Geography of Climate Change Adaptation in U.S. Agriculture*

JINGFANG ZHANG[1] EMIR MALIKOV[2] RUIQING MIAO[3] PRASENJIT GHOSH[4]

[1]Alcorn State University
[2]University of Nevada, Las Vegas
[3]Auburn University
[4]University of Southern Indiana

February 28, 2025

Abstract

Geography is a salient feature in agricultural adaptation to a warming climate. Facing heterogeneous natural-resource and climatic endowments, farmers in different locations choose adaptive strategies that are best suited to their environments, resulting in inhomogeneous adaptation across space. We provide novel evidence of this *explicitly spatial* heterogeneity in heat sensitivity of U.S. crop yields and their adaptation thereto. We generalize a popular long-differences approach by explicitly incorporating geographic information of crop-producing counties in a semiparametric fashion, using local kernel averaging. This lets us control for spatially clustered local heterogeneity that may be non-neutral in that it moderates climate effects on agriculture. Obtained measurements of historical adaptation are also more granular and account for local contexts, as do projected yield changes due to climate change. We find that corn and soybean adaptation to overheat mainly occurred in the Northern Great Plains and Upper Midwest. There is a geographic bifurcation in expected climate change effects by the mid-century, with some regions projected to experience large yield declines and others to benefit from significant yield gains. Considering the net offset potential of this bifurcation, our average yield impact projections are generally smaller relative to traditional approaches.

Keywords: Adaptation, Agriculture, Climate Change, Crop Yields, Regional Heterogeneity, Spatially Varying Coefficients

*We thank Ellen Bruno, Marshall Burke, Walter Falcon, Brittney Goodrich, Nic Irwin, David Lobell, Bruce McCarl, Rodolfo Nayga, Sofia Villas-Boas, and Brian Wright for constructive comments. We are grateful to Wendiam Sawadgo for his support with the cover crop data and to Yong Liu for his help with the genetically engineered crop adoption data. We also thank seminar participants at Stanford University, Texas A&M University, UC Berkeley, UC Davis, University of Wisconsin-Madison, the 2022 AAEA Annual Meeting, the 2022 AERE Summer Conference, and the 2023 NC1034 Annual Meeting and Research Conference for helpful feedback. All errors are ours. *E-mail*: jzhang@alcorn.edu (Zhang), emir.malikov@unlv.edu (Malikov), miaorong@auburn.edu (Miao), pghosh@usi.edu (Ghosh). *Data Sharing & Data Availability Statement:* The data that support the findings of this study are openly available, with the sources cited in the paper. *Conflict of Interest & Financial Disclosure Statement:* The authors declare no known interests related to this manuscript.

1 Introduction

The changing climate has been posing an increasing threat to sustainable agricultural production as extreme heat and drought episodes become increasingly frequent (Semenov and Shewry, 2011; Rahmstorf and Coumou, 2011; Field et al., 2012; Gourdji et al., 2013; Trnka et al., 2014). Understanding adaptation to a warming climate is critical to measuring the damages of climate change for agriculture. In the spirit of a typical analysis of average treatment effects on the treated, prior studies that examine whether—and to what extent—the adaptation to climate change occurs in agriculture almost exclusively focus on identification of the *average* adaptation (e.g., Burke and Emerick, 2016; Blanc and Schlenker, 2017; Malikov et al., 2020; Chen and Gong, 2021; Mérel and Gammans, 2021; Yu et al., 2021; Cui and Xie, 2022; Moscona and Sastry, 2022a).[1] While interesting in its own right, by construction, such a global estimand sheds little light on *local* adaptation experiences of farmers which, in all likelihood, exhibit substantial geographical heterogeneity. Crop producers in different locations deal with heterogeneous natural-resource and climatic endowments, likely employing different farming practices. Such persistent geographic differences may also prompt farmers to choose various adaptation strategies that are more optimally suited to the specific environment they face, leading to inhomogeneous adaptation outcomes across space. Understanding this (naturally occurring) spatial heterogeneity is first-order for producing more granular measurements of historical adaptation and, by extension, more accurate projections of future yield losses associated with climate change, particularly in large and climatically diverse countries.

In this paper, we contribute to the growing literature on economic geography of climate change by providing novel evidence of *explicitly spatial* heterogeneity in heat sensitivity of U.S. agriculture and adaptation thereof to a warming climate. When modeling the long-run relationship between agriculture and climate, we allow the time-variant responsiveness of mean crop yields to climate (particularly, to excessively high temperatures) to vary across geographic locations, thus capturing local heterogeneity in farmers' adaptation capabilities. To measure this cross-location variability, we employ a semiparametric specification capable of accommodating spatially inhomogeneous county-specific relationships between climate and agriculture that can systematically vary across geography and over time.

Concretely, we let temporally varying coefficients in the mean projection of crop yields on climate variables in a county be nonparametric functions of the county's geographic location. This enables us to control for local heterogeneity that needs not be additively separable (i.e., climate-neutral), as typically restricted by means of intercept-shifting county fixed effects. Our treatment of the cross-county spatial heterogeneity is more flexible in that we let it be nonneutral so that it can also moderate local climate effects on agricultural yields by, in ef-

[1]The two notable exceptions are Butler and Huybers (2013) and Keane and Neal (2020); more on these papers later.

fect, also shifting slopes. As such, our analytical strategy is more general than popular conventional methodologies for modeling the climate-agriculture relationship—both the "fixed-effects" (e.g., Schlenker and Roberts, 2009; Chen et al., 2016; Miao et al., 2016; Cui, 2020a) and "long differences" approaches (e.g., Burke and Emerick, 2016; Yu et al., 2021)—because not only do we allow the estimated relationship to vary between individual counties but, most of all, we do so in a manner that explicitly recognizes the contiguous *geography* of climate change. Of note, for identification we only require that marginal effects of climate vary across space smoothly, beyond which we continue to maintain the assumption of strict exogeneity of within-county climate variation customarily made in panel-data studies.

The spatiotemporally varying coefficients in our model are set to parsimoniously capture the myriad unobserved and observed factors pertaining to each county's geographic location that may influence the sensitivity of agricultural yields to climate variation, including agricultural practices, the quality of soil, local institutions and regulations, as well as many persistent features of the local climatic system which shape farming.[2] Technological opportunities and management strategies vary across space as well. Farmers dealing with particular land quality and other geotopographic endowments correspondingly adopt different field management practices, e.g., the application of fertilizers, irrigation, use of improved seeds, employment of rotation and tillage types. Farmers' perception of climate change across different locations also need not be the same (see Burke and Emerick, 2016). For instance, a local extreme heat event in early periods might signify a warming climate from local farmers' point of view and prompt them to adopt adaptation and mitigation strategies more proactively than typically. Spatially heterogeneous institutional and regulatory environments also prompt farmer's differential choices of adaptation strategies across regions (see World Bank, 2008; Bogdanski, 2012; Scherr et al., 2012). For example, farmers with fewer financial constraints or under supportive agricultural policies are usually more willing to adopt climate-smart practices (e.g., see Giller et al., 2009; Adenle et al., 2015).

Since the standard fixed-effects estimators only identify the average sensitivity of agriculture to the annual weather variation instead of the long-run climate change (see Blanc and Schlenker, 2017; Chen and Gong, 2021), Burke and Emerick's (2016) alternative "long differences" approach has emerged as, arguably, the dominant modeling paradigm to study climate change adaptation. The idea is simple: estimating the climate-agriculture relationship using temporal differences in the longer-run local averages, we can identify the effect of "climate" on agriculture. In our analysis, therefore, we too adopt this modeling paradigm but generalize it in a critical aspect. Namely, both the original Burke and Emerick's (2016) long-differences methodology and its recent time-varying extension by Yu et al. (2021) focus

[2]While some of these factors—notably, regulations and farming practices—may be endogenous with respect to agricultural productivity, the county's geographic location which we effectively use as their proxy is however immune to these concerns given its plausibly strict exogeneity.

on measuring *average* (over cross-sectional units and, by implication, space) causal effects of climate on agricultural productivity. To identify these effects, they implicitly assume that confounding cross-sectional heterogeneity is strictly additive (shifts the intercept only) and thus can be fully controlled for via additively separable fixed effects. Using both data-driven methods and formal inference, we find that the latter is not corroborated empirically. Our analysis reveals strong evidence that local heterogeneity—proxied by geographic location—also plays a significant role in moderating the yield-climate relationship, influencing marginal effects of climate. Given the naturally occurring correlation between the county location and local climate variation, ignoring such non-additive spatial heterogeneity can result in omitted time-varying confounders, thus hindering identification of even the average climate effect via standard fixed-effects estimators. With the data rejecting spatial invariance of slopes, we therefore build an approach that explicitly accommodates non-neutral spatiotemporal heterogeneity in the climate effects on agriculture by allowing regression parameters to change with location and over time.[3] As such, our paper contributes to the climate literature on a methodological front by providing a framework which generalizes the popular long-differences approach in a practically important aspect.

Our analysis is based on county-level corn and soybean yield and climate data in the rain-fed region of the United States during the 1958–2019 period. With data-driven cross-validation and formal specification tests rejecting a go-to spatially invariant specification across an array of popular models for measuring marginal effects of climate, we find that sensitivity and adaptation of crop yields to a warming climate vary significantly across space. This variation is not haphazard either. For corn yields, 54% of counties are estimated to have experienced statistically significant decreases in overheat sensitivity (termed "adaptation"), 12% to have experienced statistically significant *increases* (termed "maladaptation"), and 34% to have had *no* statistically significant changes (termed "no adaptation"). For soybeans, the three corresponding numbers are 75%, 2%, and 23%. Geographically, corn and soybean adaptation to overheat mainly occurred in the Northern Great Plains and Upper Midwest. On acreage-weighted average, our model estimates that yield sensitivity of corn and soybeans to overheat respectively declined by 73% and 49% over 1958–2019. Of note, spatially invariant specifications tend to produce larger estimates of declines in

[3]Notably, Mérel and Gammans (2021) model long-run adaptation by using a quadratic-in-weather panel approach. While they do not explicitly model spatial heterogeneity, their specification inherently allows varying locations to exhibit distinct marginal responses to climate. However, consistent with the prior literature, their econometric approach continues to assume that the confounding cross-sectional heterogeneity is strictly additive—a restriction that our analysis seeks to relax. Cui (2020b) and Cui and Zhong (2024) investigate climate change adaptation by replacing annual weather variables with their 30-year moving averages in a standard annual fixed-effect panel model, and estimate the responsiveness of crop acreage to climate change in different regions, either by splitting the sample (Cui, 2020) or by interacting climate variables with region dummies (Cui and Zhong, 2024). Similar to Mérel and Gammans (2021), they do not directly incorporate spatial heterogeneity at the unit level while also assuming that all unobserved cross-sectional confounders have strictly additive effects. Furthermore, those studies do not focus on temporally varying responses of agriculture to climate change, which is a key feature of our analysis.

overheat sensitivity. This underscores potential perils of abstracting away from naturally occurring non-neutral spatial heterogeneity when measuring marginal effects of climate on agriculture, which may result in overestimated evidence of (mal)adaptation.

Accounting for significant spatial heterogeneity when projecting expected damages of a warming climate between the end of our sample period (2015–2019) and the mid-century (2048–2052), we find a clear geographic bifurcation in future climate change effects on yields. Under the baseline 'adaptation as usual' scenario, some corn-producing regions in the upper South (Arkansas, Tennessee, and parts of Kentucky) and the lower Northeast (some areas in Pennsylvania and Ohio) are projected to experience decliness in yield by 2048–2052. Whereas, the Midwest is expected to benefit from significant corn yield gains due to a warming climate. Owing to its spatial flexibility, which enables us to capture this bifurcation, our methodology generally produces smaller yield loss/gain projections, compared to more traditional spatially invariant alternatives. As such, our yield loss projection are much smaller relative to earlier studies (e.g., Burke and Emerick, 2016; Yu et al., 2021). On acreage-weighted average for the whole rain-fed U.S., depending on a climate change scenario, by 2048–2052 our model predicts 1–27% yield losses for corn and 33–50% yield losses for soybeans relative to their 2015–2019 levels, although some average projections for corn are statistically insignificant. This result is intuitive given the spatial bifurcation in future climate change effects on crop productivity, with the offset potential in the net average effect. Across regions, however, the effects are not net-zero.

To summarize, the contribution of our paper is as follows. We expand the frontier of climate economics literature by studying explicitly spatial heterogeneity in heat sensitivity of the U.S. agriculture and its adaptation to a warming climate. Our analysis relaxes the empirically uncorroborated space-invariance assumption which, if violated, may jeopardize identification of (average) marginal effects of climate. To this end, we generalize a popular "long differences" approach to accommodate non-neutral local heterogeneity. Our modeling framework is more flexible in a sense that it can parsimoniously accounts for many (un)observed local factors that may moderate the effects of climate on agricultural production. Our paper shows that, without considering spatial variation in local adaptation, standard approaches tend to overestimate agricultural damages of climate change.

Although understudied, our focus on spatial heterogeneity in the climate sensitivity of agricultural production is not without precedent. In this regard, our paper complements the earlier work by Butler and Huybers (2013) and Keane and Neal (2020) who investigate non-neutral cross-county heterogeneity in the effects of weather (instead of climate) on mean crop yields.[4] Unlike Butler and Huybers' (2013) approach, ours measures the adaptation

[4]Some studies investigate time-varying sensitivity of crop yields to weather variation (e.g., Roberts and Schlenker, 2011, 2012; Lobell et al., 2014), but spatial heterogeneity is not their focus. Notably, Schlenker and Roberts (2009) also consider regional differences in yield responses to weather variation, but they investigate it using region-based sample splitting (e.g., northern vs. middle vs. southern states), which allows for spatial heterogeneity only at a coarse aggregate level. Our

to a warming climate in a flexible way without needing to rely on ad-hoc time-invariant parameterizations of heat sensitivity of yields: instead, we let the latter change over time arbitrarily. On the other hand, to identify cross-county and cross-time heterogeneity in marginal effects of climate, in contrast to Keane and Neal (2020), we do not assume additive time and unit fixed effects in slopes, meaning that spatial heterogeneity in climate sensitivity of yields in our analysis need not be time-invariant. The critical implication is that our methodology, unlike Keane and Neal's (2020), facilitates the analysis of cross-location differences in the *adaptation* to a warming climate *over time*.[5]

More importantly, although these prior studies also examine the variation in climate-agriculture relationship across counties and even interpret such heterogeneity as "spatial," neither one explicitly incorporates *spatial* information into their modeling. As such, conceptually, a more appropriate characterization of the heterogeneity that they document between counties is perhaps "cross-sectional." In contrast, our approach to measuring cross-county heterogeneity in climate change effects and adaptation thereto is implemented by explicitly recognizing the geographic location of each county. This is a non-trivial distinction because both climate and soil quality are inherently linked to the county's location; both are spatially contiguous and not assigned arbitrarily. By letting the climate effects on yields expressly depend on location via smooth slope functions and estimating them nonparametrically by locally averaging over spatially proximate counties, we directly leverage this contiguity and clustering across space in the data. To this end, the cross-county heterogeneity in climate change adaptation that our model is able to identify is unambiguously spatial.

2 Empirical Approach

We first introduce our econometric model of a spatiotemporally varying relationship between climate and agriculture and then discuss how it nests more traditional approaches as special cases.

Let us begin with the conventional formulation of a reduced-form relationship between an agricultural outcome y_{it} (e.g., the logarithm of crop yield in our paper) and strictly ex-

analysis measures spatially heterogeneous climate sensitivity at the unit level.

[5]Concretely, Keane and Neal (2020) assume an additive structure of county-year-specific slope coefficients as $\boldsymbol{\beta}_{it} = \boldsymbol{\beta} + \boldsymbol{\lambda}_i + \boldsymbol{\theta}_t$, with subscripts i and t respectively indexing counties and years. Such a coefficient structure a priori yields temporal changes in slopes between, say, t_1 and t_2 that do not vary across counties: $\boldsymbol{\theta}_{t_1} - \boldsymbol{\theta}_{t_2}\ \forall i$. Analogously, cross-county differences in slopes between, say, i_1 and i_2 are a priori time-invariant: $\boldsymbol{\lambda}_{i_1} - \boldsymbol{\lambda}_{i_2}\ \forall t$. As a result, the Keane and Neal (2020) approach imposes that all counties adapt to climate change over time to the same extent and that "level differences" in climate sensitivity across counties are time-invariant. Our nonparametric treatment of $\boldsymbol{\beta}_{it}$ does not impose such strong restrictions. Also, on a more technical note, for consistency our approach to modeling spatial heterogeneity requires large-n asymptotics, whereas the alternatives can deliver consistent estimation only when T (Butler and Huybers, 2013) or even both T and n (Keane and Neal, 2020) diverge. While theoretical, these nuances can have important practical implications in finite samples, given that most yield-climate analyses utilize large-n-small-T panels.

ogenous weather variables $\mathbf{z}_{it}$ in county i in year t:

$$y_{it} = \alpha + \boldsymbol{\beta}'\mathbf{z}_{it} + \mu_i + \epsilon_{it} \qquad\qquad \forall\ i = 1,\dots,n;\ t = 1,\dots,T, \tag{1}$$

where α is the common intercept term, $\boldsymbol{\beta}$ is a vector of coefficients measuring sensitivity of the mean of agricultural outcome to changes in $\mathbf{z}$, μ_i captures unobservable county-level heterogeneity, and ϵ_{it} is an *i.i.d.* noise with $\mathbb{E}\left[\epsilon_{it}|\mathbf{z}_{i1},\dots,\mathbf{z}_{iT},\mu_i\right] = 0$.

Arguably, the popularity of the above panel-data specification in the empirical climate economics literature is mainly driven by its ability to control for unobserved correlated confounders via unit fixed effects, thereby mitigating the omitted variable bias concerns when seeking to identify "average treatment effects on the treated" via $\boldsymbol{\beta}$. However, a key feature of the model in (1) and its typical variants is that they posit the mean yield-climate relationship that is fixed across space (and over time, but let us abstract away from the latter for now). They also implicitly assume that cross-county heterogeneity in this relationship—say, due to the differential soil quality and other geotopographic factors—is strictly neutral and thus can be fully controlled for via additively separable fixed effects $\{\mu_i\}$. However, given the inherent importance of geography for both climate and agriculture, location may also influence marginal effects of $\mathbf{z}_{it}$ on crop yields. That is, in practice, local heterogeneity is likely *non-neutral*, moderating the yield-climate relationship by shifting not only the intercept but also the slopes. If the latter is the case, then ignoring this spatial heterogeneity in slopes may jeopardize identification of even the average causal effects of climate via $\boldsymbol{\beta}$ in space-invariant models such as (1).

To fix ideas, consider the mean yield-climate relationship with non-neutral local heterogeneity:

$$y_{it} = \alpha + \underbrace{\left[\boldsymbol{\beta} + \boldsymbol{b}_i\right]'}_{\boldsymbol{\beta}_i}\mathbf{z}_{it} + \mu_i + \epsilon_{it} = \alpha + \boldsymbol{\beta}'\mathbf{z}_{it} + \mu_i + \left(\boldsymbol{b}_i'\mathbf{z}_{it} + \epsilon_{it}\right), \tag{2}$$

where $\boldsymbol{b}_i$ is cross-unit spatial heterogeneity in slopes. From the second equality, it is evident that a model ignoring spatial variation in slopes would suffer from an omitted time-varying confounder $\boldsymbol{b}_i'\mathbf{z}_{it}$ that no standard fixed-effects transformation can remove. Given the naturally expected correlation between spatial heterogeneity $\boldsymbol{b}_i$ and local weather $\mathbf{z}_{it}$ (and very likely μ_i too), the strict exogeneity of $\mathbf{z}_{it}$ necessary to identify $\boldsymbol{\beta}$ in a panel-data setup would be violated, viz., $\mathbb{E}\left[\boldsymbol{b}_i'\mathbf{z}_{it} + \epsilon_{it}|\mathbf{z}_{i1},\dots,\mathbf{z}_{iT},\mu_i\right] = \mathbb{E}\left[\boldsymbol{b}_i|\mathbf{z}_{i1},\dots,\mathbf{z}_{iT},\mu_i\right]'\mathbf{z}_{it} \neq \mathbf{0}$. Basically, the issue at hand is correlated coefficient heterogeneity that a standard linear fixed-effects (within) estimator cannot handle, suffering from what Chamberlain (1982) called "heterogeneity bias" (also see Graham and Powell, 2012; Laage, 2024, for related discussions and references therein). With that in mind, in this paper, we therefore aim to explicitly accommodate non-neutral cross-location heterogeneity in climate effects on agriculture.

Since fixed-effects estimation of panel-data models relies on a year-to-year within-county variation, even if they were well-identified, the $\boldsymbol{\beta}_i$ slopes in (2) would reflect sensitivity of crop yields to the annual *weather* variation instead of the long-run climate change (see Burke and Emerick, 2016; Blanc and Schlenker, 2017; Chen and Gong, 2021). Given that it is the latter which is the object of real interest, Burke and Emerick (2016) have popularized the idea of modeling the yield-climate relationship using longer-run averages over two separate subperiods, with the rationale being that the long-difference regression leveraging exogenous cross-county variation in long-range temporal changes of local averages can identify marginal effects of *climate* change on yields. In what follows, we too adopt this modeling paradigm but generalize it to allow both spatial and temporal—that is, *spatiotemporal*—heterogeneity in marginal effects, which we accomplish by allowing regression parameters to vary across county locations and over time subperiods.

Splitting the sample period $1,\ldots,T$ into a finite set of mutually exclusive multi-year subperiods $\mathbb{T} = \{a, b, c, \ldots\}$ and letting s_i denote the time-invariant location of county i, we arrive at the following generalization of (1):

$$y_{it} = \sum_{\tau\in\mathbb{T}} \alpha_\tau(s_i)\mathbb{1}(t\in\tau) + \sum_{\tau\in\mathbb{T}} \boldsymbol{\beta}_\tau(s_i)'\mathbb{1}(t\in\tau)\mathbf{z}_{it} + \mu_i + \epsilon_{it} \qquad \forall\ i=1,\ldots,n;\ t=1,\ldots,T, \quad (3)$$

where $\{\mathbb{1}(t\in\tau);\ \tau\in\mathbb{T}\}$ is a series of subperiod indicator variables, and all parameters are modeled as smooth nonparametric subperiod-specific functions of the county's geographic location. Thus, our model captures a more flexible relationship between climate and agriculture that can vary both temporally (over subperiods τ) and spatially (between county locations s_i).[6] By incorporating geographic information into the model, we obtain parameters that differ between counties. This provides an indirect way to control for observed and unobserved cross-county local heterogeneity (such as different soil quality, institutions, regulations, and farming practices) that moderates climate effects on agricultural productivity. As such, county-level heterogeneity in (3) is no longer restricted to be additively separable.

Of note, by virtue of modeling cross-county differences as an explicit *smooth* function of the county's location, we are able to parsimoniously accommodate the contiguity/clustering of local heterogeneity across space that naturally arises due to the geography of climate and topography of land. Thus, the cross-county heterogeneity in the yield-climate relationship that our formulation is able to identify is unambiguously "spatial." This is distinct from Butler and Huybers's (2013) and Keane and Neal's (2020) alternative approaches to modeling cross-county heterogeneity as purely "cross-sectional" with no spatial structure, which is akin to just letting coefficients be $\boldsymbol{\beta}_i$ as in (2) or $\boldsymbol{\beta}_{it}$ if one were to extend (2) to also

[6] While fully nonparametric in the spatial dimension, our model is, in effect, piece-wise linear in the time dimension. We choose such a specification in part because allowing parameters to also be nonparametric functions of time would necessitate the invocation of large-T-large-n asymptotics for consistency which is impractical in studies like ours given that $n \gg T$.

incorporate time heterogeneity. In our case, spatiotemporally varying marginal effects are essentially regularized as $\boldsymbol{\beta}_{it} \equiv \boldsymbol{\beta}_\tau(s_i)$ which smoothly—as opposed to arbitrarily—vary with space across counties.

Averaging (3) over all years in a subperiod τ, we obtain a long-run average relationship between mean crop yields and climate (i.e., average weather over years):

$$\overline{y}_{i\tau} = \alpha_\tau(s_i) + \boldsymbol{\beta}_\tau(s_i)'\overline{\mathbf{z}}_{i\tau} + \mu_i + \overline{\epsilon}_{i\tau} \qquad \forall\ i = 1,\ldots,n;\ \tau = a,b,c,\ldots,\mathbb{T}, \tag{4}$$

where $\overline{x}_{i\tau} = \sum_{t\in\tau} x_{it} \big/ \sum_t \mathbb{1}(t \in \tau)$ for any variable x, and all parameters are period- and location-specific, in effect, making them vary at the observation level. The intercept $\alpha_\tau(s_i)$ captures a local climate-neutral but time-varying contribution of the county's location-specific factors on mean crop yield. Slope parameters $\boldsymbol{\beta}_\tau(s_i)$ measure a local effect of climate on the mean crop yield in period τ moderated by *non-additive* spatial heterogeneity, and μ_i represents the remaining additive components of time-invariant county unobservables.

Altogether, a nontrivial distinction between (4) and its analogue derived from standard models akin to (1) is that yield sensitivity to climate variation is no longer constant over time and across space. This is a critical generalization because it accommodates the potential for (mal)adaptation to climate change and, importantly, expressly allows it to be of a heterogeneous degree across different regions. Namely, differencing (4) over two non-adjacent subperiods, say a and c, with a being the earlier period, we obtain a "long-differenced" relationship between the mean yield and climate:

$$\Delta\overline{y}_{i(c,a)} = \underbrace{\left[\alpha_c(s_i) - \alpha_a(s_i)\right]}_{\alpha^*_{(c,a)}(s_i)} + \boldsymbol{\beta}_a(s_i)'\Delta\overline{\mathbf{z}}_{i(c,a)} + \big[\underbrace{\boldsymbol{\beta}_c(s_i) - \boldsymbol{\beta}_a(s_i)}_{\boldsymbol{\beta}^*_{(c,a)}(s_i)}\big]'\overline{\mathbf{z}}_{ic} + \Delta\overline{\epsilon}_{i(c,a)} \quad \forall\ i = 1,\ldots,n, \tag{5}$$

where $\Delta\overline{x}_{i(c,a)} = \overline{x}_{ic} - \overline{x}_{ia}$ for any variable x, and the newly defined $\alpha^*_{(c,a)}(s_i) \equiv \alpha_c(s_i) - \alpha_a(s_i)$ and $\boldsymbol{\beta}^*_{(c,a)}(s_i) \equiv \boldsymbol{\beta}_c(s_i) - \boldsymbol{\beta}_a(s_i)$ respectively measure local changes in the intercept and slope functions between periods a and c.[7] Therefore, by identifying the change in sensitivity of the ith county's mean crop yields to climate variation in the longer run, the slopes $\boldsymbol{\beta}^*_{(c,a)}(s_i)$ indirectly provide us with the information about (mal)adaptation to climate change by local agriculture: a decrease (resp., increase) in sensitivity of yields to harmfully excessive heat would indicate adaptation (resp., maladaptation). In our model (5), such an adaptation is

[7] Just like in the conventional time-and-location-invariant "long differences" approach of Burke and Emerick (2016), the identification of (functional) coefficients is based on temporal within-county variation in climate variables, which allows controlling for additive time-invariant confounders at the county level. This becomes even more obvious once we recall that, with two time periods (as is the case with a and c here), the difference estimator is equivalent to within estimator which, in turn, is known to be equivalent to a pooled regression with fixed effects formulated as a linear projection on within-unit time averages of regressors using the so-called Mundlak (1978) device. That is, the estimation of (5), which is expressed in differences, effectively corresponds to a pooled estimation of $\overline{y}_{i\tau} = \sum_\tau \alpha_\tau(s_i)D_{i\tau} + \sum_\tau \boldsymbol{\beta}_\tau(s_i)'D_{i\tau}\overline{\mathbf{z}}_{i\tau} + \boldsymbol{\gamma}\overline{\overline{\mathbf{z}}}_{i\cdot} + \overline{\epsilon}_{i\tau}\ \forall\tau = \{a,c\}$, where $\{D_{i\tau}\}$ are time period dummies, and from where it is evident that the effects of both $\overline{\mathbf{z}}_{ia}$ and $\overline{\mathbf{z}}_{ic}$ are measured keeping the within-unit "mean of means" $\overline{\overline{\mathbf{z}}}_{i\cdot} \equiv \frac{1}{2}\sum_\tau \overline{\mathbf{z}}_{i\tau}$ constant.

explicitly allowed to vary spatially, reflective of heterogeneous local conditions. Although we ought to emphasize that, given our reduced-form formulation of the yield-climate relationship, one is to interpret $\boldsymbol{\beta}^*_{(c,a)}(s_i)$ as capturing the *net cumulative* effect of all and any various adaptive methods used by farmers.

Nested Specifications. Our flexible model constitutes a semiparametric generalization of the popular time-and-location-invariant "long differences" approach by Burke and Emerick (2016) and its recent time-varying extension by Yu et al. (2021). In fact, our spatiotemporally varying model in (5) nests these two as special cases. When $\alpha_\tau(s_i) = \alpha$ and $\boldsymbol{\beta}_\tau(s_i) = \boldsymbol{\beta}$ are restricted for all τ and s_i, it collapses to the Burke and Emerick (2016) specification:

$$\Delta\overline{y}_{i(c,a)} = \boldsymbol{\beta}'\Delta\overline{\mathbf{z}}_{i(c,a)} + \Delta\overline{\epsilon}_{i(c,a)} \qquad \forall\ i = 1,\ldots,n, \tag{6}$$

in which slopes are both spatially and temporally invariant and thus constant.

If one were to "fix" the yield-climate relationship only in the spatial dimension by having $\alpha_\tau(s_i) = \alpha_\tau$ and $\boldsymbol{\beta}_\tau(s_i) = \boldsymbol{\beta}_\tau$ for all s_i, our model would then reduce to a time-varying specification à la Yu et al. (2021), in which slopes may change over time but are restricted to be common to all locations:

$$\Delta\overline{y}_{i(c,a)} = \alpha^*_{(c,a)} + \boldsymbol{\beta}'_a\Delta\overline{\mathbf{z}}_{i(c,a)} + {\boldsymbol{\beta}^*_{(c,a)}}'\overline{\mathbf{z}}_{ic} + \Delta\overline{\epsilon}_{i(c,a)} \qquad \forall\ i = 1,\ldots,n, \tag{7}$$

where $\alpha^*_{(c,a)} \equiv \alpha_c - \alpha_a$ and $\boldsymbol{\beta}^*_{(c,a)} \equiv \boldsymbol{\beta}_c - \boldsymbol{\beta}_a$.

It may also be of interest to consider a third special case nested within our model, namely, a spatially varying but time-invariant coefficient specification that (5) simplifies to when $\alpha_\tau(s_i) = \alpha(s_i)$ and $\boldsymbol{\beta}_\tau(s_i) = \boldsymbol{\beta}(s_i)$ for all time periods τ. In such an instance, one arrives at a spatially varying extension of the Burke and Emerick (2016) specification:

$$\Delta\overline{y}_{i(c,a)} = \boldsymbol{\beta}(s_i)'\Delta\overline{\mathbf{z}}_{i(c,a)} + \Delta\overline{\epsilon}_{i(c,a)} \qquad \forall\ i = 1,\ldots,n, \tag{8}$$

as can be easily seen by comparing (8) to (6).

On a final note, our spatially varying approach can also be applied to extend the more traditional fixed-effects estimator à la Schlenker and Roberts (2009). We discuss this in more detail in Appendix A.

2.1 Semiparametric Estimation

Given our semiparametric functional-coefficient specification of the reduced-form relationship between mean crop yields and climate, we estimate our model in long differences given in (5) via *local* least squares. We employ local-constant kernel fitting.

Parameters of interest are the unknown nonparametric s_i-location-specific coefficients $\mathbf{\Theta}(s_i) = [\alpha^*_{(c,a)}(s_i), \boldsymbol{\beta}_a(s_i)', \boldsymbol{\beta}^*_{(c,a)}(s_i)']'$ in (5). Assuming that these coefficient functions are smooth and twice continuously differentiable in the neighborhood of s, we can approximate parameter functions $\mathbf{\Theta}(s_i)$ at points s_i in the vicinity of location s using a local constant: $\mathbf{\Theta}(s_i) \approx \mathbf{\Theta}(s)$. Therefore, for locations $\{s_i\}$ close to s, a spatially-varying long-differenced mean yield-climate relationship in (5) is approximated via

$$\Delta \overline{y}_{i(c,a)} \approx \alpha^*_{(c,a)}(s) + \boldsymbol{\beta}_a(s)' \Delta \overline{\mathbf{z}}_{i(c,a)} + \boldsymbol{\beta}^*_{(c,a)}(s)' \overline{\mathbf{z}}_{ic} + \Delta \overline{\epsilon}_{i(c,a)}, \tag{9}$$

which, given the quasi-random strict exogeneity of climate variation, can be consistently estimated using locally weighted least squares. The corresponding kernel estimator is

$$\widehat{\mathbf{\Theta}}(s) = \left[\sum_i \overline{\mathbf{x}}_{i(c,a)} \overline{\mathbf{x}}'_{i(c,a)} \mathbb{K}_h(s_i, s) \right]^{-1} \sum_i \overline{\mathbf{x}}_{i(c,a)} \Delta \overline{y}_{i(c,a)} \mathbb{K}_h(s_i, s), \tag{10}$$

where $\overline{\mathbf{x}}_{i(c,a)} = [1, \Delta \overline{\mathbf{z}}'_{i(c,a)}, \overline{\mathbf{z}}'_{ic}]'$ is a vector of regressors. A product kernel $\mathbb{K}_h(s_i, s) = K\left(\frac{s_{1i} - s_1}{h_1}\right) \times K\left(\frac{s_{2i} - s_2}{h_2}\right)$ weights each long-differenced county i on the basis of closeness of its geographic coordinates (i.e., longitude and latitude) $s_i = (s_{1i}, s_{2i})$ to those of the location s, with $K(\cdot)$ being a kernel weighting function, s_1 and s_2 respectively denoting the longitude and latitude of location s, and h_1 and h_2 being the corresponding bandwidths. These bandwidths control the degree of smoothing and weighting, and slowly converge to 0 as the sample size n grows. The kernel $K(\cdot)$ is non-negative, symmetric and integrates to 1; we employ a popular second-order Gaussian kernel.[8]

The estimator in (10) illustrates well the way we explicitly model a contiguous nature of spatial heterogeneity in our framework. Namely, by letting marginal effects of climate depend on the county's location via smooth functions $\mathbf{\Theta}(s_i)$, the estimated slope heterogeneity is continuous over space as we estimate these slopes for each county by locally averaging over geographically proximate counties.

Inference. Due to its semiparametric nature, computation of the asymptotic variance of estimator in (10) is not as simple and its use in finite samples may also be not as easy to justify. We therefore employ Efron's (1982) bias-corrected bootstrap for statistical inference, which we also use to obtain confidence intervals for functions of $\mathbf{\Theta}(s_i)$, such as the (mal)adaptation index and yield change projections. For details, see Appendix B.

[8] Recall that we opt to model spatial parameter heterogeneity as a function of the county's geographic location, which is as a capture-all proxy for many regulatory and farming practice factors, because it is immune to the endogeneity concern given its plausible strict exogeneity. The socioeconomic factors that may correlate with county location, such as GE crop adoption rate, cover crop adoption rate, and crop insurance coverage, are not included explicitly because they are likely endogenous with respect to crop yields. Land quality can also be endogenous in the long run because it is influenced by farming practice and land-use changes (Lark et al., 2020; Pahalvi et al., 2021; Koudahe et al., 2022; Weldewahid et al., 2023).

3 Data

Annual county-level yield data for corn and soybeans over 1958–2019 are obtained from the U.S. Department of Agriculture (USDA) National Agricultural Statistics Service (NASS). We focus only on the rainfed counties east of the 100th Meridian because i) rainfed counties account for about 97% of both corn and soybean production in the U.S. over the sample period, and ii) crop production in the western counties is heavily influenced by subsidized irrigation systems. We exclude counties that produce these crops for fewer than two years. Our final data sample includes 1,534 counties for corn and 1,042 counties for soybeans. We obtain the longitude and latitude of county centroids from the U.S. Census Bureau.

Historical weather data are from Schlenker and Roberts (2009), who have extended the dataset to 2019.[9] It includes daily total precipitation as well as the maximum and minimum temperatures for 4-km grid cells covering the entire U.S. over the period 1950–2019. Following the convention (e.g., see Schlenker and Roberts, 2009; Burke and Emerick, 2016; Malikov et al., 2020; Yu et al., 2021), we use the growing degree days (GDD) to model a non-linear relationship between temperature and crop yields. Daily GDD is a measurement of time that crops are exposed to temperatures between the lower and upper thresholds during a specific day, and the annual GDD over the entire growing season is defined as the accumulation of daily GDD over the growing season. Following Burke and Emerick (2016), Yu et al. (2021), and the Economic Research Service (2022) of the USDA, we define the growing season as April 1st to September 30th for both crops.

Schlenker and Roberts (2009) find that temperatures over 29°C and 30°C generate harmful effects on corn and soybean production, respectively. Therefore, we set upper boundaries of the GDD calculation for each crop at their respective critical thresholds, with the lower threshold always set at 8°C. We denote this variable as $\text{GDD}_{8-r_0{}^\circ\text{C}}$, where r_0 respectively equals 29 and 30 for corn and soybeans, and use it to capture the effects of "normal" temperature on yields. To quantify the overheat effect of high temperatures (and the potential adaptation by farmers to combat it in the face of a warming climate), we use a measure of harmful GDD computed for each crop using temperatures in excess of their respective r_0 thresholds. We label this overheat GDD variable as $\text{GDD}_{r_0{}^\circ\text{C}+}$.

Figure 1 plots maps of the average yield for the two crops and the corresponding GDD and overheat GDD in the last five years of our sample period, 2015–2019 (see the top three rows in the figure). Taking a quick glance at these maps, we already can see the empirical imperative to account for the apparent spatial heterogeneity (and clustering therein) in both yields and climate, when relating agricultural productivity to climate. Spatial differences in crop yields are unarguably related to many local factors and, perhaps more prominently, to the differential soil quality (see the bottom row of Figure 1 for soil quality maps associated

[9]The dataset is available at http://www.columbia.edu/ ws2162/links.html.

with each crop). However, we later show that controlling for these factors via additively separable location (i.e., county) fixed effects is insufficient to fully capture spatial differences in the climate-yield relationship, which motivates a more spatially flexible approach of ours.

Although not the focus of our analysis, we also control for precipitation, which we do along the lines of Burke and Emerick (2016) and Yu et al. (2021). To accommodate potential nonlinearities in precipitation effects on yields, we construct two precipitation-related variables: *i*) total precipitation below a threshold, measuring the severity of water deficiency, and *ii*) total precipitation above the same threshold, measuring the magnitude of water abundance. Appendix C details construction of these precipitation variables and also provides summary statistics of historical yield and weather data (see Table C.1).

Predicted future climate data over 2048–2052 are obtained from the Multivariate Adaptive Constructed Analogs (MACA).[10] We select data from two widely used global climate models. One is the HadGEM2-ES365 model, which tends to predict large temperature increases, and the other is the NorESM1-M model, which predicts small temperature increases. For each one of these climate prediction models, we obtain future climate data predicted under two greenhouse gas representative concentration pathways (RCPs)—RCP4.5 and RCP8.5—that represent medium and the warmest scenarios, respectively. These weather predictions are summarized in Table C.2 in Appendix C.

4 Estimates of Spatially Heterogeneous Adaptation to Climate Change

Using our spatiotemporally varying approach, in this section we explore spatial heterogeneity in agricultural adaptation to climate change in the U.S. We first document non-trivial heterogeneity in county-specific estimates of climate sensitivity and adaptation of yields and then explore potential factors that can help explain the observed variation in local adaptation. Since the first-order threats to agricultural production by a warming climate are arguably posed by the rising temperatures associated with it, we focus on temperature-related variables and, particularly, the overheat GDD.

The estimation is done in long differences for one crop at a time with a log-linear specification.[11] We select two five-year periods that correspond to the beginning and the end of our data sample—the 1958–1962 and 2015–2019 periods—and estimate the long-run average yield-climate relationship using our flexible spatiotemporally varying model in long differences given in (5) and the three restricted specifications in (6) through (8) that it nests.[12]

[10] The weblink is https://climate.northwestknowledge.net/MACA/index.php.

[11] All regressions are weighted by the harvested acreage of a corresponding crop in the county in 1960 to facilitate an acreage-based interpretation of the results.

[12] We choose 1958–1962 and 2015–2019 for our main analysis to obtain the longest possible gap between two periods within our data sample. For sensitivity analysis (see Section 4.4) we further explore results under ten combinations of different starting and ending periods for the long-differences models.

All these models are listed, conveniently labeled, and described in Table 1. Of the four, the first two (spatially varying) models are semiparametric. To estimate them, we need to select the optimal bandwidths that control the degree of spatial smoothing across neighboring counties. Because the county location does not change over time, we employ data-driven leave-one-*location*-out cross-validation to select them. Our analysis treats geographic coordinates, measured in decimal degrees, as continuous variables because both longitude s_{1i} and latitude s_{2i} are interval variables.[13]

4.1 Spatial Heterogeneity in the Agriculture-Climate Relationship

Before proceeding to our main analysis of cross-location heterogeneity in agricultural adaptation (or maladaptation) to a changing climate, we first explore if there is significant spatial heterogeneity in the yield-climate relationship to begin with. To this end, we estimate a restricted version of our spatiotemporally varying model by "fixing" it across time (model $\mathrm{S_1T_0}$), and compare its results to those from the standard time-and-location-invariant model $\mathrm{S_0T_0}$ by Burke and Emerick (2016). By abstracting away from temporal changes in climate change effects for the time being, we are able to focus solely on cross-county differences in heat sensitivity of crop yields.

Because model $\mathrm{S_1T_0}$ identifies county-specific heat sensitivity, we obtain a distribution of estimated slope parameters $\boldsymbol{\beta}(s_i)$ that measure *local* effects of climate on mean crop yields across all counties in our sample. Table 2 summarizes their point estimates. In the far right column, the table also reports "globally constant" coefficient estimates from the $\mathrm{S_1T_0}$ model's spatially invariant analogue, $\mathrm{S_0T_0}$, as a benchmark.

The results from our semiparametric model are largely in line with prior studies (e.g., Burke and Emerick, 2016; Keane and Neal, 2020; Malikov et al., 2020; Yu et al., 2021). The exposure to normal temperatures has a positive effect on crop yields. Cross-county estimates of sensitivity to normal GDD indicate that the exposure to an additional degree-day of normal temperatures leads to a median increase in corn yields of 0.8% and soybean yields of 0.6%. On the other hand, the exposure to overheat temperatures has an expectedly adverse effect on yields. Our estimates suggest that an additional unit of overheat GDD leads to a median reduction in corn and soybean yields by 3.2% and 4%, respectively.

More importantly, consistent with non-neutral spatial heterogeneity, the estimated $\mathrm{S_1T_0}$ model in Table 2 reveals a significant variation among county-specific climate-sensitivity parameters for both crops. For example, within an interquartile range of local point estimates, the magnitude of sensitivity to overheat GDD changes by 72% (from –5.67 to –1.58)

[13] Their treatment as continuous variables also makes sense because, given our use of a kernel from an *exponential* family, product kernels $\mathbb{K}_h(s_i,s) = K((s_{1i}-s_1)/h_1)\times K((s_{i2}-s_2)/h_2)$ that weight each neighboring county i based on their closeness to the location (s_1,s_2) using longitude and latitude separately, in actual effect, weight them using bandwidth-weighted Euclidean distances between each county i and the location (s_1,s_2).

for corn and by 64% (from –6.11 to –2.22) for soybeans. The corresponding within-quartile changes for normal GDD are 112% (from 0.55 to 1.16) and 64% (from 0.45 to 0.74). We visualize this variability in the yield-climate relationship moderated by spatial heterogeneity in Figure 2 (rows 1 and 3 from the top), which plots histograms of estimated semiparametric county-specific coefficients along with their location-invariant counterparts depicted using vertical lines. Varying estimates of crop responsiveness to GDD and overheat GDD show fairly wide dispersion, which the popular spatially invariant S_0T_0 specification is unable to capture by design because it *a priori* imposes a constant-slope restriction.

This significant cross-location heterogeneity in temperature sensitivity of yields can be seen even more clearly from maps in Figure 2 that show geographical distributions of estimated slopes. What is also evident from these maps is that sensitivity to climate is not merely inhomogeneous across counties but it tends to cluster in space. For instance, the bottom-row maps in Figure 2 show that corn and soybean yields in the upper Midwest and North Great Plains are more sensitive to overheat GDD than their counterparts in the southern areas. In fact, Moran's I test overwhelmingly rejects ($p < 0.0001$) the null of no spatial autocorrelation in all parameters for each crop. This indirectly corroborates a *non-neutral* role of local geography in moderating the yield-climate relationship. Imperatively, usual approaches such as a time-and-location-invariant S_0T_0 model, which assume that local heterogeneity is climate-neutral and thus can be accounted for via additively separable county fixed effects, are unable to fully capture spatial characteristics of the relationship between yields and climate. Figure 3, which plots spatial distributions of residuals (net of county fixed effects) from the S_0T_0 model,[14] provides a visualization of the inadequacy of additive fixed effects to fully account for all cross-location heterogeneity. After netting out location effects, the residuals continue to exhibit spatial dependence, which is also confirmed using formal Moran's I tests. At the very least, it implies that one ought to cluster standard errors when doing inference in spatially invariant models. But it is critical to recognize that treating this residual spatial correlation as merely a variance issue would be tantamount to an *untested* assumption that the residual spatial dependence is confined to random shocks. In the context of discussing eq. (2), the estimation of constant slopes $\boldsymbol{\beta}$ would be consistent only if slope heterogeneity is such that $\mathbb{E}\left[\boldsymbol{b}_i|\mathbf{z}_{i1},\ldots,\mathbf{z}_{iT},\mu_i\right]=\mathbf{0}$ which would be as strong and implausible as the assumption that μ_i were not fixed but random effects.

Although results from the S_1T_0 model already provide ample evidence of non-negligible spatial heterogeneity in the relationship between crop yields and climate, we test for both its significance and empirical relevance more formally. First, we rely on Hall et al.'s (2007) result in that local-constant kernel methods, which we employ to estimate spatially varying models, can identify irrelevant regressors via cross-validation procedure. When optimally selected, a large bandwidth parameter would effectively "smooth out" the location

[14]Concretely, from the S_0T_0 specification, the plotted residuals are computed as $\Delta\overline{y}_{i(c,a)}-\widehat{\boldsymbol{\beta}}'\Delta\overline{\mathbf{z}}_{i(c,a)}$.

variable s_i, rendering all parameters in the model globally constant. This provides an indirect *data-driven* method to assess empirical relevance of the county's geographic location in the estimation of climate change effects on agricultural productivity. For the S_1T_0 model, cross-validated bandwidths for the longitude and latitude are respectively 60.3 and 36.2 kilometers (km) for corn, and 136.9 and 28.7 km for soybeans.[15] These bandwidths are small relative to the vast geographical area covered in our study (more than 2,200 km from west to east and 2,000 km from south to north), which averts smoothing out of the location, providing strong evidence that county location plays an important role in moderating the yield-climate relationship. Thus, the data reject spatial invariance.

Our spatially varying approach is also supported by Ullah's (1985) goodness-of-fit model specification test which facilitates a joint-hypothesis inference about spatial invariance. The test is essentially a nonparametric F-test that discriminates between a "restricted" time-and-location-invariant S_0T_0 specification under the null and a more flexible "unrestricted" spatially-varying S_1T_0 specification under the alternative. The test statistic is based on the distance between residual sums of squares from the two specifications: $T_n = (RSS_r - RSS_{ur})/RSS_{ur}$, where RSS_r and RSS_{ur} are restricted and unrestricted sums of squared residuals, respectively. Intuitively, just like an F-test, the test statistic is expected to converge to 0 under the null and is positive under the alternative; hence, the test is one-sided. We approximate the null distribution of T_n via bootstrap by resampling residuals from the restricted specification; the algorithm is provided in Appendix D. With a p-value ≤ 0.001, we confidently reject the null of a location-invariant model for both corn and soybean yields.

4.2 Local Adaptation to Climate Change

Having established the presence of significant cross-location heterogeneity in climate effects on crop yields, we now investigate if there is also spatial heterogeneity in *adaptation* or *maladaptation* to climate change, which can be inferred from changes in temperature sensitivity of yields over time. To this end, we estimate our proposed spatiotemporally varying model S_1T_1 which permits coefficients to vary across both time and counties.

Table 3 summarizes our local estimates of the early-period-a temperature sensitivity (the $\beta_a(s_i)$ coefficients) and of *changes* in this sensitivity between period a and the later period c (the $\beta^*_{(c,a)}(s_i)$ coefficients).[16] The earlier-period coefficients can be used as a reference to facilitate interpretation of positive values of $\beta^*_{(c,a)}(s_i)$ as the evidence of adaptation, whereby positive effects on yield in the earlier period become "more positive" and negative effects be-

[15] To be precise, since geographic coordinates are measured in decimal degrees, the actual bandwidth values for longitude and latitude are 0.543° and 0.326° for corn, and 1.230° and 0.258° for soybeans. For convenience, here we have converted them to km using the 1° = 111km approximation that is valid at the equator.

[16] A full set of parameter estimates, including local sensitivity to precipitation, is reported in Table E.2 in Appendix E.

come “less negative” over time. Analogously, negative values of $\beta^*_{(c,a)}(s_i)$ can be interpreted as capturing maladaptation because they indicate that positive effects on yield in the earlier period become “less positive” and negative effects “more negative.”[17] For comparison, the right panel of Table 3 also reports estimates from a location-invariant S_0T_1 specification à la Yu et al. (2021).

As in the case of the S_1T_0 model, optimal cross-validated bandwidths for location variables in our spatiotemporally varying model are fairly small for both crops, which is consistent with the reported evidence that geographic location is an empirically relevant variable for measuring agricultural adaptation to climate change.[18] This is further corroborated by a formal test. Using Ullah's (1985) test, we consistently reject the spatially invariant Yu et al. (2021) specification S_0T_1 in favor of our more flexible alternative S_1T_1 at the 5% significance level for the two crops ($p < 0.035$).

Per our proposed model S_1T_1, estimates of $\beta^*_{(c,a)}(s_i)$ for normal $GDD_{8-r_0{}^\circ C}$ are generally negative whereas estimates of $\beta^*_{(c,a)}(s_i)$ for overheat $GDD_{r_0{}^\circ C+}$ are primarily positive. This also holds under the S_0T_1 model, particularly for soybeans. However, our model suggests that, on average, $\beta^*_{(c,a)}(s_i)$ for $GDD_{8-r_0{}^\circ C}$ is statistically insignificant for corn and cotton yields, with some counties showing maladaptation and some showing adaptation to normal GDD. This finding differs from that of Yu et al. (2021), who find that U.S. corn displayed statistically significant maladaptation to normal GDD in the past few decades. Given the statistical insignificance of $\beta^*_{(c,a)}(s_i)$ for $GDD_{8-r_0{}^\circ C}$ in our main model S_1T_1 and the potential for large detrimental impacts of overheat on crops (see Wagner and Schlenker, 2022), in what follows we focus our discussion on the (mal)adaptation to *overheat* GDD.

Our spatially varying estimates in Table 3 show that, as expected, the sensitivity of crop yields to overheat GDD in the early period (i.e., $\beta_a(s_i)$ for $GDD_{r_0{}^\circ C+}$) is negative, suggesting that in 1958–1962 mean crop yields would fall in response to an increase in overheat temperatures. Moreover, we find that temporal changes in overheat sensitivity are positive and statistically significant—albeit, not everywhere—and that magnitudes of these changes vary non-negligibly across counties, indicating that adaptation to climate change *is* occurring but it is *not* spatially homogeneous. Magnitudes of adaptation from a location-invariant specification are much larger than the corresponding mean/median estimates from our spatiotemporally varying model, suggesting that approaches incapable of accommodating spatial heterogeneity in slopes may overestimate the degree of adaptation.

To further explore the geography of adaptation, we include histograms and maps of local

[17] In the context of global warming this differentiation of adaptation and maladaptation is reasonable because, as agriculture is exposed to an increasing amount of normal GDD and overheat GDD, adaptation should mitigate negative effects and enlarge positive effects of temperature. If it were global cooling, definitions of adaptation and maladaptation would be the opposite.

[18] For our main model S_1T_1, when converted to kilometers, optimal bandwidths for longitude and latitude are respectively equal to 315.1 and 227.7 km for corn, and 294.5 and 308.5 km for soybeans.

adaptation estimates in Figure 4. Also included in the figure is a breakdown of counties based on the statistical significance (at the 5% level) of their historical adaptation to excessive heat. While far from uniformly across space, we do find that 54% and 75% of corn and soybeans producing counties, respectively, experienced a statistically significant decrease in heat sensitivity, helping farmers adapt to a warming climate. Geographically, these adapting counties are mainly located in the Northern Great Plains and Upper Midwest. We also find some evidence of maladaptation during 1958–2019 in some of the locations: namely, in 12% of corn-producing and 2% of soybean-producing counties. In the case of corn, maladaptation occurred mainly in Pennsylvania, Maryland and Delaware in the Northeast and Arkansas in the South, where yields became more sensitive to detrimental effects of overheat temperatures. Comparing the estimated temporal changes in overheat sensitivity in these counties to the estimates of their early-period sensitivity (see Figure E.1 in Appendix E) it becomes apparent that corn yields in virtually all these locations were insensitive to overheat before. On the other hand, for soybeans, all of the very few counties in southern Indiana and Illinois that experienced maladaptation had already been responding negatively to overheat in the past, with the overheat sensitivity getting worse over time. Different maladaptation episodes such as these suggest that there may be crop-specific causes at play, which warrants further research in the future as they would entail different policy solutions to remedy the worsening yield sensitivity to overheat that took place. All in all, our findings on agricultural adaptation differ from "average" estimates in both Yu et al. (2021), who find ubiquitous adaptation, and Burke and Emerick (2016), who find no adaptation.

To get a better feel of the extent of adaptation by farmers, we use our estimates of local adaptation $\beta^*_{(c,a)}(s_i)$ to compute two supplementary measures of adaptation which have a more concrete interpretation. First, we calculate a percentage change in sensitivity of crop yields to overheat temperatures between the two periods via $\text{sign}\{\beta^*_{(c,a)}(s_i)\} \times \left|\beta^*_{(c,a)}(s_i)/\beta_a(s_i)\right| \times 100\%$, where the ratio of $\beta^*_{(c,a)}(s_i)$ to $\beta_a(s_i)$ provides the magnitude of a proportional change in heat sensitivity, and $\beta^*_{(c,a)}$ signs it. Given the adverse effect of overheat on yields, when positive this measure corresponds to a decrease in the magnitude of a negative responsiveness, indicating adaptation. Second, we scale our local adaptation estimates using each county's average overheat GDD in the later period, viz., $\beta^*_{(c,a)}(s_i) \times \overline{\text{GDD}}_{r_0\,^\circ\text{C}+,ic}$, to obtain the measurement of adaptation in terms of crop yield gains. Unlike the "raw" adaptation estimate $\beta^*_{(c,a)}(s_i)$ that measures a nominal change in the slope of overheat GDD, this one transforms the former into a change in log-yield attributable to a change in heat sensitivity, fixing the climate at period c. We convert the change in log-yield to a percentage gain in yields via $\left(\exp\{\beta^*_{(c,a)}(s_i) \times \overline{\text{GDD}}_{r_0\,^\circ\text{C}+,ic}\} - 1\right) \times 100\%$. Both these measures are summarized in Table 4, where we also include their counterparts from a location-invariant S_0T_1 specification computed analogously but using geographically constant parameter estimates.

On acreage-weighted average, by 2015–2019 overheat sensitivity of corn and soybean yields decreased significantly—by 73% and 49%, respectively (see the column 'Weighted Mean' in Table 4)—indicating that these crops have become, generally, more heat-resilient due to adaptation. In terms of the yield change due to overheat adaptation, average gains for corn and soybeans were significant and respectively estimated at 17.7% and 10.5%, relative to their 1958–1962 mean levels. Notably, these average yield gains from our model are only about half of their counterparts obtained from a spatially invariant model S_0T_1 used by Yu et al. (2021).

To see how the degree of adaptation varied across space, consider Figure 5 that plots county-specific estimates of changes in overheat sensitivity (see maps in the top row) and crop yield gains due to local adaptation to overheat (see maps in the bottom row), with statistically insignificant point estimates—regardless of their sign or magnitude—colored using the same shade of gray. Expectedly, the pattern of spatial clustering (as well as the positive/negative delineation) here is similar to that observed for "raw" estimates of local adaptation in Figure 4. For corn, the figure shows that areas with the highest percentage changes in sensitivity to overheat GDD may not necessarily have had the largest yield gains. More specifically, the highest percentage changes tend to have occurred in northern areas whereas the largest yield gains tended to occur in southern areas of the Corn Belt. At least in part, this is because the northern part of the studied region experienced the largest changes in the magnitude of overheat sensitivity (see maps in Figure 4) whereas the southern part of the studied region had the highest values of overheat GDD (see maps in Figure 1). We observe that some areas in a few Midwestern states (e.g., Kansas, Missouri, Nebraska, and Iowa) and Southern states (e.g., Geogia, South Carolina, and Alabama) show the largest yield gains in corn due to adaptation, whereas producers in western Tennessee and northern Mississippi as well as the Northeast region including Pennsylvania and Maryland suffer from a decrease in corn yields due to maladaptation. In the case of soybeans, consistent with our earlier findings, maladaptation to overheat temperatures is practically nonexistent. Significant adaptation occurred in the western part of the Midwest as well as in Mississippi and Arkansas.

4.3 Explaining Spatial Variation in Adaptation

In this section we explore factors and mechanisms that may explain cross-location variation in the adaptation to overheat temperatures. We first examine the relationships between adaptation and local overheat temperatures, and then investigate if adaptation is significantly associated with farming policies, technologies, practices, and natural endowments.

In top-row plots in Figure 6, we examine how the change in overheat sensitivity of crop yields, which substantially varies across locations, relates to local intensity of overheating temperatures. For the two crops, we observe that counties experiencing fewer days of excessively high temperatures in period c are the ones that have adapted the most since the earlier period a (relative to locations with much higher mean overheat GDD). Although this finding might at first seem quite counter-intuitive, it is not. Recall that plotted $\beta^*_{(c,a)}(s_i)$ slopes measure a *change* in local overheat sensitivity over time since period a. Then, given a naturally diminishing capacity to adapt to high temperatures and the presumed optimality of farmer adaptation behavior, the decline in overheat sensitivity with the intensity of excessive temperatures is consistent with a narrative in which farmers from locations that experienced more overheat in the earlier period a had already adapted more. Consequently, given rising temperatures, locations that were spared from overheat before had the most adaptation to do. As such, adaptive methods become less effective at mitigating marginal damages when overheat GDD is high and increases. This is consistent with arguments in Butler and Huybers (2013) and Keane and Neal (2020) and is also corroborated by our data. Namely, the two bottom-row graphs in Figure 6 plot local overheat sensitivity in period a and show that crop yields in locations with high overheat GDD already had a significantly smaller sensitivity to begin with, presumably because farmers there had already been taking adaptive measures, an argument that can be traced back to Mendelsohn et al. (1994).

Besides overheat temperatures, other factors may also help explain spatial variation in farmers' adaptation. We focus on four major aspects that may substantially influence farming practices and outcomes in U.S. agriculture: adoption of genetically engineered (GE) crops, cover crops, crop insurance, and land quality. The rationale for considering land quality is obvious; the choice of other three factors is motivated as follows.

Since 1996, GE crops have been being rapidly and widely adopted by farmers in the U.S. GE seeds can have traits that make them resistant to certain insects or tolerant to herbicides, or both (see Chemeris et al., 2022). Studies (e.g., Lee et al., 2022) have found that the adoption of GE crops increases crop yields. However, there is no consensus on whether the GE crop adoption has increased resilience of crops to a changing climate. For example, Goodwin and Piggott (2020) find that the GE corn in the twelve Corn Belt states has increased yield resiliency to climate change, while Lobell et al. (2020) conjecture that the adoption of GE crops is associated with an *increased* relative sensitivity of yields to climatic stresses because GE traits tend to make crops less responsive to pests or weeds.

Planting cover crops after harvesting cash crops to cover the soil is an important means to improve soil fertility and health (Jian et al., 2020). Between 2012 and 2017, a cover crop adoption in the U.S. increased by 50%, from 10.3 million acres to 15.4 million acres (Wallander et al., 2021). On the one hand, cover crops can reduce soil erosion and plant nutrient losses caused by leaching and runoff (Dabney et al., 2001; Reeves, 2018). On the other hand, cover crop transpiration depletes soil water which has a negative effect on production (see Unger and Vigil, 1998; Martinez-Feria et al., 2016). Perhaps, this is why no consensus has been reached regarding the impact of cover crops on cash crop yields (e.g., Cherr et al., 2006; Blanco-Canqui et al., 2015; Decker et al., 2022). Our analysis can shed new light on the relation between cover crop adoption and yield sensitivity to climate.

Evidence on effects of subsidized crop insurance on adaptation is also mixed. Some studies argue that crop insurance contributes to agricultural adaptation as an expansion in acreage and wealth due to crop insurance can increase the demand for more advanced land management, new technologies, and practices (e.g., Aldana et al., 2011), while others find that—likely due to moral hazard—crop insurance discourages farmers from adapting to extreme heat or drought conditions through reduction in on-farm risk management, expansion to lower-quality farmland, changes in input use, and depression of adoption of certain technologies such as drought-tolerant traits (Annan and Schlenker, 2015; Connor and Katchova, 2020; Miao, 2020; Ghosh et al., 2021; Chemeris et al., 2022). At the same time, others find that crop insurance has only a modest impact on U.S. farmers' land and input uses (e.g., Goodwin et al., 2004; Weber et al., 2016), tempering the arguments that crop insurance encourages or discourages adaptation. No study, however, links farmers' long-run adaptation to crop insurance prevalence.[19] We provide first insights on this relation.

Before we proceed with our analysis, a few remarks are in order. First, we do not explicitly incorporate these four factors in our methodology used to estimate local adaptation because we purposefully seek to model a reduced-form relationship between crop yields and the exogenous climate. Instead, they are proxied using the (also exogenous) geographic location of counties. Consequently, the estimated adaptation captures adaptive methods working through all possible channels, including the aforementioned four factors. Even more importantly, our all-inclusive estimates of local adaptation are thus not contaminated by the potential endogeneity of such channels/factors. To this end, we ought to emphasize that our analysis within this section is only associative. Although not causal, these descriptive results are still of interest because they represent the first attempt to link these factors to the long-run U.S. agricultural adaptation that is spatially inhomogeneous. Understanding these associative relationships can help us pin down potential structural links, for which to seek causal identification in future research.

In our analysis, the GE crop adoption rate is measured as the average proportion of crop planted acreage seeded using GE seeds over 2015–2019. Obtained from the USDA Economic Research Service, this variable is at the state level because county-level adoption data are unavailable. The cover crop ratio is measured as the acreage for cover crops divided by the total cropland acreage in a county. Both county-level cover crop acreage and total cropland acreage are obtained from the 2017 U.S. Census of Agriculture. Crop insurance coverage is measured by average liability (in $1,000) per harvested acre in a county over 2015–2019,

[19] By directly regressing crop yields on weather variables and their interactions with crop insurance coverage, Annan and Schlenker (2015) perhaps is the most relevant study that aims to directly associate crop insurance to crops' sensitivity to overheat. Nevertheless, their analysis is based on annual yield and weather data and does not explore spatiotemporal heterogeneity in sensitivity to weather.

with the insurance liability data obtained from the USDA Risk Management Agency. Land quality is measured using the land capability class (LCC), which ranges from 1 to 8, with LCC 1–2 indicating land with little or no limitation on crop production, and LCC 5 or above indicating land unsuitable for crop production (Natural Resources Conservation Service, 2018). We construct the land quality variable by using the ratio of LCC 1–2 land to total non-developed land in a county. The LCC data are obtained from the USDA Natural Resources Conservation Service. Table C.3 and Figure C.1 in Appendix C present a summary of these variables, from which we can see that these variables exhibit a non-trivial spatial variation.

To investigate whether, and to what extent, the variation in these variables can explain spatial differences in adaptation of crop yields, we run linear quantile regressions of our local estimates of adaptation to overheat temperatures (i.e., $\beta^*_{(c,a)}(s_i)$ for $\mathrm{GDD}_{r_0 {}^\circ\mathrm{C}+}$) on local overheat GDD, GE crop adoption rate, cover crop adoption rate, crop insurance coverage, and land quality for each crop. We use the quantile regression because of its robustness to outliers. Standard errors are clustered at the climate division level to allow for spatial correlation across proximate counties.[20] As earlier, regressions are weighted by the average crop harvested acreage in 2015–2019. Table 5 reports quantile coefficients for the first quartile, median, and third quartile of the local adaptation variable.

We find that these variables have heterogeneous associations with agricultural adaptation, depending on the adaptation quartile and crop type. Specifically, as already discussed earlier, a temporal change in overheat sensitivity is negatively, and generally statistically significantly related to overheat GDD. Overall, the prevalence of negative signs on the GE crop adoption ratio across all quartiles and crops indicates a negative relation between it and adaptation. This is consistent with Lobell et al. (2020) who postulate that adoption of GE crops is associated with increased sensitivity of crops to climatic stresses. However, we find little evidence that this association is statistically significant for corn and soybeans. Similar conclusions can be drawn about land quality in that its coefficients are generally negative and statistically insignificant. The results in Table 5 also show that the cover crop adoption ratio is negatively associated with adaptation, with statistically significant coefficients across different quartiles and crops.[21] Finally, we find that the crop insurance coverage is not associated with adaptation in a statistically significant manner, which corroborates findings in Goodwin et al. (2004), Weber et al. (2016) and Burke and Emerick (2016) that crop insurance only has a modest impact on farmer behavior.

To conclude, the data suggest that GE crops, crop insurance, and even land quality, generally, are not predictive of agricultural adaptation, whereas a cross-county variation in cover crop adoption and overheat temperatures does help explain spatial differences in agri-

[20] Note that the generated nature of local adaptation estimates does not complicate inference in these regressions because they are used as outcome variables. Hence, no "generated *regressor*" problem.

[21] Because our analysis is only associative, this should not be interpreted as evidence that cover crops reduce agricultural adaptation (Seifert et al., 2018).

cultural adaptation. Exploring and attempting to causally identify structural links between these processes should be a promising avenue for future research.

4.4 Robustness Analysis

We examine whether our main findings continue to hold when we vary the gap width over which we long-difference. Specifically, we re-estimate our spatiotemporally varying model S_1T_1 using data with different starting periods (i.e., the a periods) centered on 1960, 1970, 1980, and 1990[22] and different gap widths between periods a and c: 20-year, 30-year, 40-year, and 50-year. Given the sample period of our analysis, these starting periods and gap widths result in ten different combinations of periods a and c. Table E.3 in Appendix E reports values of $\beta^*_{(c,a)}(s_i)$ for $\mathrm{GDD}_{r_0{}^\circ\mathrm{C}+}$ estimated under these ten combinations. This parameter measures a change in overheat sensitivity of crop yields between periods a and c, so it is not expected to stay exactly the same as starting periods or gap widths vary. Nevertheless, we find that coefficient estimates in our main results presented in Section 4.2 are, in general, qualitatively comparable to those in Table E.3.

In our main specification, the mean of the estimated $\beta^*_{(c,a)}(s_i)$ for $\mathrm{GDD}_{r_0{}^\circ\mathrm{C}+}$ is 0.4820 and 0.6042 for corn and soybean yields, respectively (see Table 3). In Table E.3, under seven out of ten starting-period and gap-width combinations, the mean estimated value of this coefficient for corn is also positive, ranging from 0.0610 to 0.8525. Three out of ten generate negative but small mean coefficients (i.e., –0.0021, –0.1050, and –0.1166), and one of them is statistically insignificant. These negative values can plausibly be explained by the extreme drought in 2012, because all three combinations use 2008–2012 as the ending period. For soybean yields, the mean estimate of overheat $\beta^*_{(c,a)}(s_i)$ under nine out of ten combinations is positive, ranging from 0.1424 to 0.5634. Mean estimates also increase with the gap between two periods, which is intuitive as a longer temporal gap would allow a larger magnitude of adaptation.

Figure E.2 in Appendix E presents geographical distributions of these temporal changes in overheat sensitivity. For corn yields, we see a consistent (mal)adaptation pattern across all starting-period and gap-width combinations. Generally, we find that the upper Midwest and lower Southeast experienced adaptation (green colors) to overheat GDD, whereas the regions in between tended to experience no adaptation (gray color) or maladaptation (red colors). For soybeans, it is still the upper Midwest that shows overheat adaptation in most cases. For completeness, we also report the corresponding yield gains or losses due to adaptation or maladaptation across all ten combinations; Figure E.3 in Appendix E maps them. As expected, spatial patterns in this figure are similar to those in Figure E.2.

[22]Concretely, these starting periods are 1958–1962, 1968–1972, 1978–1982, and 1988–1992.

5 Projection of Future Crop Yield Changes

In this section, we project expected damages of climate change on U.S. crop yields between the end of our sample period and the mid-21st century. For these projections, we use predicted future weather data from two global climate models—HadGEM2-ES365 and NorESM1-M—under two global warming scenarios: RCP4.5 (mild warming) and RCP8.5 (severe warming). We conduct this projection analysis based on regression results from our flexible S_1T_1 model and compare these projections to those based on two existing alternatives: Yu et al.'s (2021) S_0T_1 and Burke and Emerick's (2016) S_0T_0 specifications. Contrasting projections across models, we can assess practical implications of explicitly allowing for spatiotemporally inhomogeneous historical effects of climate on agricultural production, as opposed to focusing on "average effects," when measuring expected damages of a warming climate in the future.

We use 2015–2019 as the base period (the later period c used in the long-differences estimation for our main results) and 2048–2052 as the future period (labeled d) for the projections. To compute the future climate change, we difference five-year averages of climate variables between these two periods to obtain $\Delta\overline{\mathbf{z}}_{i(d,c)} = \overline{\mathbf{z}}_{id} - \overline{\mathbf{z}}_{ic}$. Lastly, one also needs to take a stance on future adaptation when forecasting yield changes. As discussed at length in the introduction, spatiotemporally varying coefficients in our flexible S_1T_1 model are designed to capture the myriad natural and socioeconomic factors (both observed and unobserved) that pertain to each county's geographic location—thus, naturally exhibiting spatial continuity—and influence the sensitivity of crop yields to climate variation. The natural factors include local topographic features, natural resources, and climatic patterns, while the socioeconomic factors may include, but not limited to, farming practice, technological opportunities, as well as local institutions and regulations. Albeit at different rates, all these factors evolve over time, determining the adaptation of farming to a changing climate. To account for this in our yield projections while minimizing excessive extrapolation and avoiding many additional assumptions, we consider a straightforward scenario under which the evolvement of these factors continue into the future at the same rates as those in our sample period. We dub this an 'adaptation as usual' scenario, whereby the adaptation between our based period (2015–2019) and the future period (2048–2052) is assumed to occur at the average historical rate observed over 1958–2019. (We also consider an alternative, more conservative 'status quo' scenario; more on this later.)

Namely, we project future yield changes by assuming that the historical adaptation linearly persists into the future. Per our model in eq. (5), the predicted change in log-yield due to climate change between the periods a and c, considering the adaptation of crops to climate *but* netting the influence of climate-neutral technical change (i.e., setting $\alpha^*_{(c,a)}(s_i) = 0$), can be written as

$$\Delta\widehat{\widehat{y}}_{i(c,a)} = \widehat{\boldsymbol{\beta}}_c(s_i)'\overline{\mathbf{z}}_{ic} - \widehat{\boldsymbol{\beta}}_a(s_i)'\overline{\mathbf{z}}_{ia} = \big[\widehat{\boldsymbol{\beta}}_a(s_i) + \widehat{\boldsymbol{\beta}}^*_{(c,a)}(s_i)\big]'\overline{\mathbf{z}}_{ic} - \widehat{\boldsymbol{\beta}}_a(s_i)'\overline{\mathbf{z}}_{ia}.$$

Analogously, with no relocation of crop production, the projected net log-yield difference between the current period c and the future period d in each location s_i is given by

$$\begin{aligned}\Delta\widehat{\widehat{y}}_{i(d,c)} &= \boldsymbol{\beta}_d(s_i)'\overline{\mathbf{z}}_{id} - \widehat{\boldsymbol{\beta}}_c(s_i)'\overline{\mathbf{z}}_{ic} = \big[\widehat{\boldsymbol{\beta}}_c(s_i) + \boldsymbol{\beta}^*_{(d,c)}(s_i)\big]'\overline{\mathbf{z}}_{id} - \widehat{\boldsymbol{\beta}}_c(s_i)'\overline{\mathbf{z}}_{ic} \\ &= \big[\widehat{\boldsymbol{\beta}}_a(s_i) + \widehat{\boldsymbol{\beta}}^*_{(c,a)}(s_i) + \boldsymbol{\beta}^*_{(d,c)}(s_i)\big]'\overline{\mathbf{z}}_{id} - \big[\widehat{\boldsymbol{\beta}}_a(s_i) + \widehat{\boldsymbol{\beta}}^*_{(c,a)}(s_i)\big]'\overline{\mathbf{z}}_{ic},\end{aligned}$$

where note that $\boldsymbol{\beta}^*_{(d,c)}(s_i) \equiv \boldsymbol{\beta}_d(s_i) - \widehat{\boldsymbol{\beta}}_c(s_i)$ is unknown as we do not know the future climate sensitivity of yields, $\boldsymbol{\beta}_d(s_i)$.

Under the assumption that historical adaptation for the log-yield was linear over time and will persists as such in the future until the period d, we can forecast $\boldsymbol{\beta}^*_{(d,c)}(s_i)$ as $\widehat{\boldsymbol{\beta}}^*_{(d,c)}(s_i) = \frac{2050-2017}{2017-1960}\widehat{\boldsymbol{\beta}}^*_{(c,a)}(s_i)$, where the years 1960, 2017, 2050 are the midpoints of the period a (1958-1962), c (2015-2019), and d (2048-2052), respectively. To emphasize, because we focus solely on the impact of climate change, any potential climate-*neutral* technical change is netted out in our calculation by fixing intercept functions over time. This predicted log-yield change is converted to the percentage yield change from the present period c to the future period d using $(\exp\{\Delta\widehat{\widehat{y}}_{i(d,c)}\} - 1) \times 100\%$.

Since the increasing frequency and magnitude of overheat is a key feature of the expected climate change and also a major factor affecting crop yields (Schlenker and Roberts, 2009; Burke and Emerick, 2016), we first examine the impact of future overheat GDD changes on yields. The left panel of Table 6 reports projections based on the S_1T_1 model which flexibly accounts for spatial heterogeneity, while the right panel reports counterpart projections based on its spatially invariant alternative S_0T_1. We find that under the 'adaptation as usual' scenario the impact of rising overheat temperatures in the future, overall, is projected to boost corn yields but still harm soybean yields. This is driven by the magnitude of adaptation which was historically larger for corn than soybeans (see Table 4). In addition to the finding that the effect sizes (regardless of the sign) are generally larger under a more severe warming scenario, we can make a few other notable observations. First, our projections of future yield changes due to global warming are not always statistically different from zero, particularly for soybeans. Second, comparing the results across the two models, we see that the weighted mean projections from the S_1T_1 model are generally more conservative (i.e., 7 to 30 percentage points lower) than those produced by the S_0T_1 specification à la Yu et al. (2021). This suggests that conventional space-invariant approaches, which confine local heterogeneity strictly to intercept-shifting fixed effects under the assumption that any potential slope heterogeneity is orthogonal to climate (see Section 2), may be overestimating adaptation to rising overheat temperatures (see Table 4).

We visualize the results in Table 6 in Figure 7 that maps local projections from our S_1T_1 model for each crop, with statistically insignificant predictions—regardless of their sign or magnitude—colored using the same shade of gray. Unsurprisingly, the figure reveals that the yield impact of future overheat changes is not spatially homogeneous. In the case of corn production, changes in overheat by 2050 are projected to increase yields in the Midwest but decrease in the upper South (Arkansas, Tennessee, and part of Kentucky) and the lower Northeast (e.g., some areas in Pennsylvania and Ohio). Given the significant role of the Midwest in corn production, it is unsurprising that we find statistically significant projections on *average* (see the first column in Table 6). There is also evidence of dichotomous effects on soybean yields, with Indiana, Illinois, and parts of Ohio predicted to experience yield losses, whereas producers in Nebraska are to see their soybean yields increase due to changes in overheat GDD. This spatial bifurcation in future overheat effects on soybean productivity with the offset potential in the net explains why we find statistically insignificant projections on average for soybeans. The geographical pattern in the yield impact seen in Figure 7 is largely consistent with that for historical overheat adaptation seen in first-row maps in Figure 5. That is, areas with the largest projected future yield decreases overlap with areas that historically experienced maladaptation or no adaptation to overheat.

Total projections of future yield changes inclusive of the effects of normal temperatures and precipitation (in addition to overheat) are quite different from projections using only overheat GDD change (see Table E.4 and Figure E.4 in Appendix E). On average, the total climate change impact on both corn and soybean yields is negative, even as we allow for linear adaptation. For corn, although the adaptation to overheat temperatures boosts yields, the maladaptation to normal GDD (see Table 3) reduces them, resulting in a negative—though statistically insignificant—overall impact of climate change. For soybeans, the maladaptation to normal GDD exacerbates the already negative impact of overheat, producing a large negative impact projection on yields.

To draw conclusions about a "representative" county that would correspond to the object of analysis of the conventional spatially invariant methodologies that argue to focus on *average* causal effects of climate, in Table 7 we aggregate local county-specific projections, weighting them using crop acreage in 2017 (the midpoint of the "present" 2015–2019 period). For comparison, we include total projections from our preferred model S_1T_1 as well as the S_0T_1 and S_0T_0 alternatives. Average yield loss projections for corn based on our spatiotemporally varying methodology are smaller than those obtained using these two alternative models.[23] Our model projects total yield losses for corn ranging from –0.68%

[23] Overall, a time-invariant S_0T_0 model tends to predict much larger yield losses than time-varying S_0T_1 and S_1T_1 models. This is because, as first documented by Yu et al. (2021) and corroborated by our findings, time-varying models allow for historical adaptation which feeds into the computation of future projections through estimates of the "present" yield-climate relationship.

to –27.40% and, notably, these losses are largely statistically *in*significant. As discussed, this statistically insignificant result reflect the opposing effects of adaptation to overheat and maladaptation to normal temeperatures. For soybean yields, our S_1T_1 model projects the smallest yield losses among the three specifications under both NorESM1-M scenarios. But under HadGEM2-ES365 scenarios, it projects slightly larger losses than those by S_0T_1, although these projections are still about only a half of what the time-invariant S_0T_0 alternative predicts. As projected by our model, the future soybean yield reduction expected in a typical county ranges between statistically significant 33.17% and 50.04%.

Overall, total projections of future climate change impacts on corn yields from our spatiotemporally varying model are much smaller than those reported in earlier studies. For instance, Yu et al. (2021), employing a S_0T_1-like approach, document that climate change would lead to a 39%–68% yield loss for corn and a 86%–92% yield loss for soybeans by 2050 relative to yields in 2013–2017. Burke and Emerick (2016), using a S_0T_0-like model, report 7% to 64% of corn yield reduction by 2050. Although our projections are not perfectly comparable to these studies due to differences in data and future climate change scenarios used in analyses, most of these differences are likely attributable to our reliance on more granular measurements of local heat sensitivity of crop yields and their adaptation thereto when projecting future losses, instead of using globally "average" coefficients.

Retrospectively, our future yield projection analysis is inherently subject to significant model uncertainty because it requires a stance on future adaptation behavior which is well-known to be difficult to forecast as past technological change has historically been a poor predictor of future technical change. As such, in addition to our baseline 'adaptation as usual' scenario, it is also of interest to examine a more conservative 'status quo' scenario whereby, in addition to no climate-neutral technical change (i.e., $\alpha^*_{(d,c)}(s_i) = 0$), we also impose that no technological adaptation (i.e., $\boldsymbol{\beta}^*_{(d,c)}(s_i) = 0$) is to occur between the end of our sample period and 2048–2052. Effectively, we fix coefficients in the yield-climate relationship at their 2015–2019 values, resulting in a projected future log-yield change due to a warming climate in each location s_i given by $\Delta\widehat{y}_{i(d,c)} = \widehat{\boldsymbol{\beta}}_c(s_i)'\Delta\overline{\mathbf{z}}_{i(d,c)}$, where $\widehat{\boldsymbol{\beta}}_c(s_i) = \widehat{\boldsymbol{\beta}}_a(s_i) + \widehat{\boldsymbol{\beta}}^*_{(c,a)}(s_i)$. The results are reported in Appendix F. Turning the future (mal)adaptation off, we find that the impact of rising overheat temperatures by the mid-century becomes negative for corn yield and more negative for soybean yield, compared to projections under the 'adaptation as usual' scenario. However, the total future climate change impact on crop yields under this 'status quo' scenario is on par with what we project under the 'adaptation as usual' scenario because, recall, the latter also implies "maladaptation as usual." In other words, the potential consequences of maladaptation in the future are substantial enough that they negate the benefits of adaptation, implying that 'adaptation as usual' and 'status quo' scenarios are in effect similar for the purposes of valuating economic costs of future climate change.

6 Concluding Remarks

Although many prior studies have examined whether, or to what extent, adaptation to climate change occurs, most exclusively focus on identification of the *average* adaptation, pooling over farmers located across different geographic locations. Such a global estimand sheds little light on local adaptation experiences of farmers that exhibit substantial heterogeneity. Understanding this (naturally occurring) spatial heterogeneity is important for producing more granular measurements of historical adaptation and, by extension, more accurate projections of expected yield losses associated with a warming climate, particularly in large and climatically diverse countries. In this paper, we extend the literature by providing novel evidence of explicitly spatial heterogeneity in heat sensitivity of U.S. agriculture and its adaptation to climate change. We accomplish this by generalizing a popular long-differences methodology to explicitly incorporate geographic information of crop-producing counties in a flexible semiparametric fashion, which we implement using local kernel averaging. This enables us to control for spatially clustered, local heterogeneity that may be non-neutral, moderating climate effects by shifting all parameters—the intercept *and* slopes—in the relationship between climate and agriculture.

Based on data for the rain-fed region of the United States in 1958–2019, we show significant cross-location heterogeneity in climate sensitivity of crop yields and their adaptation to climate change. For corn and soybeans, 54% and 75% of producing counties, respectively, are estimated to have experienced a statistically significant decrease in overheat sensitivity of yields, thereby adapting to a warming climate. The remaining counties experienced either statistically significant increases (i.e., maladaptation) or no changes in overheat sensitivity (i.e., no adaptation). Geographically, corn and soybean adaptation mainly occurred in the Northern Great Plains and Upper Midwest. On acreage-weighted average, our model estimates that overheat sensitivity of corn and soybean yields decreased by 73% and 49%, respectively.

Importantly, we find that measurements of (mal)adaptation produced by traditional spatially invariant specifications tend to be larger, suggesting the potential to overestimate (mal)adaptation when abstracting away from naturally occurring non-neutral spatial heterogeneity. Relatedly, in most cases, projections of future climate change impacts on crop yields by 2050 based on our spatially flexible model are the smallest compared to popular alternative specifications, and are statistically insignificant for corn. This suggests that existing projections of yield loss due to climate change, and thereby the expected social cost of carbon, are likely overestimated. For example, Rennert et al. (2022) estimate the social cost of carbon to be $185 per ton of CO_2, among which $84 (about 45%) is attributed to an agricultural impact of climate change. Our findings could therefore have important implications for reassessing social costs of carbon.

We also investigate how the newly documented spatially inhomogeneous adaptation to overheat temperatures varies with local climate, GE crop adoption, cover crop adoption, crop insurance, and land quality. We find that adaptation is negatively associated with local overheat temperatures and cover crop adoption rates. But the relation with the GE crop adoption, crop insurance coverage levels, or land quality is insignificant. These results contribute to the debate about factors that may influence agricultural adaptation. For example, unlike previous studies such as Annan and Schlenker (2015), who document a negative impact of crop insurance on yield sensitivity to overheat, and Lee et al. (2021), who report that GE varieties contribute to adaptation of corn, we do not find evidence that either crop insurance or GE crop adoption help explain adaptation of U.S. corn and soybeans.

Our findings, perhaps, have opened more questions about agricultural adaptation to climate change. They attest to complexity of adaptation and illustrate that large-scale adaptation approaches, such as crop insurance and advanced seeds, may not suit all locations because local technologies and endowments differ. This would suggest that the R&D efforts and agricultural policy designs that aim to enhance agricultural adaptation to climate change should be tailored to local contexts more. However, doing so might inhibit technological spillovers and cause productivity disparities across regions as documented by Evenson (1989) and Moscona and Sastry (2022b). Therefore, balancing climate change adaptation and cross-region productivity equity may come to be a policy dilemma.

While the present study deepens our understanding of the geography of climate change adaptation in U.S. agriculture, some limitations present opportunities for future research. First, a growing concern of climate change is the increasing frequency of extreme weather events such as heat waves, heavy precipitation, and multi-year droughts (Chen et al., 2025; NOAA, 2025). Due to the unique design of the long-difference approach (i.e., using average weather data to represent climate), it is not well-suited for reflecting agricultural responses to extreme weather events. A careful examination of spatial and temporal patterns of these extreme events and an investigation of the spatial heterogeneity of U.S. agricultural adaptation to these events following a semiparametric approach similar to that developed in this study could be a fruitful direction for future research.

Moreover, since our analysis is reduced-form, estimated local marginal effects of climate (and adaption inferred therefrom) capture all possible channels through which climate may affect yields. We cannot distinguish specific (mal)adaptation channels, such as crop switching, crop rotation, land-use change, price effects, climate-related agricultural policy, innovation, and agricultural value chains; and we cannot identify drivers of said (mal)adaptation. Nevertheless, by offering an approach to measuring adaptation on a more granular scale while also incorporating a naturally occurring geographic clustering therein, our study makes an early step to improving our understanding of spatial heterogeneity in adaptation. Future research may focus on disentangling individual mechanisms, quantifying their impact on climate change adaptation, and providing further insights into why and how adaptation varies geographically and how adverse climate change impacts on agriculture can be further mitigated.

References

Adenle, A. A., Azadi, H., and Arbiol, J. (2015). Global assessment of technological innovation for climate change adaptation and mitigation in developing world. *Journal of Environmental Management*, 161:261–275.

Aldana, U., Foltz, J. D., Barham, B. L., and Useche, P. (2011). Sequential adoption of package technologies: The dynamics of stacked trait corn adoption. *American Journal of Agricultural Economics*, 93(1):130–143.

Annan, F. and Schlenker, W. (2015). Federal crop insurance and the disincentive to adapt to extreme heat. *American Economic Review*, 105(5):262–66.

Blanc, E. and Schlenker, W. (2017). The use of panel models in assessments of climate impacts on agriculture. *Review of Environmental Economics and Policy*, 11(2):258–279.

Blanco-Canqui, H., Shaver, T. M., Lindquist, J. L., Shapiro, C. A., Elmore, R. W., Francis, C. A., and Hergert, G. W. (2015). Cover crops and ecosystem services: Insights from studies in temperate soils. *Agronomy Journal*, 107(6):2449–2474.

Bogdanski, A. (2012). Integrated food–energy systems for climate-smart agriculture. *Agriculture & Food Security*, 1(1):1–10.

Burke, M. and Emerick, K. (2016). Adaptation to climate change: Evidence from US agriculture. *American Economic Journal: Economic Policy*, 8(3):106–40.

Butler, E. E. and Huybers, P. (2013). Adaptation of US maize to temperature variations. *Nature Climate Change*, 3(1):68–72.

Chamberlain, G. (1982). Multivariate regression models for panel data. *Journal of Econometrics*, 18(1):5–46.

Chemeris, A., Liu, Y., and Ker, A. P. (2022). Insurance subsidies, climate change, and innovation: Implications for crop yield resiliency. *Food Policy*, 108:102232.

Chen, L., Brun, P., Buri, P., Fatichi, S., Gessler, A., Mccarthy, M. J., Pellicciotti, F., Stocker, B., and Karger, D. N. (2025). Global increase in the occurrence and impact of multiyear droughts. *Science*, 387(6731):278–284.

Chen, S., Chen, X., and Xu, J. (2016). Impacts of climate change on agriculture: evidence from China. *Journal of Environmental Economics and Management*, 76:105–124.

Chen, S. and Gong, B. (2021). Response and adaptation of agriculture to climate change: Evidence from China. *Journal of Development Economics*, 148:102557.

Cherr, C., Scholberg, J. S., and McSorley, R. (2006). Green manure approaches to crop production: A synthesis. *Agronomy Journal*, 98(2):302–319.

Connor, L. and Katchova, A. L. (2020). Crop insurance participation rates and asymmetric effects on US corn and soybean yield risk. *Journal of Agricultural and Resource Economics*, 45(1):1–19.

Cui, X. (2020a). Climate change and adaptation in agriculture: Evidence from US cropping patterns. *Journal of Environmental Economics and Management*, 101:1–24.

Cui, X. (2020b). Climate change and adaptation in agriculture: Evidence from us cropping patterns. *Journal of Environmental Economics and Management*, 101:102306.

Cui, X. and Xie, W. (2022). Adapting agriculture to climate change through growing season adjustments: Evidence from corn in China. *American Journal of Agricultural Economics*, 104(1):249–272.

Cui, X. and Zhong, Z. (2024). Climate change, cropland adjustments, and food security: Evidence from china. *Journal of Development Economics*, 167:103245.

Dabney, S. M., Delgado, J. A., and Reeves, D. W. (2001). Using winter cover crops to improve soil and water quality. *Communications in Soil Science and Plant Analysis*, 32(7-8):1221–1250.

Decker, H. L., Gamble, A. V., Balkcom, K. S., Johnson, A. M., and Hull, N. R. (2022). Cover crop monocultures and mixtures affect soil health indicators and crop yield in the southeast united states. *Soil Science Society of America Journal*, 86(5):1312–1326.

Economic Research Service (2022). Cotton sector at a glance. Online document of the U.S. Department of Agriculture, available at: https://www.ers.usda.gov/topics/crops/cotton-wool/cotton-sector-at-a-glance/ (accessed October 8, 2022).

Efron, B. (1982). *The jackknife, the bootstrap and other resampling plans*. The Society for Industrial and Applied Mathematics (SIAM), Philadelphia, PA.

Evenson, R. E. (1989). Spillover benefits of agricultural research: Evidence from U.S. experience. *American Journal of Agricultural Economics*, 71(2):447–452.

Field, C. B., Barros, V., Stocker, T. F., and Dahe, Q. (2012). *Managing the risks of extreme events and disasters to advance climate change adaptation: Special report of the intergovernmental panel on climate change*. Cambridge University Press.

Ghosh, P. N., Miao, R., and Malikov, E. (2021). Crop insurance premium subsidy and irrigation water withdrawals in the western united states. *The Geneva Papers on Risk and Insurance – Issues and Practice*, pages 1–25.

Giller, K. E., Witter, E., Corbeels, M., and Tittonell, P. (2009). Conservation agriculture and smallholder farming in Africa: The heretics' view. *Field Crops Research*, 114(1):23–34.

Goodwin, B. K. and Piggott, N. E. (2020). Has technology increased agricultural yield risk? Evidence from the crop insurance Biotech Endorsement. *American Journal of Agricultural Economics*, 102(5):1578–1597.

Goodwin, B. K., Vandeveer, M. L., and Deal, J. L. (2004). An empirical analysis of acreage effects of participation in the federal crop insurance program. *American Journal of Agricultural Economics*, 86(4):1058–1077.

Gourdji, S. M., Sibley, A. M., and Lobell, D. B. (2013). Global crop exposure to critical high temperatures in the reproductive period: historical trends and future projections. *Environmental Research Letters*, 8(2):024041.

Graham, B. S. and Powell, J. L. (2012). Identification and estimation of average partial effects in "irregular" correlated random coefficient panel data models'. *Econometrica*, 80(5):2105–2152.

Hall, P., Li, Q., and Racine, J. S. (2007). Nonparametric estimation of regression functions in the presence of irrelevant regressors. *The Review of Economics and Statistics*, 89(4):784–789.

Jian, J., Lester, B. J., Du, X., Reiter, M. S., and Stewart, R. D. (2020). A calculator to quantify cover crop effects on soil health and productivity. *Soil and Tillage Research*, 199:104575.

Keane, M. and Neal, T. (2020). Climate change and US agriculture: Accounting for multidimensional slope heterogeneity in panel data. *Quantitative Economics*, 11(4):1391–1429.

Koudahe, K., Allen, S. C., and Djaman, K. (2022). Critical review of the impact of cover crops on soil properties. *International Soil and Water Conservation Research*, 13(3):343–354.

Laage, L. (2024). A correlated random coefficient panel model with time-varying endogeneity. *Journal of Econometrics*, 242. Article 105804.

Lark, T. J., Spawn, S. A., Bougie, M., and Gibbs, H. K. (2020). Cropland expansion in the united states produces marginal yields at high costs to wildlife. *Nature Communications*, 11:4295.

Lee, S., Ji, Y., and Moschini, G. (2022). Agricultural innovation and adaptation to climate change: Insights from us maize. *Journal of the Agricultural and Applied Economics Association*, 1(2):165–179.

Lee, S., Ji, Y., Moschini, G., et al. (2021). Agricultural innovation and adaptation to climate change: Insights from genetically engineered maize. *Working Paper*.

Lobell, D. B., Deines, J. M., and Tommaso, S. D. (2020). Changes in the drought sensitivity of US maize yields. *Nature Food*, 1(11):729–735.

Malikov, E., Miao, R., and Zhang, J. (2020). Distributional and temporal heterogeneity in the climate change effects on US agriculture. *Journal of Environmental Economics and Management*, 104:102386.

Mammen, E. (1993). Bootstrap and wild bootstrap for high dimensional linear models. *The Annals of Statistics*, 21(1):255–285.

Martin, J. H. and Leonard, W. H. (1949). *Principles of field crop production*. Macmillan, New York.

Martinez-Feria, R. A., Dietzel, R., Liebman, M., Helmers, M. J., and Archontoulis, S. V. (2016). Rye cover crop effects on maize: A system-level analysis. *Field Crops Research*, 196:145–159.

Mendelsohn, R., Nordhaus, D., and Shaw, D. (1994). The impact of global warming on agriculture: A ricardian analysis. *American Economic Review*, 84(4):753–771.

Mérel, P. and Gammans, M. (2021). Climate econometrics: Can the panel approach account for long-run adaptation? *American Journal of Agricultural Economics*, 103(4):1207–1238.

Miao, R. (2020). Climate, insurance and innovation: The case of drought and innovations in drought-tolerant traits in US agriculture. *European Review of Agricultural Economics*, 47(5):1826–1860.

Miao, R., Khanna, M., and Huang, H. (2016). Responsiveness of crop yield and acreage to prices and climate. *American Journal of Agricultural Economics*, 98(1):191–211.

Moscona, J. and Sastry, K. (2022a). Does directed innovation mitigate climate damage? Evidence from US agriculture. *Quarterly Journal of Economics*, forthcoming.

Moscona, J. and Sastry, K. A. (2022b). Inappropriate technology: Evidence from global agriculture. Working paper, Harvard University.

Mundlak, Y. (1978). On the pooling of time series and cross section data. *Econometrica*, 46(1):69–85.

Natural Resources Conservation Service (2018). National soil survey handbook. *U.S. Department of Agriculture.*

NOAA (2025). U.S. billion-dollar weather and climate disasters. Technical report, National Oceanic and Atmospheric Administration (NOAA) National Centers for Environmental Information (NCEI). Available at: `https://www.ncei.noaa.gov/access/billions/`. DOI: 10.25921/stkw-7w73.

Pahalvi, H. N., Rafiya, L., Rashid, S., Nisar, B., and Kamili, A. N. (2021). *Chemical Fertilizers and Their Impact on Soil Health*, pages 1–20. Springer International Publishing, Cham.

Rahmstorf, S. and Coumou, D. (2011). Increase of extreme events in a warming world. *Proceedings of the National Academy of Sciences*, 108(44):17905–17909.

Reeves, D. (2018). Cover crops and rotations. *Crops Residue Management*, pages 125–172.

Rennert, K., Errickson, F., Prest, B. C., Rennels, L., Newell, R. G., Pizer, W., Kingdon, C., Wingenroth, J., Cooke, R., Parthum, B., Smith, D., Cromar, K., Diaz, D., Moore, F. C., Müller, U. K., Plevin, R. J., Raftery, A. E., Ševčíková, H., Sheets, H., Stock, J. H., Tan, T., Watson, M., Wong, T. E., and Anthoff, D. (2022). Comprehensive evidence implies a higher social cost of co2. *Nature*, 610(7933):687–692.

Scherr, S. J., Shames, S., and Friedman, R. (2012). From climate-smart agriculture to climate-smart landscapes. *Agriculture & Food Security*, 1(1):1–15.

Schlenker, W. and Roberts, M. J. (2009). Nonlinear temperature effects indicate severe damages to US crop yields under climate change. *Proceedings of the National Academy of Sciences*, 106(37):15594–15598.

Seifert, C. A., Azzari, G., and Lobell, D. B. (2018). Satellite detection of cover crops and their effects on crop yield in the midwestern united states. *Environmental Research Letters*, 13(6):1–9.

Semenov, M. A. and Shewry, P. R. (2011). Modelling predicts that heat stress, not drought, will increase vulnerability of wheat in Europe. *Scientific Reports*, 1(1):1–5.

Trnka, M., Rötter, R. P., Ruiz-Ramos, M., Kersebaum, K. C., Olesen, J. E., Žalud, Z., and Semenov, M. A. (2014). Adverse weather conditions for European wheat production will become more frequent with climate change. *Nature Climate Change*, 4(7):637–643.

Ullah, A. (1985). Specification analysis of econometric models. *Journal of Quantitative Economics*, 1(2):187–209.

Unger, P. W. and Vigil, M. F. (1998). Cover crop effects on soil water relationships. *Journal of Soil and Water Conservation*, 53(3):200–207.

Wagner, G. and Schlenker, W. (2022). Declining crop yields limit bioenergy potential. *Nature*, 609:250–251.

Wallander, S., Smith, D., Bowman, M., and Claassen, R. (2021). Cover crop trends, programs, and practices in the united states. Economic Information Bulletin Number 222, Economic Research Service, the U.S. Department of Agriculture.

Weber, J. G., Key, N., and O'Donoghue, E. (2016). Does federal crop insurance make environmental externalities from agriculture worse? *Journal of the Association of Environmental and Resource Economists*, 3(3):707–742.

Weldewahid, Y., Habtu, S., Taye, G., Teka, K., and Gessesse, T. A. (2023). Effects of long-term irrigation practice on soil quality, organic carbon and total nitrogen stocks in the drylands of ethiopia. *Journal of Arid Environments*, 214:104982.

World Bank (2008). Local institutions and climate change adaptation. *Social Development Notes – The Social Dimensions of Climate Change*, 113.

Yu, C., Miao, R., and Khanna, M. (2021). Maladaptation of US corn and soybeans to a changing climate. *Scientific Reports*, 11(1):1–12.

Table 1. Estimated Models

Model	*Description*	*Spatially Varying?*	*Time Varying?*	*Estimating Equation*
S_1T_1	Our main spatiotemporally varying coefficient model	✓	✓	eq. (5)
S_1T_0	A spatially varying but time-invariant coefficient model	✓	×	eq. (8)
S_0T_1	A time-varying but spatially invariant coefficient model a là Yu et al. (2021)	×	✓	eq. (7)
S_0T_0	A both time-and-location-invariant model a là Burke and Emerick (2016)	×	×	eq. (6)

Note: All models are estimated in long differences.

Table 2. Estimated Local Sensitivity of Crop Yields to Temperature

	Spatially Varying but Time-Invariant Model S_1T_0				*Space- and Time-Invariant* Model S_0T_0
	Mean	1st Qu.	Median	3rd Qu.	Fixed Coefficient Estimate
Corn					
$GDD_{8-r_0{}^\circ C}$	0.8973	0.5469	0.7899	1.1573	0.9756
	(0.8785, 0.911)	(0.5247, 0.5573)	(0.787, 0.7999)	(1.1134, 1.1839)	(0.8774, 1.0611)
$GDD_{r_0{}^\circ C+}$	–3.8424	–5.6650	–3.1826	–1.5844	–4.2546
	(–3.9699, –3.8006)	(–5.9469, –5.4658)	(–3.3438, –2.9957)	(–1.8028, –1.4757)	(–4.7949, –3.7079)
Soybeans					
$GDD_{8-r_0{}^\circ C}$	0.6067	0.4542	0.5758	0.7429	0.6245
	(0.5662, 0.6358)	(0.4182, 0.4953)	(0.5167, 0.6045)	(0.7038, 0.785)	(0.5476, 0.6822)
$GDD_{r_0{}^\circ C+}$	–4.2763	–6.1139	–3.9924	–2.2202	–3.9847
	(–4.7814, –4.0539)	(–6.7654, –5.8597)	(–4.6785, –3.3023)	(–2.5185, –1.7077)	(–4.6936, –3.1745)

Notes: The left panel summarizes point estimates of the responsiveness of crop yields to temperature variation $\boldsymbol{\beta}(s_i) \times 100$ from the spatially varying but time-invariant model S_1T_0. The right panel reports their counterparts $\boldsymbol{\beta} \times 100$ from a spatially and temporally invariant model S_0T_0. All models control for precipitation variables. The two-sided 95% bias-corrected confidence intervals clustered at the climate division level are in parentheses. For corn and soybeans, r_0 equals 29 and 30, respectively. The reported point estimates are semi-elasticities interpretable as percentage changes in the mean crop yield per unit change in climate variables. The expanded version of this table that includes estimated sensitivity to precipitation variables is presented in Table E.1 in Appendix E.

Table 3. Estimated Time-Varying Local Sensitivity of Crop Yields to Temperature

	Spatially and Temporally Varying Model S_1T_1				*Spatially Invariant* Model S_0T_1
	Mean	1st Qu.	Median	3rd Qu.	Fixed Point Estimate
Corn					
$\beta_a(s_i)$ for $\mathrm{GDD}_{8-r_0\,°\mathrm{C}}$	–0.0024	–0.0577	–0.0240	0.0591	0.1105
	(–0.0422, 0.0155)	(–0.1045, –0.0259)	(–0.0574, –0.0103)	(0.0238, 0.0777)	(0.0555, 0.1701)
$\beta_a(s_i)$ for $\mathrm{GDD}_{r_0\,°\mathrm{C}+}$	–0.6076	–1.267	–0.4927	–0.0250	–1.5653
	(–0.6606, –0.4473)	(–1.4114, –0.8868)	(–0.6357, –0.2094)	(–0.1326, 0.2383)	(–1.9274, –1.2595)
$\beta^*_{(c,a)}(s_i)$ for $\mathrm{GDD}_{8-r_0\,°\mathrm{C}}$	–0.0064	–0.0846	0.0050	0.0587	–0.0704
	(–0.0147, 0.0128)	(–0.1010, –0.0680)	(–0.0098, 0.0360)	(0.0451, 0.0870)	(–0.0954, –0.0457)
$\beta^*_{(c,a)}(s_i)$ for $\mathrm{GDD}_{r_0\,°\mathrm{C}+}$	0.4820	0.0399	0.3311	0.8936	1.1666
	(0.3762, 0.5080)	(–0.1682, 0.1097)	(0.1839, 0.3631)	(0.7152, 0.9444)	(0.975, 1.3637)
Soybeans					
$\beta_a(s_i)$ for $\mathrm{GDD}_{8-r_0\,°\mathrm{C}}$	0.0724	0.0214	0.0695	0.1219	0.0808
	(0.0343, 0.1149)	(–0.0164, 0.0771)	(0.0270, 0.1204)	(0.0468, 0.1696)	(0.0228, 0.1354)
$\beta_a(s_i)$ for $\mathrm{GDD}_{r_0\,°\mathrm{C}+}$	–1.1141	–1.5248	–0.9711	–0.7456	–1.3388
	(–1.4228, –0.8325)	(–2.1129, –1.1609)	(–1.2043, –0.6677)	(–1.0054, –0.4841)	(–1.7646, –0.9705)
$\beta^*_{(c,a)}(s_i)$ for $\mathrm{GDD}_{8-r_0\,°\mathrm{C}}$	–0.0384	–0.0620	–0.0348	–0.0129	–0.0555
	(–0.0493, –0.0288)	(–0.0820, –0.0502)	(–0.0414, –0.0216)	(–0.0219, 0.0020)	(–0.0741, –0.0355)
$\beta^*_{(c,a)}(s_i)$ for $\mathrm{GDD}_{r_0\,°\mathrm{C}+}$	0.6042	0.3171	0.5195	0.8801	0.8450
	(0.4530, 0.7902)	(0.1080, 0.4543)	(0.3419, 0.6069)	(0.7191, 1.2066)	(0.5787, 1.0933)

Notes: The left panel summarizes point estimates of the responsiveness of crop yields to temperature variation in the early period $\boldsymbol{\beta}_a(s_i) \times 100$ and its *change* over time $\boldsymbol{\beta}^*_{(c,a)}(s_i) \times 100$ from the spatiotemporally varying model S_1T_1. The right panel reports their counterparts $\boldsymbol{\beta}_a \times 100$ and $\boldsymbol{\beta}^*_{(c,a)} \times 100$ from a spatially-fixed but temporally varying model S_0T_1. All models control for precipitation variables. Two-sided 95% bias-corrected confidence intervals clustered at the climate division level are in parentheses. For corn and soybeans, r_0 equals 29 and 30, respectively. The reported point estimates are semi-elasticities interpretable as percentage changes in the mean crop yield per unit change in climate variables. The expanded version of this table that includes estimated sensitivity to precipitation variables is presented in Table E.2 in Appendix E.

Table 4. Evidence of Local (Mal)Adaptation to Overheat Temperatures

	Spatially and Temporally Varying Model S_1T_1				*Spatially Invariant* Model S_0T_1
	Weighted Mean	1st Qu.	Median	3rd Qu.	Fixed Point Estimate
	Percentage Changes in Local Overheat Sensitivity of Crop Yields				
Corn	73.29	33.39	64.14	88.81	74.53
	(49.25, 79.51)	(–90.4, 48.36)	(49.46, 82.09)	(61.49, 106.05)	(62.11, 89.87)
Soybeans	48.98	39.04	54.58	67.15	63.12
	(35.29, 72.47)	(16.12, 52.83)	(42.12, 70.62)	(54.89, 95.35)	(46.04, 84.10)
	Crop Yield Gains due to Local Adaptation (in %)				
Corn	17.68	2.03	9.71	26.69	36.15
	(14.55, 18.53)	(–4.42, 4.60)	(4.77, 10.90)	(16.92, 31.46)	(29.42, 43.43)
Soybeans	10.49	2.86	9.16	19.43	18.46
	(6.65, 12.49)	(1.15, 4.39)	(5.68, 11.39)	(13.96, 22.29)	(12.3, 24.51)

Notes: The top left panel summarizes point estimates of the percentage change in responsiveness of crop yields to overheat GDD computed based on the spatiotemporally varying model S_1T_1. We calculate it via $\text{sign}\{\beta^*_{(c,a)}(s_i)\} \times \left|\beta^*_{(c,a)}(s_i)/\beta_a(s_i)\right| \times 100\%$. The bottom left panel summarizes point estimates of the percentage changes in crop yield due to adaptation to overheat GDD based on the spatiotemporally varying model S_1T_1. We calculate it via $\left(\exp\{\beta^*_{(c,a)}(s_i) \times \overline{\text{GDD}}_{r^\circ\text{C}+,ic}\} - 1\right) \times 100\%$. The two right panels reports their counterparts from a spatially-fixed but temporally varying model S_0T_1. Weighted mean is calculated using crop acreages in 1960. Two-sided 95% bias-corrected confidence intervals clustered at the climate division level are in parentheses.

Table 5. Explaining Spatial Variation in Agricultural (Mal)Adaptation

	Corn			**Soybeans**		
	1st Qu.	Median	3rd Qu.	1st Qu.	Median	3rd Qu.
Overheat GDD $\times 10^{-3}$	–0.1129***	–0.1271***	–0.1163***	–0.0139	–0.0559*	–0.0839***
GE crop adoption ratio	0.0059	–0.0379	–0.0644	0.0024	–0.1412	–0.0906
Cover crop adoption ratio	–0.0502***	–0.0388***	–0.0204*	–0.0187	–0.0462**	–0.0309**
Liability per acre	0.0131*	0.0054	–0.0012	0.0066	0.0057	–0.0009
Land quality ratio	–0.004*	–0.0025	–0.0003	–0.0065***	–0.002	0.001

Notes: The table reports coefficient estimates from quantile regressions of county-specific adaptation on five local factors. Adaptation here is simply measured as $\boldsymbol{\beta}^*_{(c,a)}(s_i)$, the temporal change in responsiveness of crop yields to overheat temperatures from the spatiotemporally varying model S_1T_1. Regressors include: overheat GDD (divided by 1,000 to scale coefficients) in period 2015–2019; the GE crop adoption rate measured by the proportion of crop planted acreage seeded using GE seeds; cover crop ratio measured by the acreage for cover crop divided by the total cropland area in a county; insurance liability per acre measured by the average liability per harvested acreage (in $1,000); and land quality ratio measured by the ratio of land with land capability class 1 or 2 (with little or no limitation on crop production) to total land in a county. Regressions are weighted by the average crop harvested acreage between 2015–2019. Standard errors are clustered at the climate division level. Significance levels: $^*p < 0.05$; $^{**}p < 0.01$; $^{***}p < 0.001$.

Table 6. Projections of the Impact of Future Rising Overheat Temperature on Crop Yields

	Spatiotemporally Varying Model S_1T_1				*Spatially Invariant* Model S_0T_1
	Weighted Mean	1st Qu.	Median	3rd Qu.	Weighted Mean
			Corn		
Had RCP 4.5	57.23	–10.56	23.87	88.21	73.84
	(20.80, 117.99)	(–34.72, 22.45)	(–8.25, 70.73)	(26.05, 130.51)	(12.12, 155.18)
Had RCP 8.5	70.88	–15.63	26.46	121.79	96.74
	(19.66, 142.11)	(–42.71, 28.70)	(–12.93, 91.82)	(29.65, 178.89)	(9.36, 225.07)
Nor RCP 4.5	23.24	–1.46	17.78	31.12	36.67
	(9.44, 40.73)	(–18.73, 11.56)	(3.79, 33.06)	(17.38, 39.39)	(15.94, 58.01)
Nor RCP 8.5	44.13	–7.6	21.95	63.92	63.87
	(14.42, 97.51)	(–28.48, 19.53)	(–3.91, 60.06)	(26.33, 96.08)	(13.84, 126.41)
			Soybeans		
Had RCP 4.5	–13.55	–36.44	–10.62	20.97	9.71
	(–41.82, 22.67)	(–63.40, –6.58)	(–35.86, 25.37)	(–10.83, 81.86)	(–32.51, 64.84)
Had RCP 8.5	–20.92	–48.02	–16.22	22.73	9.48
	(–54.42, 25.61)	(–76.83, –11.52)	(–45.65, 31.79)	(–17.35, 109.5)	(–43.76, 91.58)
Nor RCP 4.5	2.83	–8.29	0.92	15.44	10.08
	(–8.01, 17.63)	(–19.96, 3.97)	(–10.35, 13.19)	(2.35, 34.19)	(–8.88, 27.43)
Nor RCP 8.5	–6.64	–25.95	–10.39	18.62	9.76
	(–29.71, 24.8)	(–46.78, –2.15)	(–33.22, 15.06)	(–9.61, 67.13)	(–28.09, 53.72)

Notes: The left panel summarizes point estimates of the projected change (in %) in crop yields due to changes in overheat GDD (i.e., $\text{GDD}_{r_0{}^\circ\text{C}+}$) based on the spatiotemporally varying model S_1T_1, using the predicted future weather data from two global climate models, HadGEM2-ES365 and NorESM1-M, under two warming scenarios: RCP4.5 (mild warming) and RCP8.5 (severe warming). The right panel reports the counterpart estimates based on the spatially invariant but time-varying model S_0T_1. The 'adaptation as usual' projections of the change in yields from the present period c (2015–2019) to the future period d (2048–2052) are computed as $\left(\exp\{\Delta\widehat{\overline{y}}_{i(d,c)}|_{\text{GDD}_{r_0{}^\circ\text{C}+}}\} - 1\right) \times 100\%$, where $\Delta\widehat{\overline{y}}_{i(d,c)}|_{\text{GDD}_{r_0{}^\circ\text{C}+}} = [\widehat{\beta}_a(s_i) + \widehat{\beta}^*_{(c,a)}(s_i) + \beta^*_{(d,c)}(s_i)]'\overline{\text{GDD}_{r_0{}^\circ\text{C}+}}_{id} - [\widehat{\beta}_a(s_i) + \widehat{\beta}^*_{(c,a)}(s_i)]'\overline{\text{GDD}_{r_0{}^\circ\text{C}+}}_{ic}$ and $\widehat{\beta}^*_{(d,c)}(s_i) = \frac{2050-2017}{2017-1960}\widehat{\beta}^*_{(c,a)}(s_i)$. Weighted mean is calculated using crop acreages in 2017. Two-sided 95% bias-corrected confidence intervals clustered at the climate division level are in parentheses.

Table 7. Total Projections of the Future Climate Change Impact on Crop Yields

	Model	**Corn**	**Soybeans**
Had RCP 4.5	S_1T_1 (preferred model)	–7.44	–45.28
		(–23.75, 22.60)	(–61.16, –29.26)
	S_0T_1 (à la Yu et al. (2021))	–23.48	–44.62
		(–46.05, 7.53)	(–58.44, –23.26)
	S_0T_0 (à la Burke and Emerick (2016))	–88.29	–88.67
		(–94.35, –74.52)	(–95.06, –73.08)
Had RCP 8.5	S_1T_1 (preferred model)	–0.68	–50.04
		(–22.96, 35.88)	(–68.58, –27.69)
	S_0T_1 (à la Yu et al. (2021))	–13.46	–45.04
		(–43.64, 32.25)	(–65.38, –14.15)
	S_0T_0 (à la Burke and Emerick (2016))	–95.13	–96.17
		(–98.13, –85.99)	(–98.82, –86.88)
Nor RCP 4.5	S_1T_1 (preferred model)	–27.40	–33.17
		(–32.77, –14.56)	(–37.48, –24.20)
	S_0T_1 (à la Yu et al. (2021))	–41.04	–44.47
		(–52.17, –26.51)	(–53.12, –38.08)
	S_0T_0 (à la Burke and Emerick (2016))	–28.29	–37.62
		(–44.97, –5.62)	(–53.67, –17.51)
Nor RCP 8.5	S_1T_1 (preferred model)	–16.99	–37.55
		(–28.68, 8.13)	(–48.91, –21.30)
	S_0T_1 (à la Yu et al. (2021))	–29.58	–45.02
		(–47.01, –5.48)	(–57.16, –29.04)
	S_0T_0 (à la Burke and Emerick (2016))	–68.30	–76.33
		(–83.12, –38.20)	(–88.68, –50.07)

Notes: The table reports weighted averages (in %) of the projected change in crop yields due to climate change based on models S_1T_1, S_0T_1 and S_0T_0. We use predicted future weather data from two global climate models, HadGEM2-ES365 and NorESM1-M, under two warming scenarios: RCP4.5 (mild warming) and RCP8.5 (severe warming). The 'adaptation as usual' projections of the change from the present period c (2015–2019) to the future period d (2048–2052) are computed as $\left(\exp\{\Delta\widehat{\overline{y}}_{i(d,c)}\} - 1\right) \times 100\%$, where $\Delta\widehat{\overline{y}}_{i(d,c)} = [\widehat{\boldsymbol{\beta}}_a(s_i) + \widehat{\boldsymbol{\beta}}^*_{(c,a)}(s_i) + \boldsymbol{\beta}^*_{(d,c)}(s_i)]'\overline{\mathbf{z}}_{id} - [\widehat{\boldsymbol{\beta}}_a(s_i) + \widehat{\boldsymbol{\beta}}^*_{(c,a)}(s_i)]'\overline{\mathbf{z}}_{ic}$ and $\widehat{\boldsymbol{\beta}}^*_{(d,c)}(s_i) = \frac{2050-2017}{2017-1960}\widehat{\boldsymbol{\beta}}^*_{(c,a)}(s_i)$. Weighted mean is calculated using crop acreages in 2017. Two-sided 95% bias-corrected confidence intervals clustered at the climate division level are in parentheses.

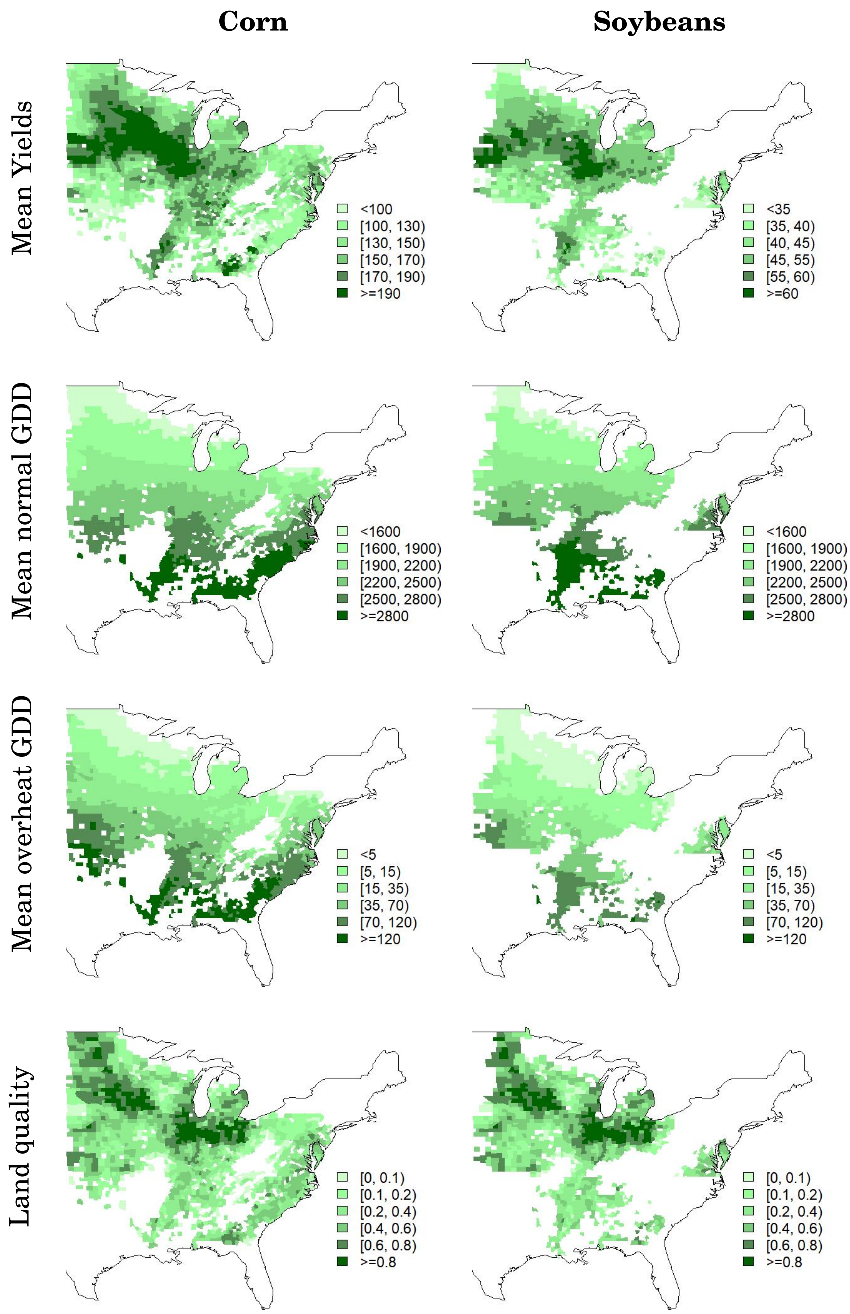

Figure 1. Spatial Distributions of Mean Yields, Mean Normal GDD, Mean Overheat GDD, and Land Quality in 2015–2019

Notes: Crop yields are obtained from the USDA NASS and are measured in bushels per acre for corn and soybeans. The historical weather data are obtained from Schlenker and Roberts (2009). Normal GDD measures the time that crops are exposed to temperature between lower and upper thresholds over the entire growing season which is defined to run from April 1 to September 30. We set the lower boundary of the GDD calculation at 8°C and upper boundary for each crop at their respective critical thresholds: 29°, and 30° for corn and soybeans, respectively. Overheat GDD measures the time that crops are exposed to temperatures in excess of their respective upper thresholds. The land quality is measured by the ratio of LCC 1–2 land (with little or no limitation on crop production) to the total non-developed land in a county. The land capability class (LCC) classification data are obtained from the USDA Natural Resources Conservation Service.

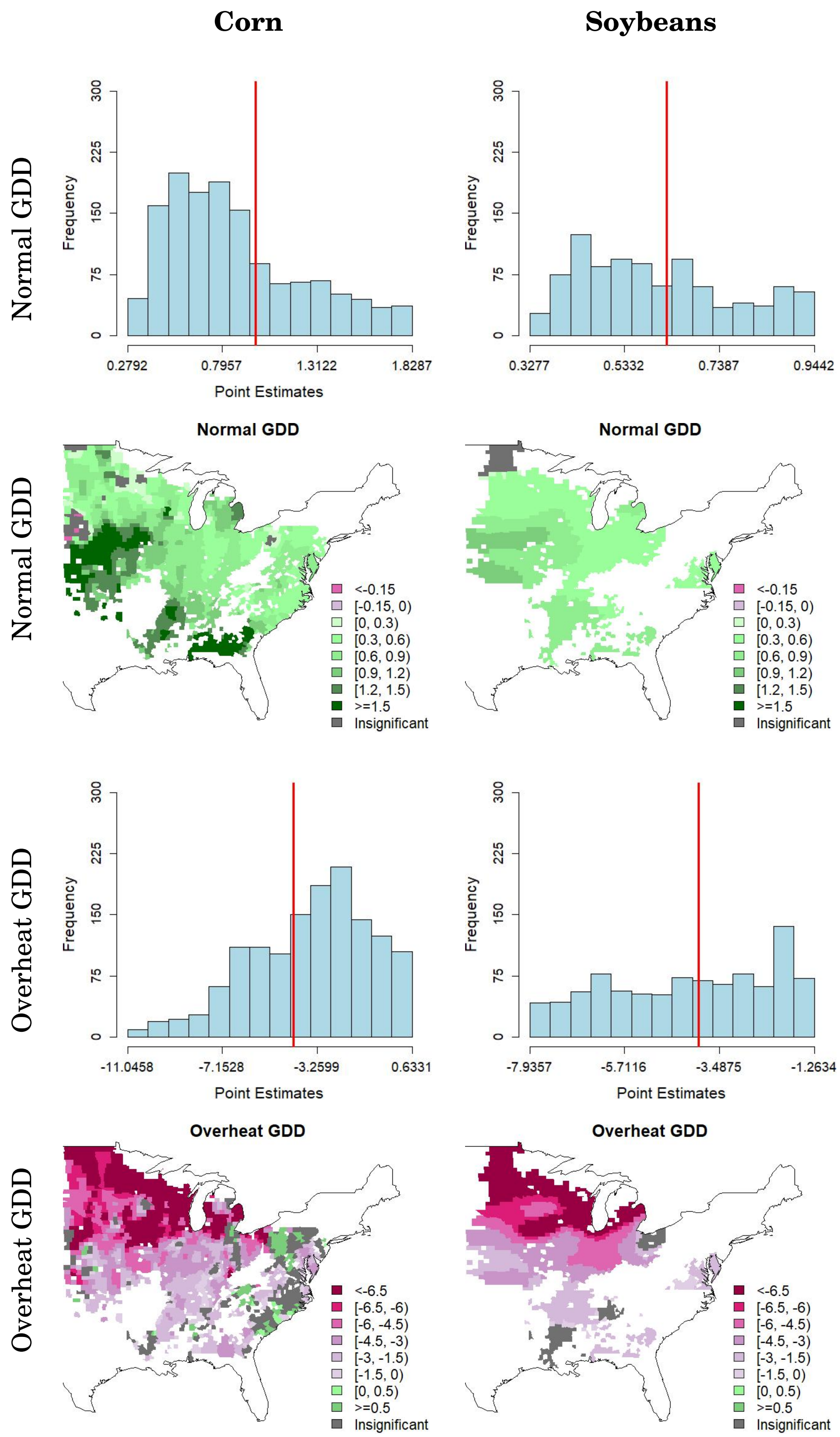

Figure 2. Distributions of Estimated Local Sensitivity of Crop Yields to Temperature

Notes: Histograms summarize point estimates of the responsiveness of crop yields to temperature variation, $\boldsymbol{\beta}(s_i) \times 100$, from the spatially varying but time-invariant model S_1T_0. Maps plot their spatial distribution. The vertical red lines in the histograms show the counterpart estimates $\boldsymbol{\beta} \times 100$ from a fixed-coefficient, spatially and temporally invariant model S_0T_0. All models control for precipitation variables. The plotted point estimates are semi-elasticities interpretable as percentage changes in the mean crop yield per unit change in climate variables.

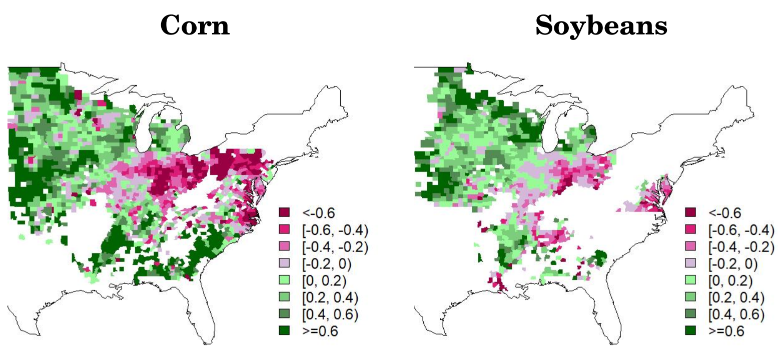

Figure 3. Spatial Distributions of Residuals from a Spatially Invariant Model Net of (Additive) Location Fixed Effects

Note: Maps plot (long-differenced) residuals from the spatially and temporally invariant model $\mathrm{S_0T_0}$ computed as $\Delta\overline{y}_{i(c,a)} - \widehat{\boldsymbol{\beta}}'\Delta\overline{\mathbf{z}}_{i(c,a)}$.

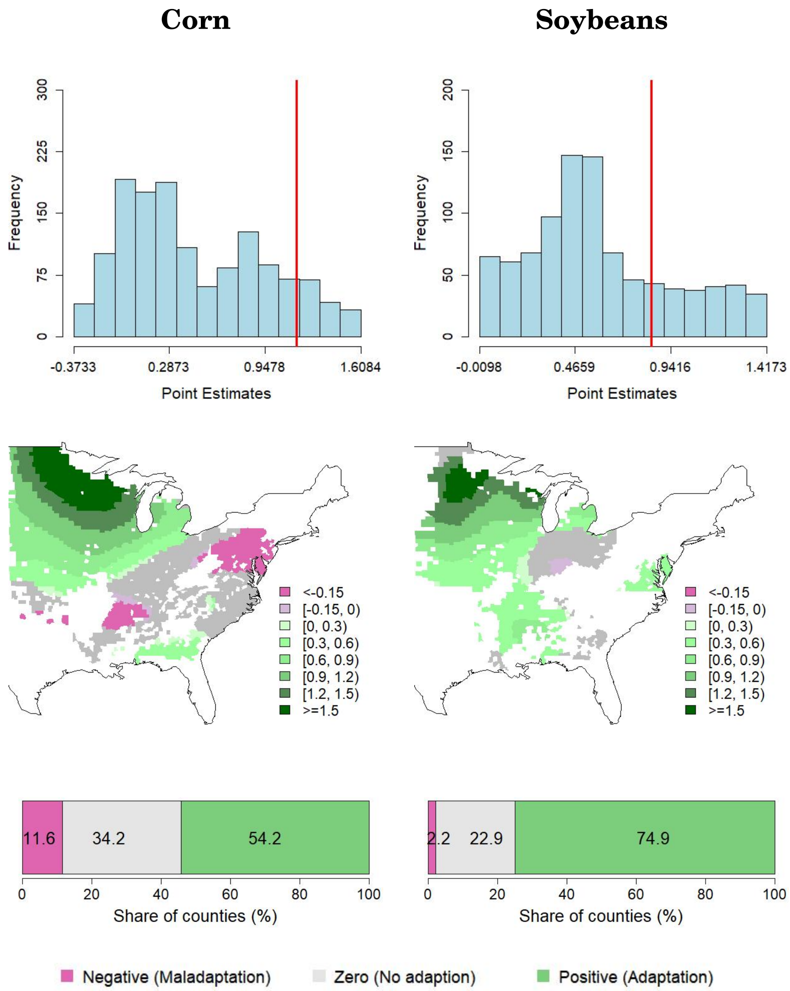

Figure 4. Estimated Temporal Changes in Local Sensitivity of Crop Yields to Overheat Temperatures

Notes: Histograms summarize point estimates of the *change* in responsiveness of crop yields to overheat GDD over time, $\beta^*_{(c,a)}(s_i) \times 100$, from the spatiotemporally varying model $\mathrm{S}_1\mathrm{T}_1$. Maps plot their spatial distribution: regardless of their magnitude or sign, all statistically insignificant estimates are shown using the same shade of gray. Barplot reports the breakdown of counties based on the statistical significance of point estimates of $\beta^*_{(c,a)}(s_i)$. "Negative" if statistically significant but has a negative sign; "zero" if statistically insignificant; and "positive" if the county-specific point estimate is statistically significant at the 5% level and has a positive sign. The vertical red lines in the histograms show the counterpart estimates $\beta^*_{(c,a)} \times 100$ from a spatially-fixed but temporally varying model $\mathrm{S}_0\mathrm{T}_1$. All models control for precipitation variables. The plotted point estimates are semi-elasticities interpretable as percentage changes in the mean crop yield per unit change in climate variables.

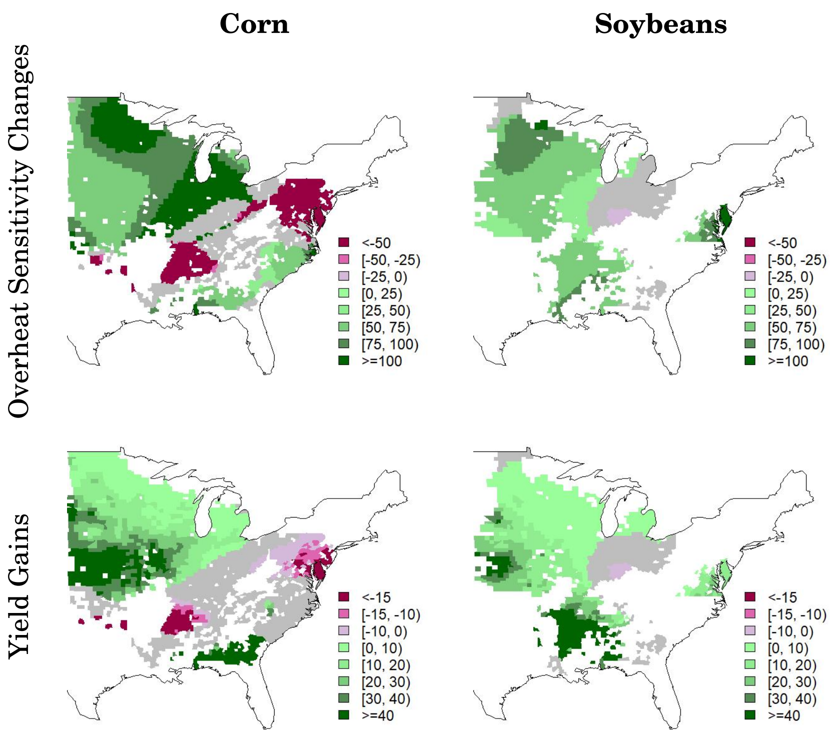

Figure 5. Spatial Distributions of Percentage Changes in Overheat Sensitivity and the Associated Crop Yield Gains due to Local Adaptation or Maladaptation

Notes: Maps in the top row plot point estimates of the percentage change in the sensitivity of crop yields to overheat GDD between periods a and c. The percentage change is calculated via $\text{sign}\{\beta^*_{(c,a)}(s_i)\} \times \left|\beta^*_{(c,a)}(s_i)/\beta_a(s_i)\right| \times 100\%$. Maps in the bottom row plot point estimates of the associated percentage changes in crop yield due to adaptation or maladaptation to overheat GDD. We calculate it via $\left(\exp\{\beta^*_{(c,a)}(s_i)\overline{\text{GDD}}_{r;\,^\circ\text{C}+,ic}\} - 1\right) \times 100\%$. For all maps, calculations are based on estimates from the spatiotemporally varying model S_1T_1. Regardless of their magnitude or sign, all statistically insignificant (at the 5% level) estimates are shown using the same shade of gray. Green colors indicate statistically significant adaptation, red colors indicate statistically significant maladaptation, and gray color indicates no significant adaptation or maladaptation.

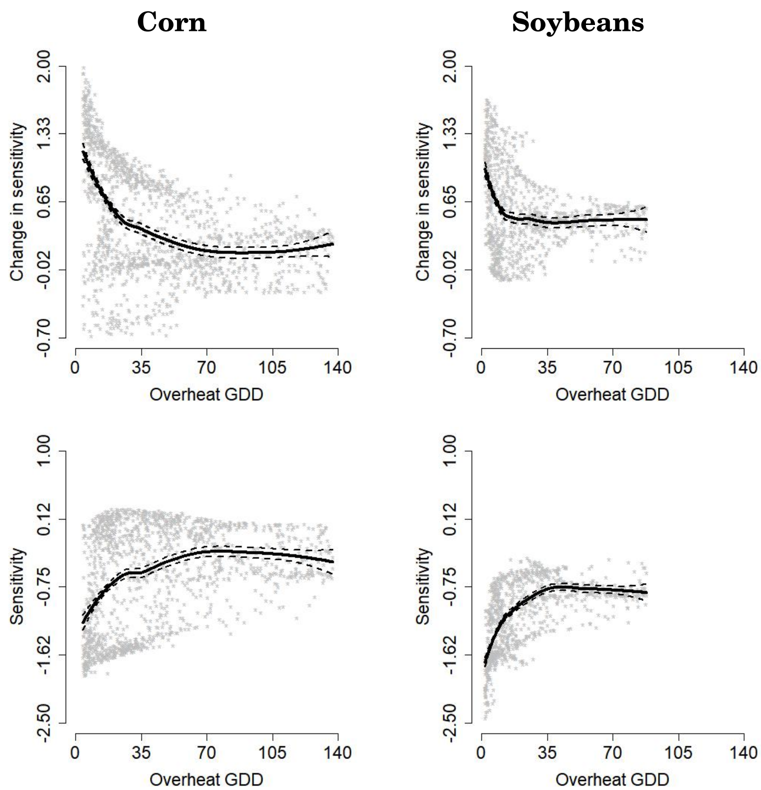

Figure 6. Variation of Local Overheat GDD Adaptation (top row) and Local Overheat GDD Sensitivity (bottom row) across Overheat GDD

Notes: The top-row graphs plot point estimates of the *change* in responsiveness of crop yields to overheat GDD between periods a and c (the $\beta^*_{(c,a)}(s_i) \times 100$ parameter) from the spatiotemporally varying model S_1T_1 against the mean overheat GDD in each county in period c (i.e., 2015–2019). The bottom-row graphs plot point estimates of the responsiveness of crop yields to overheat GDD in period a (the $\beta_a(s_i) \times 100$ parameter) from the spatiotemporally varying model S_1T_1 against the mean overheat GDD in each county in period a (i.e., 1958–1962). Fitted local-linear smoothing mean regressions (solid line) with the corresponding 95% confidence intervals (dashed lines) are superimposed on the scatterplots. To minimize influence of outliers, counties in the bottom or top 5% of the distribution of mean overheat GDD are omitted.

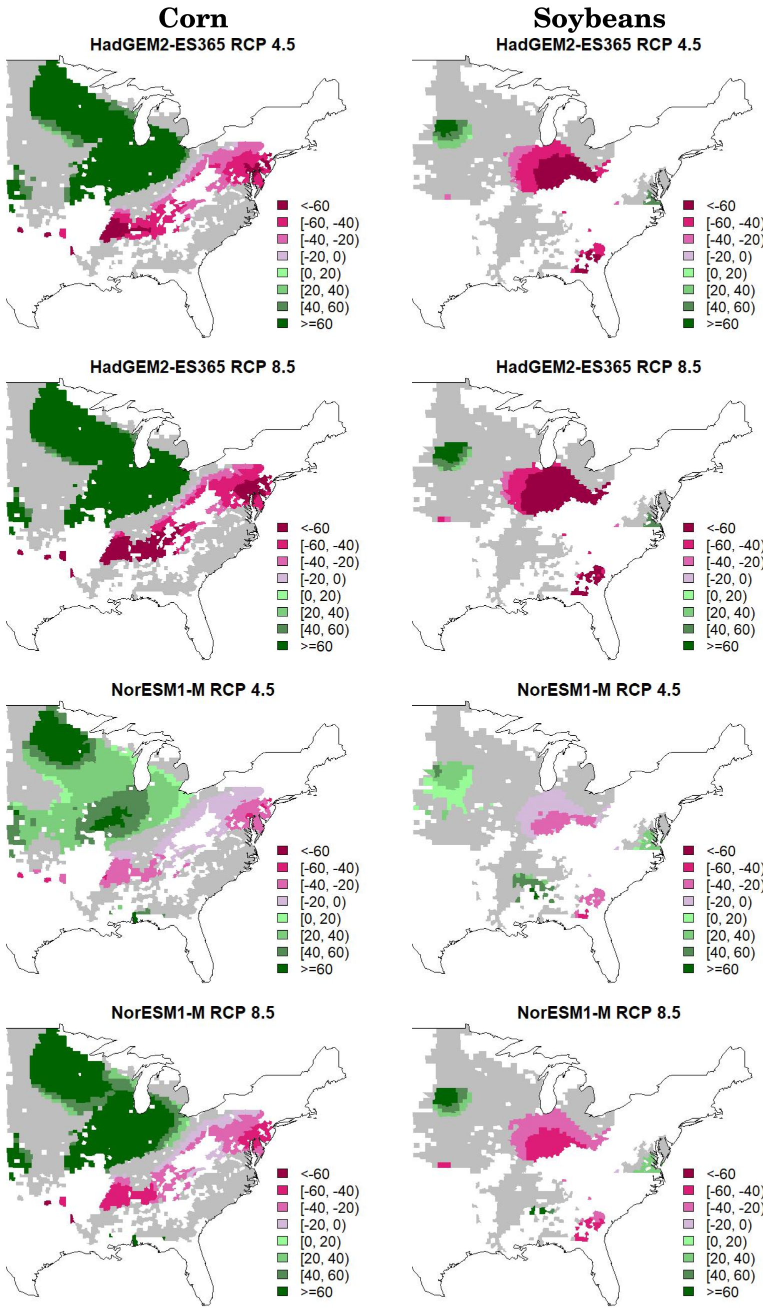

Figure 7. Spatial Distributions of Projections of the Future Rising Overheat Temperature Impact on Crop Yields

Notes: Maps plot point estimates of the projected change (in %) in crop yields due to changes in overheat GDD (i.e., $\text{GDD}_{r_0{}^\circ\text{C+}}$) based on the spatiotemporally varying model S_1T_1, using the predicted future weather data from two global climate models, HadGEM2-ES365 and NorESM1-M, under two warming scenarios: RCP4.5 (mild warming) and RCP8.5 (severe warming). The 'adaptation as usual' projections of the change in yields from the present period c (2015–2019) to the future period d (2048–2052) are computed as $\left(\exp\{\Delta\widehat{\widehat{y}}_{i(d,c)}|_{\text{GDD}_{r_0{}^\circ\text{C+}}}\} - 1\right) \times 100\%$, where $\Delta\widehat{\widehat{y}}_{i(d,c)}|_{\text{GDD}_{r_0{}^\circ\text{C+}}} = [\widehat{\beta}_a(s_i) + \widehat{\beta}^*_{(c,a)}(s_i) + \beta^*_{(d,c)}(s_i)]'\overline{\text{GDD}_{r_0{}^\circ\text{C+}}}_{id} - [\widehat{\beta}_a(s_i) + \widehat{\beta}^*_{(c,a)}(s_i)]'\overline{\text{GDD}_{r_0{}^\circ\text{C+}}}_{ic}$ and $\widehat{\beta}^*_{(d,c)}(s_i) = \frac{2050-2017}{2017-1960}\widehat{\beta}^*_{(c,a)}(s_i)$. Regardless of their magnitude or sign, all statistically insignificant projections (at the 5% level) are shown using the same shade of gray.

Appendix

A Spatially Varying Extension of the Fixed-Effects Estimator

Consider a spatially varying generalization of the standard fixed-effects specification of the relationship between crop yields and weather in (1):

$$y_{it} = \alpha(s_i) + \boldsymbol{\beta}(s_i)\mathbf{z}_{it} + \mu_i + \epsilon_{it}, \tag{A.1}$$

which, following Schlenker and Roberts (2009), maintains that all parameters are time-invariant. Just like in the case of the traditional fixed-effects estimator, we can estimate (A.1) in a within-transformed form to remove μ_i. Namely, averaging the regression over time and subtracting the result from (A.1), we obtain

$$\widetilde{y}_{it} = \boldsymbol{\beta}(s_i)\widetilde{\mathbf{z}}_{it} + \widetilde{\epsilon}_{it}, \tag{A.2}$$

where $\widetilde{y}_{it} \equiv y_{it} - \overline{y}_i$ is a demeaned outcome, with $\overline{y}_i$ being the county-specific time average of y_{it}, and all other "tilde" variables are defined analogously.

To estimate the unknown nonparametric location-specific coefficients $\boldsymbol{\beta}(\cdot)$, assume that these slopes are smooth and twice continuously differentiable in the neighborhood of s and approximate them in the vicinity of location s using a local constant via $\boldsymbol{\beta}(s_i) \approx \boldsymbol{\beta}(s)$. Hence, for locations $\{s_i\}$ close to s, the spatially-varying within-transformed regression is given by $\widetilde{y}_{it} \approx \boldsymbol{\beta}(s)\widetilde{\mathbf{z}}_{it} + \widetilde{\epsilon}_{it}$ which can be consistently estimated using kernel-weighted least squares.

B Inference

To approximate the sampling distribution of the parameter estimator $\widehat{\boldsymbol{\Theta}}(s_i)$ and secondary functions thereof, we use a wild residual bootstrap. To account for the fact that spatially proximate counties share some common climate characteristics, we adapt the *block* bootstrap algorithm to accommodate the potential spatial cluster dependence in residuals across counties. More concretely, we allow for spatial clustering across counties that belong to the same climatic region by following Malikov et al. (2020) in using climate divisions defined by the U.S. National Oceanic and Atmospheric Administration as "blocks" when bootstrapping.[24] Defining G spatial blocks $\{\mathbb{G}_1,\ldots,\mathbb{G}_G\}$ with each $\mathbb{G}_g$ denoting a set of counties located in a given U.S. climate division, the wild cluster bootstrap algorithm is then given by the following.

1. Estimate the spatiotemporally varying coefficient model via (10) using the original data. Denote the obtained estimates for each location s_i as $\widehat{\boldsymbol{\Theta}}^0(s_i) = [\widehat{\alpha}^*_{(c,a)}(s_i), \widehat{\boldsymbol{\beta}}_a(s_i)', \widehat{\boldsymbol{\beta}}^*_{(c,a)}(s_i)']'$. Let the corresponding residuals be $\widehat{\Delta\epsilon}_{i(c,a)}$ for all $i = 1,\ldots,n$.
2. For a bootstrap replication b, generate a common bootstrap weight ω_g^b for each spatial cluster

[24] Clustering at the level of US states yield quantitatively and qualitatively similar results (see Table E.5).

$g = 1,\ldots,G$ from the Mammen (1993) two-point mass distribution:

$$\omega_g^b = \begin{cases} \frac{1+\sqrt{5}}{2} & \text{with prob. } \frac{\sqrt{5}-1}{2\sqrt{5}} \\ \frac{1-\sqrt{5}}{2} & \text{with prob. } \frac{\sqrt{5}+1}{2\sqrt{5}}. \end{cases} \tag{B.3}$$

Next, for each county observation $i = 1,\ldots,n$, generate a new bootstrap disturbance as follows: $\Delta\bar{\epsilon}^b_{i(c,a)} = \left(\sum_{g=1}^{G} \omega_g^b \mathbb{1}\{i \in \mathbb{G}_g\}\right) \times \widehat{\Delta\bar{\epsilon}}_{i(c,a)}$.

3. Generate a new bootstrap outcome variable via $\Delta\bar{y}^b_{i(c,a)} = \widehat{\mathbf{\Theta}}^0(s_i)'\mathbf{x}_{i(c,a)} + \Delta\bar{\epsilon}^b_{i(c,a)}$ for all $i = 1,\ldots,n$.
4. Reestimate the model via (10) but using $\{\Delta\bar{y}^b_{i(c,a)}\}$ in place of $\{\Delta\bar{y}_{i(c,a)}\}$ to obtain the bootstrap coefficient estimates $\widehat{\mathbf{\Theta}}^b(s_i)$ for all s_i.
5. Repeat steps 2 through 4 $\mathscr{B} = 999$ times.

After obtaining the empirical distribution of $\mathscr{B}$ bootstrap parameter replicas plus the original estimate for each location s_i, i.e., $\left\{\widehat{\mathbf{\Theta}}^0(s_i), \widehat{\mathbf{\Theta}}^1(s_i), \ldots, \widehat{\mathbf{\Theta}}^{\mathscr{B}}(s_i)\right\}$, we perform inference on $\mathbf{\Theta}(s_i)$ using bias-corrected percentile confidence intervals. For two-tailed hypotheses, the interval is defined by the $[A_1 \times 100]^{\text{th}}$ and $[A_2 \times 100]^{\text{th}}$th percentiles of the bootstrap distribution, with $A_1 = \Phi\left(2\widehat{z}_0 + \Phi^{-1}(A/2)\right)$ and $A_2 = \Phi\left(2\widehat{z}_0 + \Phi^{-1}(1 - A/2)\right)$, where A is the confidence level, $\Phi(\cdot)$ is the standard normal cdf along with its quantile function $\Phi^{-1}(\cdot)$, and the parameter $\widehat{z}_0 = \Phi^{-1}\left(\sum_{b=0}^{\mathscr{B}} \mathbb{1}\left\{\widehat{\mathbf{\Theta}}^b(s_i) < \widehat{\mathbf{\Theta}}(s_i)\right\}/(\mathscr{B}+1)\right)$ is a bias-correction factor measuring median bias. Analogous procedure is applied to functions of $\mathbf{\Theta}(s_i)$ of interest, such as the (mal)adaptation index and yield change projections.

C Data Summary Statistics

Construction of precipitation variables. For a crop, precipitation below the threshold is calculated as $\max\{p_0 - p, 0\}$, where p_0 is the threshold and p is the actual precipitation. It is meant to measure the severity of water deficiency, with larger magnitudes indicating severer deficiencies. On the other hand, precipitation above the threshold is given by $\max\{p - p_0, 0\}$, measuring water abundance above the threshold. For corn and soybeans, we set the precipitation threshold p_0 at 42 cm, following Burke and Emerick (2016). For cotton, we set the threshold at 58.8 cm, aiming to retain the same ratio of precipitation threshold to upper bound of water demand as that of corn. Specifically, Martin and Leonard (1949) document that corn (respectively, cotton) requires 50.8–76.2 cm (respectively, 70-106.7 cm) of water per growing season. We obtain 58.8 cm by using $106.7 \times 42/76.2$. We respectively denote the precipitation below and above the threshold as $\text{Prec}_{p<p_0}$ and $\text{Prec}_{p>p_0}$.

Table C.1. Summary Statistics of Historical Variables (1958–2019)

Variable	Mean	1st Qu.	Median	3rd Qu.	Sd
			Corn		
Yield	90.42	58.00	86.00	118.00	42.02
$\text{GDD}_{8-r_0\,°\text{C}}$	2229.40	1879.98	2223.80	2571.27	452.32
$\text{GDD}_{r_0\,°\text{C}+}$	58.43	16.08	41.20	85.55	55.64
$\text{Prec}_{p<p_0}$	0.42	0.00	0.00	0.00	1.98
$\text{Prec}_{p>p_0}$	21.06	9.80	19.49	30.04	14.90
Longitude	–87.79	–93.31	–87.68	–83.00	6.67
Latitude	38.32	35.29	38.54	41.33	4.27
			Soybeans		
Yield	30.81	22.50	29.00	38.00	11.00
$\text{GDD}_{8-r_0\,°\text{C}}$	2264.80	1919.35	2264.64	2605.82	438.79
$\text{GDD}_{r_0\,°\text{C}+}$	38.62	9.63	26.59	57.62	37.33
$\text{Prec}_{p<p_0}$	0.38	0.00	0.00	0.00	1.83
$\text{Prec}_{p>p_0}$	21.31	9.90	19.63	30.32	15.12
Longitude	–88.59	–93.71	–88.90	–84.22	6.25
Latitude	38.51	35.44	38.78	41.36	4.13

Notes: The crop yield data are measured in bushels per acre for corn and soybeans. Precipitation variables are measured in cm. The yield data are obtained from United States Department of Agriculture (USDA)'s National Agricultural Statistics Service (NASS). The historical weather data are obtained from Schlenker and Roberts (2009). Location information including longitude and latitude (in decimal degree) of the centroid of a county are obtained from United States Census Bureau. For corn and soybeans, r_0 equals 29 and 30, respectively, and p_0 equals 42 and 42, respectively.

Table C.2. Summary Statistics of Future Climate Variables (2048–2052)

Variable	Mean	1st Qu.	Median	3rd Qu.	Sd	Mean	1st Qu.	Median	3rd Qu.	Sd
					Corn					
	HadGEM2-ES365 RCP 4.5					**NorESM1-M RCP 4.5**				
$GDD_{8-r_0 °C}$	2623.56	2341.20	2613.86	2912.26	381.06	2417.05	2126.27	2396.51	2697.75	381.79
$GDD_{r_0 °C+}$	212.74	129.27	192.83	280.04	109.90	106.53	51.89	88.03	145.49	70.45
$Prec_{p<p_0}$	1.25	0.00	0.00	0.00	4.01	0.24	0.00	0.00	0.00	1.32
$Prec_{p>p_0}$	15.47	3.47	12.99	25.45	13.92	21.29	11.95	20.88	29.49	12.28
	HadGEM2-ES365 RCP 8.5					**NorESM1-M RCP 8.5**				
$GDD_{8-r_0 °C}$	2716.35	2473.35	2744.91	2977.45	361.73	2602.72	2330.06	2595.92	2873.98	368.25
$GDD_{r_0 °C+}$	270.98	161.91	248.20	363.64	138.64	174.41	94.25	149.01	231.08	107.20
$Prec_{p<p_0}$	0.97	0.00	0.00	0.00	3.19	0.48	0.00	0.00	0.00	2.25
$Prec_{p>p_0}$	15.07	4.52	13.38	22.64	12.74	21.97	10.88	19.90	30.12	15.70
					Soybean					
	HadGEM2-ES365 RCP 4.5					**NorESM1-M RCP 4.5**				
$GDD_{8-r_0 °C}$	2649.63	2365.64	2601.80	2925.46	389.24	2420.45	2133.16	2372.16	2680.00	381.22
$GDD_{r_0 °C+}$	168.82	96.49	144.06	227.44	95.76	74.25	32.91	57.46	101.31	54.18
$Prec_{p<p_0}$	1.33	0.00	0.00	0.00	3.93	0.17	0.00	0.00	0.00	0.97
$Prec_{p>p_0}$	14.18	2.80	11.44	23.36	12.99	20.18	11.24	19.70	27.80	11.60
	HadGEM2-ES365 RCP 8.5					**NorESM1-M RCP 8.5**				
$GDD_{8-r_0 °C}$	2756.30	2517.20	2757.96	2981.83	367.04	2633.50	2357.28	2600.35	2890.93	368.31
$GDD_{r_0 °C+}$	222.19	126.61	195.34	292.05	124.38	137.67	69.64	113.34	185.52	89.56
$Prec_{p<p_0}$	1.03	0.00	0.00	0.00	3.17	0.36	0.00	0.00	0.00	1.65
$Prec_{p>p_0}$	14.75	3.86	13.09	21.47	13.04	18.99	9.53	17.46	25.71	13.73

Notes: Predicted future weather data are obtained from two global climate models (HadGEM2-ES365 and NorESM1-M) under two warming scenarios (RCP4.5 and RCP8.5). For corn and soybeans, r_0 equals 29 and 30, respectively, and p_0 equals 42 and 42 cm, respectively.

Table C.3. Summary Statistics of Local Contextual Variables

Variable	Mean	1st Qu.	Median	3rd Qu.	Sd
			Corn		
GE adoption ratio	0.905	0.904	0.904	0.904	0.017
Cover crop ratio	0.668	0.095	0.233	0.681	1.352
Liability per acre	0.418	0.318	0.425	0.511	0.134
Land quality	0.402	0.217	0.376	0.563	0.233
			Soybeans		
GE adoption ratio	0.940	0.940	0.940	0.940	0.006
Cover crop ratio	0.322	0.060	0.120	0.243	0.926
Liability per acre	0.289	0.225	0.286	0.362	0.086
Land quality	0.458	0.269	0.427	0.645	0.233

Notes: The GE crop adoption rate is measured as the proportion of crop planted acreage seeded using GE seeds over 2015-2019. This variable is measured at the state level because the county-level adoption data are unavailable. The cover crop ratio is measured as the acreage for cover crops divided by the total cropland acreage in a county in 2017. Crop insurance coverage is measured by liability (in \$1,000) per harvested acre over 2015-2019 in a county. Land quality is measured based on the land capability class (LCC), which ranges from 1 to 8, with LCC 1–2 indicating land with little or no limitation on crop production, and LCC 5 or above indicating land unsuitable for crop production (Natural Resources Conservation Service, 2018). We construct land quality variable by using the ratio of LCC 1–2 land to the total undeveloped land in a county.

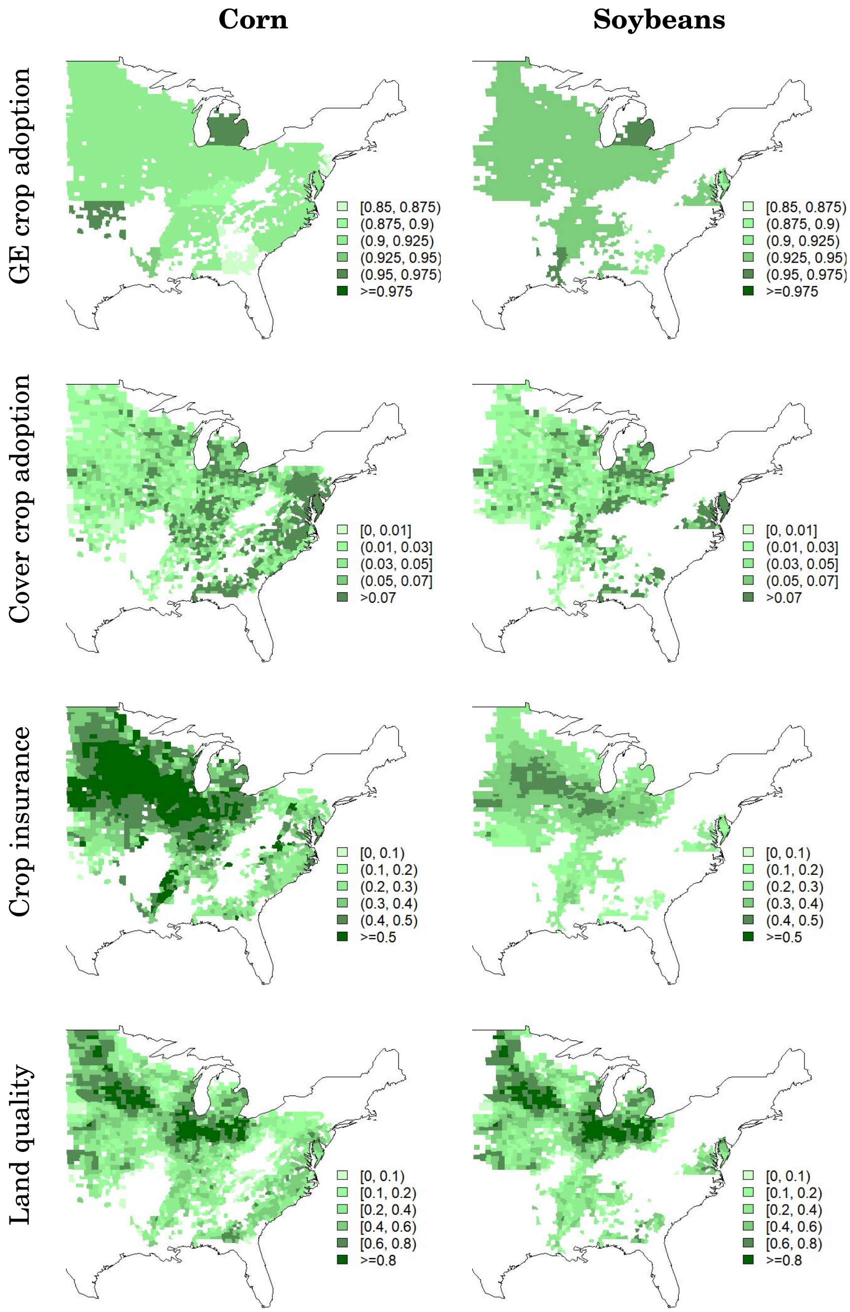

Figure C.1. Spatial Distributions of Local Contextual Variables

Notes: GE crop adoption rate is measured by the proportion of crop planted acreage seeded using GE seeds; cover crop ratio is measured by the acreage for cover crop divided by the total cropland area in a county; insurance liability per acre is measured by the average liability per harvested acreage (in $1,000); and land quality ratio is measured by the ratio of land with land capability class 1 or 2 (with little or no limitation on crop production) to total undeveloped land in a county.

D Test of Spatial Invariance

In this appendix we describe the bootstrap algorithm used to approximate the null distribution of the Ullah (1985) model specification test statistic T_n. We approximate T_n by employing bootstrap procedure as we discussed in Section B, except that we resample residuals from the restricted parametric model. Specifically, the bootstrap algorithm is as follows:

1. Compute both the spatially invariant (under H_0) and spatially varying (under H_1) models using the original data. Denote the estimates from the restricted model as $\left[\widetilde{\alpha}^*_{(c,a)}(s), \widetilde{\boldsymbol{\beta}}_a(s), \widetilde{\boldsymbol{\beta}}^*_{(c,a)}(s)\right]'$ and the estimates from the unrestricted alternative as $\left[\widehat{\alpha}^*_{(c,a)}(s), \widehat{\boldsymbol{\beta}}_a(s), \widehat{\boldsymbol{\beta}}^*_{(c,a)}(s)\right]'$ for all $i = 1,\ldots,n$. Let the residuals under the null be $\{\widetilde{\Delta\overline{\epsilon}_{i(c,a)}}\}$ and those under the alternative be $\{\widehat{\Delta\overline{\epsilon}_{i(c,a)}}\}$. Then compute the test statistic and denote it as T^0_n. Specifically, $T^0_n = \left(\sum_i(\widetilde{\Delta\overline{\epsilon}_{i(c,a)}})^2 - \sum_i(\widehat{\Delta\overline{\epsilon}_{i(c,a)}})^2\right)/\sum_i(\widehat{\Delta\overline{\epsilon}_{i(c,a)}})^2$.
2. For a bootstrap replication b, generate bootstrap weights ω^b_i for all cluster units $g = 1,\ldots,G$ from the Mammen (1993)'s two-point mass distribution:

$$\omega^b_g = \begin{cases} \frac{1+\sqrt{5}}{2} & \text{with prob. } \frac{\sqrt{5}-1}{2\sqrt{5}} \\ \frac{1-\sqrt{5}}{2} & \text{with prob. } \frac{\sqrt{5}+1}{2\sqrt{5}}. \end{cases}$$

   Next, for each observation i with $i = 1,\ldots,n$, jointly generate a new bootstrap disturbance $\{\Delta\overline{\epsilon}_{i(c,a)}\}^b = \left(\sum_{g=1}^G \omega^b_g \mathbb{1}\{i \in \mathbb{G}_g\}\right) \times \{\widetilde{\Delta\overline{\epsilon}_{i(c,a)}}\}$.
3. Generate a new bootstrap outcome variable based on the specification under H_0, that is: $\Delta\overline{y}^b_{i(c,a)} = \widetilde{\alpha}^*_{(c,a)}(s) + \widetilde{\boldsymbol{\beta}}_a(s)\Delta\overline{\mathbf{z}}_{i(c,a)} + \widetilde{\boldsymbol{\beta}}^*_{(c,a)}(s)\overline{\mathbf{z}}_{ic} + \{\Delta\overline{\epsilon}_{i(c,a)}\}^b$ for all $i = 1,\ldots,n$.
4. Recompute the restricted and unrestricted model using $\{\Delta\overline{y}^b_{i(c,a)}\}$ in place of $\{\Delta\overline{y}_{i(c,a)}\}$ for all i, obtain the bootstrap residuals under the null $\widetilde{\Delta\overline{\epsilon}_{i(c,a)}}^b$ and under the alternative $\widehat{\Delta\overline{\epsilon}_{i(c,a)}}^b$.
5. Recompute the bootstrap test statistic $T^b_n = \left(\sum_i(\widetilde{\Delta\overline{\epsilon}_{i(c,a)}}^b)^2 - \sum_i(\widehat{\Delta\overline{\epsilon}_{i(c,a)}}^b)^2\right)/\sum_i(\widehat{\Delta\overline{\epsilon}_{i(c,a)}}^b)^2$.
6. Repeat steps 2 through 5 $\mathscr{B} = 999$ times. Obtain the p-value as $\sum_b \mathbb{1}\{T^b_n \geq T_n\}/(\mathscr{B}+1)$ using the empirical distribution of $\mathscr{B}$ bootstrap replicas plus the original test statistic $\{T^0_n, T^1_n, \ldots, T^{\mathscr{B}}_n\}$. Note that $T_n = T^0_n$.

E Additional Results

Table E.1. An Expanded Set of the Estimated Local Sensitivity of Crop Yields to Climate Variation

	Spatially Varying but Time-Invariant Model S_1T_0				*Space- and Time-Invariant* Model S_0T_0
	Mean	1st Qu.	Median	3rd Qu.	Fixed Coefficient Estimate
			Corn		
$GDD_{8-r_0\,°C}$	0.8973	0.5469	0.7899	1.1573	0.9756
	(0.8785, 0.9110)	(0.5247, 0.5573)	(0.7870, 0.7999)	(1.1134, 1.1839)	(0.8774, 1.0611)
$GDD_{r_0\,°C+}$	–3.8424	–5.6650	–3.1826	–1.5844	–4.2546
	(–3.9699, –3.8006)	(–5.9469, –5.4658)	(–3.3438, –2.9957)	(–1.8028, –1.4757)	(–4.7949, –3.7079)
$Prec_{p<p_0}$	0.4658	–0.0422	0.2480	0.8788	0.0123
	(0.4428, 0.5165)	(–0.0466, –0.0293)	(0.2078, 0.3004)	(0.8345, 0.9580)	(–0.0374, 0.0367)
$Prec_{p>p_0}$	0.0068	–0.0058	0.0069	0.0209	0.0066
	(0.0052, 0.0082)	(–0.0068, –0.0039)	(0.0054, 0.0080)	(0.0186, 0.0224)	(0.0010, 0.0120)
			Soybeans		
$GDD_{8-r_0\,°C}$	0.6067	0.4542	0.5758	0.7429	0.6245
	(0.5662, 0.6358)	(0.4182, 0.4953)	(0.5167, 0.6045)	(0.7038, 0.7850)	(0.5476, 0.6822)
$GDD_{r_0\,°C+}$	–4.2763	–6.1139	–3.9924	–2.2202	–3.9847
	(–4.7814, –4.0539)	(–6.7654, –5.8597)	(–4.6785, –3.3023)	(–2.5185, –1.7077)	(–4.6936, –3.1745)
$Prec_{p<p_0}$	0.1861	–0.1257	0.0280	0.1422	0.1059
	(0.1115, 0.2192)	(–0.165, –0.0978)	(0.0123, 0.0639)	(0.0911, 0.1846)	(0.0134, 0.1534)
$Prec_{p>p_0}$	0.0079	0.0013	0.0087	0.0157	0.0105
	(0.0058, 0.0090)	(–0.0030, 0.0029)	(0.0047, 0.0102)	(0.0119, 0.0180)	(0.0061, 0.0145)

Notes: The left panel summarizes point estimates of the responsiveness of crop yields to temperature variation $\boldsymbol{\beta}(s_i) \times 100$ from the spatially varying but time-invariant model S_1T_0. The right panel reports their counterparts $\boldsymbol{\beta} \times 100$ from a spatially and temporally invariant model S_0T_0. All models control for precipitation variables. The two-sided 95% bias-corrected confidence intervals clustered at the climate division level are in parentheses. For corn and soybeans, r_0 equals 29 and 30, respectively, and p_0 equals 42 and 42 cm, respectively. The reported point estimates are semi-elasticities interpretable as percentage changes in the mean crop yield per unit change in climate variables.

Table E.2. An Expanded Set of the Estimated Time-Varying Local Sensitivity of Crop Yields to Climate Variation

	Spatially and Temporally Varying Model S_1T_1				*Spatially Invariant* Model S_0T_1
	Mean	1st Qu.	Median	3rd Qu.	Fixed Point Estimate
			Corn		
$\alpha^*_{(c,a)}(s_i)$	1.0536	–0.1474	1.0077	2.4203	2.1455
	(0.7483, 1.2036)	(–0.6487, 0.0473)	(0.5321, 1.4617)	(2.187, 2.593)	(1.7332, 2.5427)
$\beta_a(s_i)$ for $\text{GDD}_{8-r_0\,°\text{C}}$	–0.0024	–0.0577	–0.0240	0.0591	0.1105
	(–0.0422, 0.0155)	(–0.1045, –0.0259)	(–0.0574, –0.0103)	(0.0238, 0.0777)	(0.0555, 0.1701)
$\beta_a(s_i)$ for $\text{GDD}_{r_0\,°\text{C}+}$	–0.6076	–1.2670	–0.4927	–0.0250	–1.5653
	(–0.6606, –0.4473)	(–1.4114, –0.8868)	(–0.6357, –0.2094)	(–0.1326, 0.2383)	(–1.9274, –1.2595)
$\beta_a(s_i)$ for $\text{Prec}_{p<p_0}$	0.0259	–0.2703	–0.0420	0.3824	–0.0246
	(–0.0702, 0.0842)	(–0.3550, –0.1427)	(–0.0726, –0.0254)	(0.3116, 0.4886)	(–0.0507, 0.0024)
$\beta_a(s_i)$ for $\text{Prec}_{p>p_0}$	0.0029	–0.0016	0.0015	0.0068	0.0036
	(0.0000, 0.0043)	(–0.0043, 0.0016)	(–0.0012, 0.0035)	(0.0042, 0.0081)	(–0.0000, 0.0084)
$\beta^*_{(c,a)}(s_i)$ for $\text{GDD}_{8-r_0\,°\text{C}}$	–0.0064	–0.0846	0.0050	0.0587	–0.0704
	(–0.0147, 0.0128)	(–0.1010, –0.0680)	(–0.0098, 0.0360)	(0.0451, 0.0870)	(–0.0954, –0.0457)
$\beta^*_{(c,a)}(s_i)$ for $\text{GDD}_{r_0\,°\text{C}+}$	0.4820	0.0399	0.3311	0.8936	1.1666
	(0.3762, 0.5080)	(–0.1682, 0.1097)	(0.1839, 0.3631)	(0.7152, 0.9444)	(0.975, 1.3637)
$\beta^*_{(c,a)}(s_i)$ for $\text{Prec}_{p<p_0}$	0.0840	–0.0519	0.0753	0.2587	0.0463
	(0.0565, 0.1342)	(–0.1148, –0.0197)	(0.0739, 0.0971)	(0.1932, 0.3139)	(0.0132, 0.0764)
$\beta^*_{(c,a)}(s_i)$ for $\text{Prec}_{p>p_0}$	–0.0034	–0.0072	–0.0013	0.0019	–0.0037
	(–0.0049, 0.0000)	(–0.0087, –0.0047)	(–0.0032,0.0019)	(–0.0000, 0.0051)	(–0.0075, 0.0000)
			Soybeans		
$\alpha^*_{(c,a)}(s_i)$	1.4195	0.9402	1.3741	1.8844	1.7621
	(1.2344, 1.5733)	(0.7100, 1.0825)	(1.1179, 1.4978)	(1.6948, 2.1734)	(1.4441, 2.0850)
$\beta_a(s_i)$ for $\text{GDD}_{8-r_0\,°\text{C}}$	0.0724	0.0214	0.0695	0.1219	0.0808
	(0.0343, 0.1149)	(–0.0164, 0.0771)	(0.0270, 0.1204)	(0.0468, 0.1696)	(0.0228, 0.1354)
$\beta_a(s_i)$ for $\text{GDD}_{r_0\,°\text{C}+}$	–1.1141	–1.5248	–0.9711	–0.7456	–1.3388
	(–1.4228, –0.8325)	(–2.1129, –1.1609)	(–1.2043, –0.6677)	(–1.0054, –0.4841)	(–1.7646, –0.9705)
$\beta_a(s_i)$ for $\text{Prec}_{p<p_0}$	–0.0846	–0.1385	–0.1059	–0.0346	–0.0204
	(–0.1212, –0.0162)	(–0.1760, –0.0861)	(–0.1454, –0.0632)	(–0.0688, 0.0221)	(–0.0813, 0.0331)
$\beta_a(s_i)$ for $\text{Prec}_{p>p_0}$	0.0025	0.0000	0.0027	0.0040	0.0026
	(–0.0000, 0.0053)	(–0.0017, 0.0055)	(–0.0000, 0.0065)	(0.0010, 0.0076)	(–0.0011, 0.0060)
$\beta^*_{(c,a)}(s_i)$ for $\text{GDD}_{8-r_0\,°\text{C}}$	–0.0384	–0.0620	–0.0348	–0.0129	–0.0555
	(–0.0493, –0.0288)	(–0.0820, –0.0502)	(–0.0414, –0.0216)	(–0.0219, 0.0020)	(–0.0741, –0.0355)
$\beta^*_{(c,a)}(s_i)$ for $\text{GDD}_{r_0\,°\text{C}+}$	0.6042	0.3171	0.5195	0.8801	0.845
	(0.4530, 0.7902)	(0.1080, 0.4543)	(0.3419, 0.6069)	(0.7191, 1.2066)	(0.5787, 1.0933)
$\beta^*_{(c,a)}(s_i)$ for $\text{Prec}_{p<p_0}$	0.0426	–0.0000	0.0569	0.1034	0.0059
	(–0.0069, 0.0744)	(–0.0312, 0.0206)	(0.0062, 0.0893)	(0.0690, 0.1359)	(–0.0317, 0.0329)
$\beta^*_{(c,a)}(s_i)$ for $\text{Prec}_{p>p_0}$	–0.0024	–0.0038	–0.0025	–0.0012	–0.0028
	(–0.0052, 0.0000)	(–0.0062, –0.0011)	(–0.0058, 0.0000)	(–0.0054, 0.0018)	(–0.0062, 0.0013)

Notes: The left panel summarizes point estimates (all ×100, except intercept term and precipitation) of parameters in the spatiotemporally varying model S_1T_1. The right panel reports their counterparts from a spatially-fixed but temporally varying model S_0T_1. Two-sided 95% bias-corrected confidence intervals clustered at the climate division level are in parentheses. For corn and soybeans, r_0 equals 29 and 30, respectively, and p_0 equals 42 and 42 cm, respectively. The reported point estimates are semi-elasticities interpretable as percentage changes in the mean crop yield per unit change in climate variables.

Table E.3. Robustness of the Estimated Temporal Changes in Local Sensitivity of Crop Yields to Overheat Temperatures

Periods a and c	Mean	1st Qu.	Median	3rd Qu.	Mean	1st Qu.	Median	3rd Qu.
	Corn				**Soybeans**			
1958/1962 – 1978/1982	0.2449	0.0190	0.2118	0.5058	–0.2193	–0.5039	–0.1499	0.1991
	(0.1247, 0.3557)	(–0.1432, 0.0956)	(0.1180, 0.3565)	(0.3651, 0.7553)	(–0.5074, –0.0976)	(–0.7048, –0.3216)	(–0.3084, 0.0083)	(–0.0509, 0.3032)
1958/1962 – 1988/1992	0.3607	0.0915	0.2544	0.5817	0.1843	–0.1166	0.0923	0.4184
	(0.2238, 0.4381)	(–0.0173, 0.2172)	(0.1056, 0.4094)	(0.4023, 0.6515)	(0.0722, 0.3798)	(–0.3282, 0.1021)	(–0.0508, 0.3252)	(0.1997, 0.8156)
1958/1962 – 1998/2002	0.4810	0.1687	0.4423	0.8505	0.3785	0.0935	0.2158	0.6640
	(0.4453, 0.4539)	(0.0142, 0.2250)	(0.3825, 0.4360)	(0.7386, 0.8661)	(0.1165, 0.5871)	(–0.1207, 0.3763)	(–0.0327, 0.3937)	(0.2649, 0.9295)
1958/1962 – 2008/2012	0.8525	0.729	0.8758	1.0175	0.5634	0.3381	0.6564	0.7909
	(0.6872, 0.8523)	(0.5415, 0.7761)	(0.6193, 0.916)	(0.7656, 1.0549)	(0.3260, 0.7047)	(0.0575, 0.4482)	(0.4577, 0.8602)	(0.5196, 1.0106)
1968/1972 – 1988/1992	0.1208	–0.1654	0.0720	0.3539	0.3227	–0.0796	0.2612	0.5659
	(0.0499, 0.1981)	(–0.2678, –0.0610)	(–0.0074, 0.1720)	(0.2838, 0.4682)	(0.1883, 0.3773)	(–0.1474, –0.0797)	(0.1421, 0.3691)	(0.3767, 0.6648)
1968/1972 – 1998/2002	0.1689	–0.2029	0.0649	0.4591	0.3430	–0.0661	0.2627	0.5299
	(0.0688, 0.2753)	(–0.3165, –0.101)	(–0.0412, 0.1418)	(0.3010, 0.5829)	(0.1735, 0.4527)	(–0.1799, –0.0328)	(0.0694, 0.3622)	(0.3522, 0.6074)
1968/1972 – 2008/2012	–0.0021	–0.3929	–0.0860	0.2443	0.3758	0.2006	0.4627	0.6954
	(–0.1634, 0.0704)	(–0.5413, –0.3670)	(–0.1856, –0.0519)	(0.0610, 0.3447)	(0.2400, 0.3888)	(–0.1055, 0.3078)	(0.3754, 0.4805)	(0.5583, 0.7354)
1978/1982 – 1998/2002	0.0610	–0.1156	0.0582	0.2479	0.1424	–0.1158	0.1164	0.3264
	(–0.0373, 0.1081)	(–0.2026, –0.0579)	(–0.0181, 0.1255)	(0.1403, 0.3028)	(0.0625, 0.2336)	(–0.2221, –0.0399)	(0.0292, 0.1858)	(0.2302, 0.4163)
1978/1982 – 2008/2012	–0.1050	–0.3878	–0.1655	0.0953	0.1879	–0.0314	0.1345	0.3822
	(–0.2213, –0.0287)	(–0.5025, –0.2976)	(–0.2542, –0.1243)	(–0.0282, 0.1541)	(0.0897, 0.2616)	(–0.1559, 0.0329)	(0.0126, 0.2121)	(0.2497, 0.4657)
1988/1992 – 2008/2012	–0.1166	–0.4210	–0.1320	0.1693	0.1782	–0.1089	0.1315	0.3722
	(–0.1872, 0.0018)	(–0.5358, –0.3161)	(–0.2534, –0.0574)	(0.0996, 0.2998)	(0.0506, 0.2894)	(–0.2662, –0.0249)	(0.0278, 0.2281)	(0.2899, 0.5062)

Notes: The table summarizes point estimates ×100 of the *change* in responsiveness of crop yields to climate variation $\boldsymbol{\beta}^*_{(c,a)}(s_i)$ from the spatiotemporally varying model S_1T_1 using the data from different gap widths (e.g., 20-year, 30-year, 40-year, 50-year) and different starting periods centered in 1960, 1970, 1980, and 1990. For example, 20-year gap widths with starting periods centered in 1960 stands for the periods between 1958–1962 and 1978–1982. Two-sided 95% bias-corrected confidence intervals are in parentheses. The reported point estimates are semi-elasticities interpretable as percentage changes in the mean crop yield per unit change in climate variables.

Table E.4. Total Projections of the Future Climate Change Impact on Crop Yields

	Spatiotemporally Varying Model S_1T_1				*Spatially Invariant* Model S_0T_1
	Weighted Mean	1st Qu.	Median	3rd Qu.	Weighted Mean
			Corn		
Had RCP 4.5	–7.44 (–23.75, 22.60)	–37.07 (–54.25, –6.27)	30.52 (10.26, 36.91)	130.58 (77.78, 163.00)	–23.48 (–46.05, 7.53)
Had RCP 8.5	–0.68 (–22.96, 35.88)	–34.12 (–54.35, 2.63)	19.27 (–4.54, 28.29)	132.23 (54.28, 211.17)	–13.46 (–43.64, 32.25)
Nor RCP 4.5	–27.40 (–32.77, –14.56)	–47.06 (–52.65, –34.45)	10.68 (–13.69, 24.77)	83.04 (53.72, 121.2)	–41.04 (–52.17, –26.51)
Nor RCP 8.5	–16.99 (–28.68, 8.13)	–39.83 (–54.42, –18.56)	13.11 (–0.48, 16.46)	94.10 (50.09, 124.79)	–29.58 (–47.01, –5.48)
			Soybeans		
Had RCP 4.5	–45.28 (–61.16, –29.26)	–52.46 (–64.47, –33.53)	–45.66 (–58.53, –23.86)	–39.90 (–55.77, –20.66)	–44.62 (–58.44, –23.26)
Had RCP 8.5	–50.04 (–68.58, –27.69)	–59.49 (–74.35, –35.99)	–47.55 (–62.95, –18.3)	–39.27 (–59.68, –9.92)	–45.04 (–65.38, –14.15)
Nor RCP 4.5	–33.17 (–37.48, –24.20)	–47.27 (–53.76, –40.18)	–34.06 (–37.81, –24.9)	–24.56 (–30.20, –15.36)	–44.47 (–53.12, –38.08)
Nor RCP 8.5	–37.55 (–48.91, –21.30)	–46.36 (–56.03, –30.57)	–42.37 (–55.01, –29.73)	–31.19 (–44.39, –14.22)	–45.02 (–57.16, –29.04)

Notes: The left panel summarizes point estimates of the projected change (in %) in crop yields due to climate change based on the spatiotemporally varying model S_1T_1, using predicted future weather data from two global climate models (HadGEM2-ES365 and NorESM1-M) under two warming scenarios (RCP4.5 and RCP8.5). The right panel reports the counterpart estimates based on the spatially invariant but time-varying (S_0T_1) model. The 'adaptation as usual' projections of the change from the present period c (2015–2019) to the future period d (2048–2052) are computed as $\left(\exp\{\Delta\widehat{\overline{y}}_{i(d,c)}\} - 1\right) \times 100\%$, where $\Delta\widehat{\overline{y}}_{i(d,c)} = [\widehat{\boldsymbol{\beta}}_a(s_i) + \widehat{\boldsymbol{\beta}}^*_{(c,a)}(s_i) + \boldsymbol{\beta}^*_{(d,c)}(s_i)]'\overline{\mathbf{z}}_{id} - [\widehat{\boldsymbol{\beta}}_a(s_i) + \widehat{\boldsymbol{\beta}}^*_{(c,a)}(s_i)]'\overline{\mathbf{z}}_{ic}$ and $\widehat{\boldsymbol{\beta}}^*_{(d,c)}(s_i) = \frac{2050-2017}{2017-1960}\widehat{\boldsymbol{\beta}}^*_{(c,a)}(s_i)$. Weighted mean is calculated using crop acreages in 2017. Two-sided 95% bias-corrected confidence intervals are in parentheses.

Table E.5. Estimated Time-Varying Local Sensitivity of Crop Yields to Temperature (Inference with Clustering at the State Level)

	Spatially and Temporally Varying Model S_1T_1				*Spatially Invariant* Model S_0T_1
	Mean	1st Qu.	Median	3rd Qu.	Fixed Point Estimate
			Corn		
$\beta_a(s_i)$ for $\text{GDD}_{8-r_0°\text{C}}$	–0.0024	–0.0577	–0.0240	0.0591	0.1105
	(–0.0378, 0.0145)	(–0.0959, –0.0292)	(–0.0694, –0.0061)	(0.0252, 0.1016)	(0.0360, 0.2056)
$\beta_a(s_i)$ for $\text{GDD}_{r_0°\text{C}+}$	–0.6076	–1.2670	–0.4927	–0.0250	–1.5653
	(–0.6889, –0.3836)	(–1.6004, –0.9373)	(–0.6590, –0.1774)	(–0.1471, 0.3141)	(–2.0800, –1.2434)
$\beta^*_{(c,a)}(s_i)$ for $\text{GDD}_{8-r_0°\text{C}}$	–0.0064	–0.0846	0.0050	0.0587	–0.0704
	(–0.0134, 0.0076)	(–0.0946, –0.0667)	(–0.0121, 0.0318)	(0.0517, 0.0736)	(–0.1094, –0.0355)
$\beta^*_{(c,a)}(s_i)$ for $\text{GDD}_{r_0°\text{C}+}$	0.4820	0.0399	0.3311	0.8936	1.1666
	(0.3176, 0.5337)	(–0.0864, 0.0890)	(0.2201, 0.3399)	(0.6919, 0.9884)	(0.9051, 1.4896)
			Soybeans		
$\beta_a(s_i)$ for $\text{GDD}_{8-r_0°\text{C}}$	0.0724	0.0214	0.0695	0.1219	0.0808
	(0.0551, 0.1029)	(0.0026, 0.0582)	(0.042, 0.1257)	(0.0836, 0.1455)	(0.0355, 0.1275)
$\beta_a(s_i)$ for $\text{GDD}_{r_0°\text{C}+}$	–1.1141	–1.5248	–0.9711	–0.7456	–1.3388
	(–1.4168, –0.8723)	(–2.0218, –1.2134)	(–1.1701, –0.7380)	(–0.8911, –0.4973)	(–1.7669, –0.8536)
$\beta^*_{(c,a)}(s_i)$ for $\text{GDD}_{8-r_0°\text{C}}$	–0.0384	–0.0620	–0.0348	–0.0129	–0.0555
	(–0.0446, –0.0315)	(–0.0707, –0.0586)	(–0.0404, –0.0279)	(–0.0197, 0.0008)	(–0.0782, –0.0340)
$\beta^*_{(c,a)}(s_i)$ for $\text{GDD}_{r_0°\text{C}+}$	0.6042	0.3171	0.5195	0.8801	0.8450
	(0.4638, 0.7546)	(0.1058, 0.4039)	(0.4251, 0.5709)	(0.7563, 1.1203)	(0.5875, 1.1428)

Notes: The left panel summarizes point estimates of the responsiveness of crop yields to temperature variation in the early period $\boldsymbol{\beta}_a(s_i) \times 100$ and its *change* over time $\boldsymbol{\beta}^*_{(c,a)}(s_i) \times 100$ from the spatiotemporally varying model S_1T_1. The right panel reports their counterparts $\boldsymbol{\beta}_a \times 100$ and $\boldsymbol{\beta}^*_{(c,a)} \times 100$ from a spatially-fixed but temporally varying model S_0T_1. All models control for precipitation variables. Two-sided 95% bias-corrected confidence intervals clustered at the state level are in parentheses. For corn and soybeans, r_0 equals 29 and 30, respectively. The reported point estimates are semi-elasticities interpretable as percentage changes in the mean crop yield per unit change in climate variables.

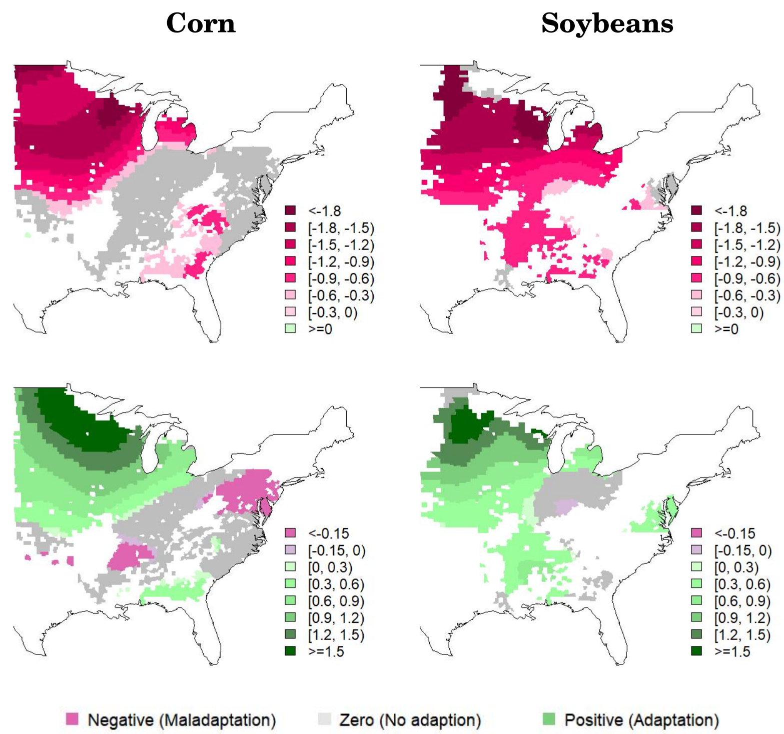

Figure E.1. Estimated Early-Period Local Sensitivity of Crop Yields to Overheat Temperatures and Temporal Changes Therein

Notes: The top-row maps plot point estimates of the early-period crop yield sensitivity to overheat GDD, $\beta_a(s_i) \times 100$, from the spatiotemporally varying model S_1T_1. The bottom-row maps plot point estimates of the *change* in that sensitivity over time, $\beta^*_{(c,a)}(s_i) \times 100$. Regardless of the effect size or sign, all statistically insignificant estimates (at the 5% level) are shown using the same shade of gray. Models control for precipitation variables. The mapped point estimates are semi-elasticities interpretable as percentage changes in the mean crop yield per unit change in climate variables.

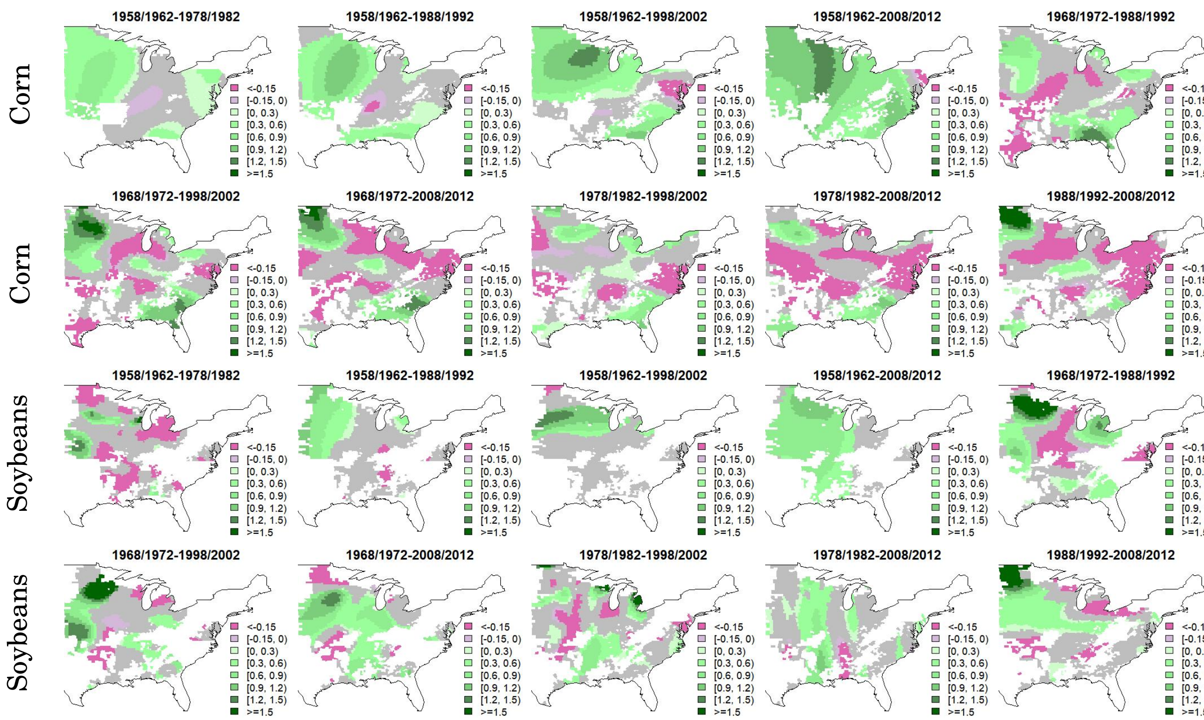

Figure E.2. Robustness of the Estimated Temporal Changes in Local Sensitivity of Crop Yields to Overheat Temperatures

Notes: Maps plot point estimates ×100 of the *change* in responsiveness of crop yields to overheat GDD (the $\beta^*_{(c,a)}(s_i)$ parameter) from the spatiotemporally varying model S_1T_1 using the data from different gap widths (e.g., 20-year, 30-year, 40-year, 50-year) and different starting periods centered in 1960, 1970, 1980, and 1990. For example, the very first map in this figure shows temporal changes in local sensitivity of crop yields to overheat GDD between two periods: 1958-1962 and 1978-1982. Green colors stand for yield gains and red colors stand for yield losses. Regardless of their magnitude or sign, all statistically insignificant estimates are shown using the same shade of gray.

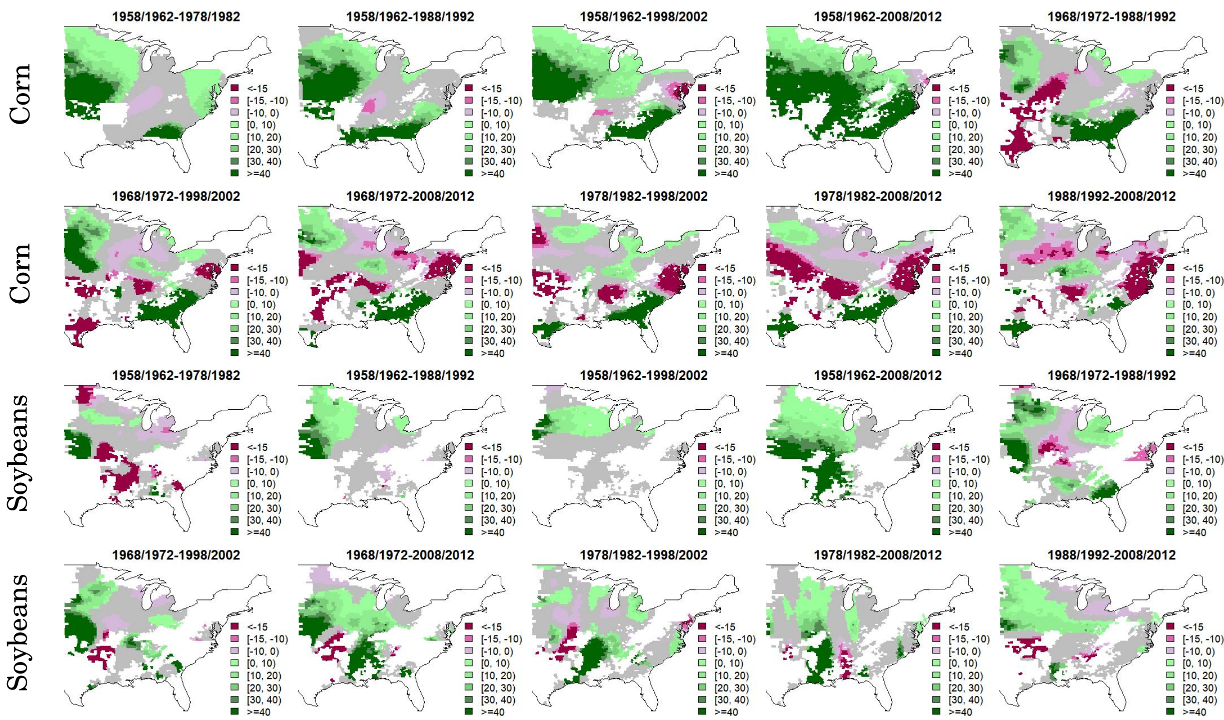

Figure E.3. Robustness of the Estimated Crop Yield Gains (Losses) due to Local Adaptation (Maladaptation)

Notes: Maps plot point estimates of the percentage change in crop yield due to adaptation to overheat GDD based on the spatiotemporally varying model S_1T_1. We calculate it via $\left(\exp\{\beta^*_{(c,a)}(s_i)\times\overline{\mathrm{GDD}}_{p^\circ\mathrm{C}+,ic}\}-1\right)\times 100\%$ using the data from different gap widths (e.g., 20-year, 30-year, 40-year, 50-year) and different starting periods centered in 1960, 1970, 1980, and 1990. For example, the very first map in this figure shows yield gains (losses) due to local adaptation (maladaptation) between two periods: 1958-1962 and 1978-1982. Green colors stand for yield gains and red colors stand for yield losses. Regardless of their magnitude or sign, all statistically insignificant estimates are shown using the same shade of gray.

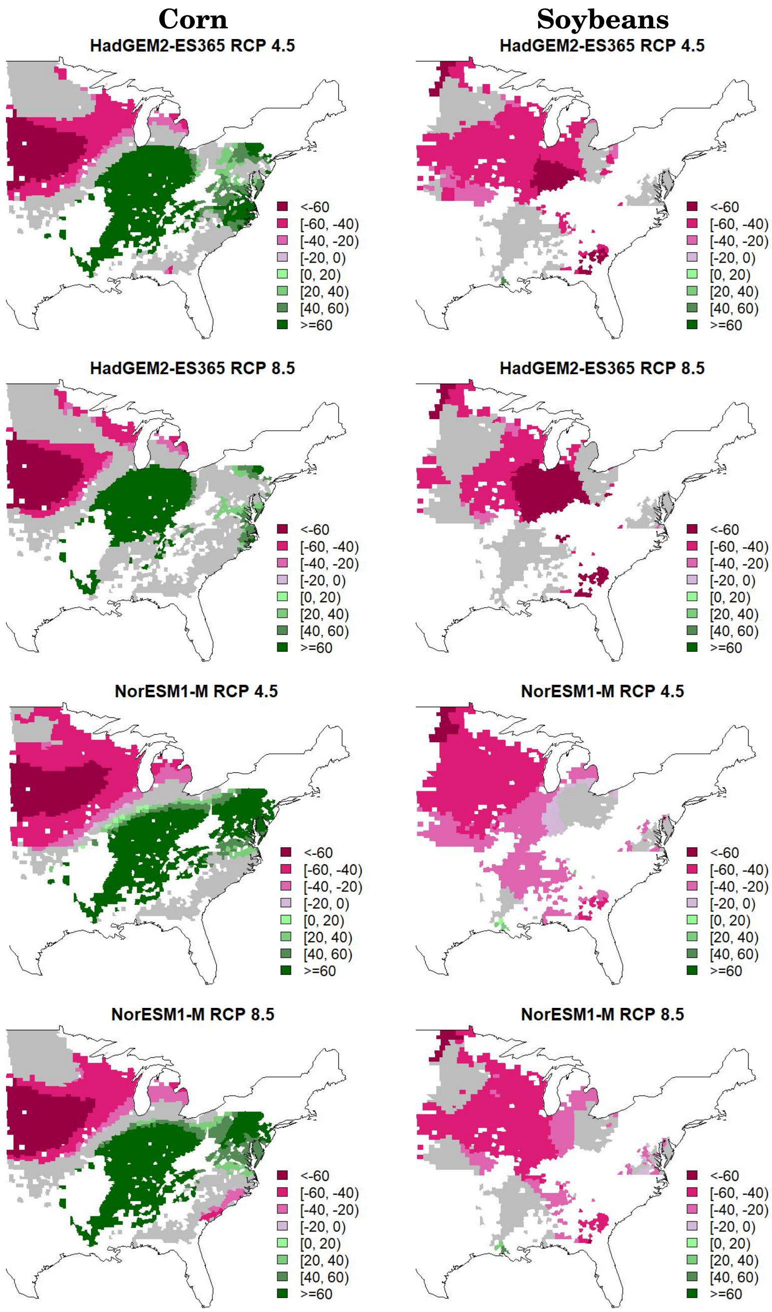

Figure E.4. Spatial Distributions of Total Projections of the Future Climate Change Impact on Crop Yields

Notes: Maps plot point estimates of the projected change (in %) in crop yields due to climate change based on the spatiotemporally varying model S_1T_1, using predicted future weather data from two global climate models (HadGEM2-ES365 and NorESM1-M) under two warming scenarios (RCP4.5 and RCP8.5). The 'adaptation as usual' pojections of the change from the present period c (2015–2019) to the future period d (2048–2052) are computed as $\left(\exp\left\{\Delta\widehat{\widehat{y}}_{i(d,c)}\right\}-1\right)\times 100\%$, where $\Delta\widehat{\widehat{y}}_{i(d,c)} = [\widehat{\boldsymbol{\beta}}_a(s_i)+\widehat{\boldsymbol{\beta}}^*_{(c,a)}(s_i)+\boldsymbol{\beta}^*_{(d,c)}(s_i)]'\overline{\mathbf{z}}_{id} - [\widehat{\boldsymbol{\beta}}_a(s_i)+\widehat{\boldsymbol{\beta}}^*_{(c,a)}(s_i)]'\overline{\mathbf{z}}_{ic}$ and $\widehat{\boldsymbol{\beta}}^*_{(d,c)}(s_i) = \frac{2050-2017}{2017-1960}\widehat{\boldsymbol{\beta}}^*_{(c,a)}(s_i)$. Regardless of their magnitude or sign, all statistically insignificant projections are shown using the same shade of gray.

F Future Crop Yield Change Projections under the Status Quo Scenario

In this appendix, we examine a more conservative 'status quo' scenario, whereby no technological adaptation (i.e., $\boldsymbol{\beta}^*_{(d,c)} = 0$), no climate-neutral technical change (i.e., $\alpha^*_{(d,c)} = 0$), and no relocation of crop production are to occur between the end of our sample period and 2048–2052. To do so, we fix coefficients in the yield-climate relationship at their 2015–2019 values. As such, a projected change in log-yield due to a warming climate in each location s_i in the future is given by $\Delta\hat{y}_{i(d,c)} = \hat{\boldsymbol{\beta}}_c(s_i)'\Delta\overline{\mathbf{z}}_{i(d,c)}$, where $\hat{\boldsymbol{\beta}}_c(s_i)$ measures climate sensitivity of crop yields in observable (historical) period c. We recover $\hat{\boldsymbol{\beta}}_c(s_i)$ using functional parameters in equation (5) as $\hat{\boldsymbol{\beta}}_c(s_i) = \hat{\boldsymbol{\beta}}_a(s_i) + \hat{\boldsymbol{\beta}}^*_{(c,a)}(s_i)$. This predicted log-yield change is converted to the percentage yield change from the present period c to the future period d using $\left(\exp\{\Delta\hat{y}_{i(d,c)}\} - 1\right) \times 100\%$.

Starting with the impact of future overheat GDD changes, the left panel of Table F.1 reports projections based on our S_1T_1 model, while the right panel reports counterpart projections based on its spatially invariant alternative S_0T_1. Aside from the obvious finding that projected effect sizes are generally larger under a more severe warming scenario, we also find the following. Our projections are not always statistically different from zero, even under severe scenarios. This is especially the case for production of corn. The most negative and significant impacts on yields in the future are predicted for soybeans. Contrasting the two models, we see that the weighted mean projections from the S_1T_1 model are generally of smaller magnitudes, which suggests that conventional space-invariant approaches like the S_0T_1 may be overestimating future damages of rising overheat temperatures.

Figure F.1 depicts the results in Table F.1 by mapping local projections from our S_1T_1 model for each crop (statistically insignificant predictions are colored gray). In the case of corn production, regions in the lower Midwest—Nebraska, Kansas, southern Iowa, northern Missouri and parts of South Dakota—and in the South—Tennessee, Georgia, South Carolina, northern Alabama—are projected to experience large declines in yields by 2050. Whereas, parts of the Corn Belt including some areas in Indiana, Ohio, Illinois, as well as parts of North Dakota are, in contrast, expected to benefit from significant gains in crop yields. Given this spatial bifurcation in future climate change effects on corn productivity with the offset potential in the net, it is unsurprising that we find statistically insignificant (effectively zero) projections *on average* (see the first column in Table F.1). Consistent with Table F.1, when statistically different from zero, local county-level projections for soybean yields are mostly negative, which is why the average projection for the U.S. is also significantly negative. The largest decline is to occur in the area of Illinois, Indiana, Ohio as well as Kansas. Minnesota is essentially the only state for which we project a mild yield increase in soybean production. The geographical pattern in the yield impact seen in Figure F.1 is largely consistent with that for historical overheat adaptation (Figure 5), whereby areas with the largest projected yield decreases strongly overlap with areas that historically experienced small or statistically insignificant adaptation.

Unlike under the 'adaptation as usual' scenario, the 'status quo' total projections of future yield changes are quite similar to projections using only overheat GDD change (see Table F.2 and Figure

F.2), corroborating earlier studies such as Schlenker and Roberts (2009) and Burke and Emerick (2016) documenting that overheat is the major factor influencing crop yields in a warming climate.[25]

In Table F.3 we aggregate local county-specific projections, weighting them using crop acreage in 2017 (the midpoint of the "present" 2015–2019 period). For comparison, we include total projections from three models. Average yield loss projections for corn based on our spatiotemporally varying methodology are smaller than those obtained using these two alternative models. Our model projects total yield losses for corn ranging from –7% to –13% and, notably, these losses are statistically *in*significant even under severe global warming scenarios. As discussed above, this statistically insignificant result is largely due to bifurcated effects of a changing climate on corn yields, with some regions experiencing yield losses and others gains (also see Figures F.1 and F.2). For soybean yields, our S_1T_1 model projects the smallest yield losses among the three specifications under both HadGEM2-ES365 scenarios. But under NorESM1-M scenarios, it projects slightly larger yield losses than those by S_0T_1, although these projections are still less than a half of what the time-invariant S_0T_0 alternative predicts (see the "Soybeans" column in Table F.3). As projected by our model, the future soybean yield reduction expected in a typical county ranges between statistically significant 12% and 48%.

[25] Note that Table F.2 in Appendix E shows that the future climate change by 2050 is predicted to result in a statistically significant median decrease in corn yields, although the weighted average decrease is still insignificant.

Table F.1. Projections of the Impact of Future Rising Overheat Temperature on Crop Yields

	Spatiotemporally Varying Model S_1T_1				*Spatially Invariant* Model S_0T_1
	Weighted Mean	1st Qu.	Median	3rd Qu.	Weighted Mean
			Corn		
Had RCP 4.5	–8.65	–39.27	–22.22	1.94	–41.88
	(–19.32, 15.75)	(–48.95, –18.59)	(–39.05, 0.29)	(–19.89, 19.40)	(–60.97, –17.03)
Had RCP 8.5	–11.39	–49.81	–27.79	2.32	–51.41
	(–25.24, 22.41)	(–61.13, –22.94)	(–47.05, –2.19)	(–24.97, 25.01)	(–71.39, –21.98)
Nor RCP 4.5	–4.77	–16.58	–8.42	0.65	–17.45
	(–8.54, 2.96)	(–20.8, –7.43)	(–15.98, 0.17)	(–6.14, 5.88)	(–28.28, –6.38)
Nor RCP 8.5	–11.07	–30.30	–15.79	1.30	–36.75
	(–17.98, 6.15)	(–38.67, –12.6)	(–29.33, 0.28)	(–12.89, 12.88)	(–54.81, –14.58)
			Soybeans		
Had RCP 4.5	–47.13	–55.86	–49.41	–40.77	–41.84
	(–63.72, –30.21)	(–69.75, –37.08)	(–64.39, –29.95)	(–57.89, –20.30)	(–59.44, –14.73)
Had RCP 8.5	–57.87	–68.68	–60.68	–51.08	–53.49
	(–74.35, –38.21)	(–82.82, –48.46)	(–75.52, –38.23)	(–68.4, –29.14)	(–72.04, –20.15)
Nor RCP 4.5	–17.24	–20.83	–17.7	–14.9	–17.4
	(–25.2, –8.03)	(–28.24, –9.85)	(–25.92, –8.41)	(–23.17, –8.44)	(–27.26, –5.46)
Nor RCP 8.5	–38.55	–46.39	–39.79	–31.89	–37.53
	(–53.27, –20.27)	(–58.7, –25.96)	(–53.74, –21.45)	(–48.41, –17.19)	(–54.31, –12.91)

Notes: The left panel summarizes point estimates of the projected change (in %) in crop yields due to changes in overheat GDD (i.e., $\mathrm{GDD}_{r_0\,°\mathrm{C}+}$) based on the spatiotemporally varying model S_1T_1, using the predicted future weather data from two global climate models, HadGEM2-ES365 and NorESM1-M, under two warming scenarios: RCP4.5 (mild warming) and RCP8.5 (severe warming). The right panel reports the counterpart estimates based on the spatially invariant but time-varying model S_0T_1. The 'status quo' projections of the change in yields from the present period c (2015–2019) to the future period d (2048–2052) are computed as $\left(\exp\left\{\Delta\widehat{y}_{i(d,c)}\big|_{\mathrm{GDD}_{r_0\,°\mathrm{C}+}}\right\} - 1\right) \times 100\%$, where $\Delta\widehat{y}_{i(d,c)}\big|_{\mathrm{GDD}_{r_0\,°\mathrm{C}+}} = \left(\widehat{\beta}_c(s_i)\text{for } \mathrm{GDD}_{r_0\,°\mathrm{C}+}\right) \times \Delta(\overline{\mathrm{GDD}_{r_0\,°\mathrm{C}+}})_{i(d,c)}$. Weighted mean is calculated using crop acreages in 2017. Two-sided 95% bias-corrected confidence intervals clustered at the climate division level are in parentheses.

Table F.2. Total Projections of the Future Climate Change Impact on Crop Yields

	Spatiotemporally Varying Model S_1T_1				*Spatially Invariant* Model S_0T_1
	Weighted Mean	1st Qu.	Median	3rd Qu.	Weighted Mean
			Corn		
Had RCP 4.5	–11.47	–38.31	–21.43	5.97	–32.08
	(–24.09, 12.61)	(–44.78, –21.66)	(–35.50, –4.02)	(–15.83, 25.76)	(–49.64, –8.46)
Had RCP 8.5	–12.64	–50.50	–28.14	6.46	–40.98
	(–27.50, 16.68)	(–59.90, –29.18)	(–44.86, –7.05)	(–19.49, 32.91)	(–60.67, –11.88)
Nor RCP 4.5	–7.29	–15.77	–7.39	1.02	–11.04
	(–12.95, 1.47)	(–18.42, –7.92)	(–13.47, –0.17)	(–5.92, 5.09)	(–19.78, –1.11)
Nor RCP 8.5	–11.61	–32.41	–13.96	3.30	–26.09
	(–20.50, 6.37)	(–39.50, –16.94)	(–24.66, –0.15)	(–11.30, 13.21)	(–42.38, –4.93)
			Soybeans		
Had RCP 4.5	–38.13	–51.32	–38.49	–26.13	–36.18
	(–55.80, –19.85)	(–66.29, –27.71)	(–53.11, –17.08)	(–44.34, –4.46)	(–55.26, –12.34)
Had RCP 8.5	–47.85	–65.30	–48.44	–34.16	–47.26
	(–66.50, –25.68)	(–81.04, –39.52)	(–64.35, –21.12)	(–54.73, –6.59)	(–68.43, –17.01)
Nor RCP 4.5	–11.75	–18.32	–14.18	–7.00	–13.57
	(–19.63, –3.50)	(–25.64, –9.08)	(–21.81, –6.99)	(–14.21, 1.45)	(–24.40, –3.45)
Nor RCP 8.5	–28.58	–39.39	–31.92	–19.96	–30.52
	(–43.90, –11.35)	(–51.72, –19.77)	(–46.63, –14.78)	(–36.93, –1.23)	(–49.81, –8.57)

Notes: The left panel summarizes point estimates of the projected change (in %) in crop yields due to climate change based on the spatiotemporally varying model S_1T_1, using predicted future weather data from two global climate models (HadGEM2-ES365 and NorESM1-M) under two warming scenarios (RCP4.5 and RCP8.5). The right panel reports the counterpart estimates based on the spatially invariant but time-varying (S_0T_1) model. The 'status quo' projections of the change from the present period c (2015–2019) to the future period d (2048–2052) are computed as $\left(\exp\{\Delta\widehat{y}_{i(d,c)}\} - 1\right) \times 100\%$, where $\Delta\widehat{y}_{i(d,c)} = \widehat{\boldsymbol{\beta}}_c(s_i)\Delta\overline{\mathbf{z}}_{i(d,c)}$. Weighted mean is calculated using crop acreages in 2017. Two-sided 95% bias-corrected confidence intervals are in parentheses.

Table F.3. Total Projections of the Future Climate Change Impact on Crop Yields

	Model	**Corn**	**Soybeans**
Had RCP 4.5	S_1T_1 (preferred model)	–11.47	–38.13
		(–24.09, 12.61)	(–55.80, –19.85)
	S_0T_1 (à la Yu et al. (2021))	–32.08	–36.18
		(–49.64, –8.46)	(–55.26, –12.34)
	S_0T_0 (à la Burke and Emerick's (2016))	–88.29	–88.67
		(–94.35, –74.52)	(–95.06, –73.08)
Had RCP 8.5	S_1T_1 (preferred model)	–12.64	–47.85
		(–27.50, 16.68)	(–66.50, –25.68)
	S_0T_1 (à la Yu et al. (2021))	–40.98	–47.26
		(–60.67, –11.88)	(–68.43, –17.01)
	S_0T_0 (à la Burke and Emerick's (2016))	–95.13	–96.17
		(–98.13, –85.99)	(–98.82, –86.88)
Nor RCP 4.5	S_1T_1 (preferred model)	–7.29	–11.75
		(–12.95, 1.47)	(–19.63, –3.50)
	S_0T_1 (à la Yu et al. (2021))	–11.04	–13.57
		(–19.78, –1.11)	(–24.40, –3.45)
	S_0T_0 (à la Burke and Emerick's (2016))	–28.29	–37.62
		(–44.97, –5.62)	(–53.67, –17.51)
Nor RCP 8.5	S_1T_1 (preferred model)	–11.61	–28.58
		(–20.50, 6.37)	(–43.90, –11.35)
	S_0T_1 (à la Yu et al. (2021))	–26.09	–30.52
		(–42.38, –4.93)	(–49.81, –8.57)
	S_0T_0 (à la Burke and Emerick's (2016))	–68.30	–76.33
		(–83.12, –38.20)	(–88.68, –50.07)

Notes: The table reports weighted averages (in %) of the projected change in crop yields due to climate change based on models S_1T_1, S_0T_1 and S_0T_0. We use predicted future weather data from two global climate models, HadGEM2-ES365 and NorESM1-M, under two warming scenarios: RCP4.5 (mild warming) and RCP8.5 (severe warming). The 'status quo' projections of the change in yields from the present period c (2015–2019) to the future period d (2048–2052) are computed as $\left(\exp\left\{\Delta\widehat{y}_{i(d,c)}\right\}-1\right)\times 100\%$, where $\Delta\widehat{y}_{i(d,c)} = \widehat{\boldsymbol{\beta}}_c(s_i)\Delta\overline{\mathbf{z}}_{i(d,c)}$. Weighted mean is calculated using crop acreages in 2017. Two-sided 95% bias-corrected confidence intervals clustered at the climate division level are in parentheses.

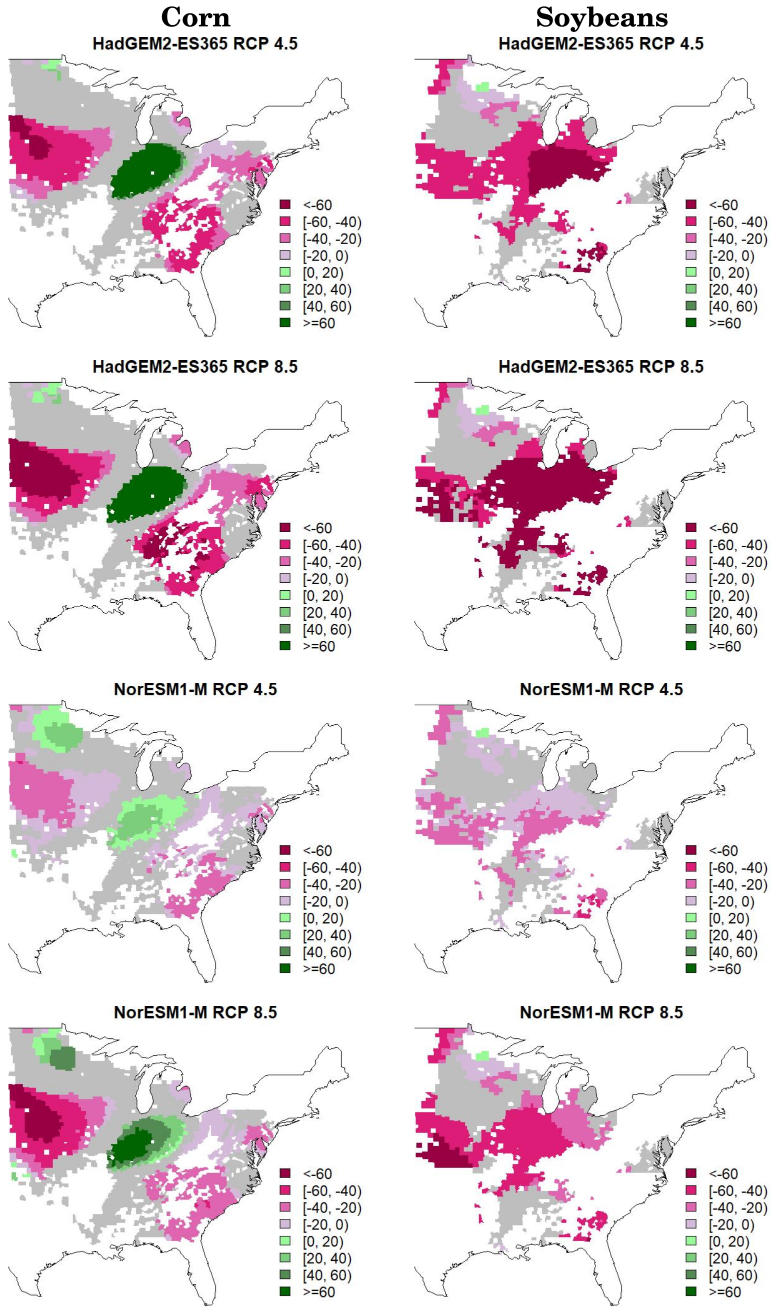

Figure F.1. Spatial Distributions of Projections of the Future Rising Overheat Temperature Impact on Crop Yields

Notes: Maps plot point estimates of the projected change (in %) in crop yields due to changes in overheat GDD (i.e., $\text{GDD}_{r_0\,^\circ\text{C}+}$) based on the spatiotemporally varying model S_1T_1, using the predicted future weather data from two global climate models, HadGEM2-ES365 and NorESM1-M, under two warming scenarios: RCP4.5 (mild warming) and RCP8.5 (severe warming). The 'status quo' projections of the change in yields from the present period c (2015–2019) to the future period d (2048–2052) are computed as $\left(\exp\left\{\Delta\widehat{y}_{i(d,c)}\big|_{\text{GDD}_{r_0\,^\circ\text{C}+}}\right\} - 1\right) \times 100\%$, where $\Delta\widehat{y}_{i(d,c)}\big|_{\text{GDD}_{r_0\,^\circ\text{C}+}} = \left(\widehat{\beta}_c(s_i)\text{for GDD}_{r_0\,^\circ\text{C}+}\right) \times \Delta(\overline{\text{GDD}_{r_0\,^\circ\text{C}+}})_{i(d,c)}$. Regardless of their magnitude or sign, all statistically insignificant projections (at the 5% level) are shown using the same shade of gray.

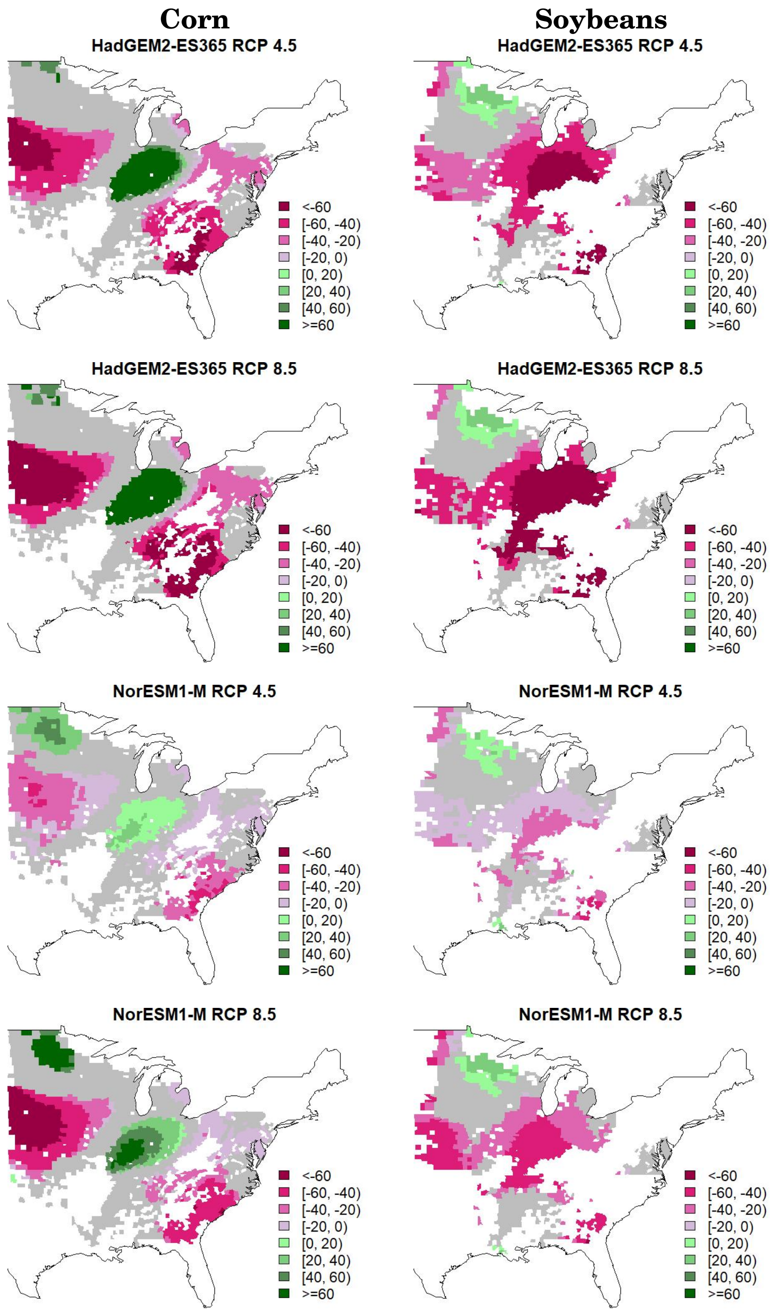

Figure F.2. Spatial Distributions of Total Projections of the Future Climate Change Impact on Crop Yields

Notes: Maps plot point estimates of the projected change (in %) in crop yields due to climate change based on the spatiotemporally varying model S_1T_1, using predicted future weather data from two global climate models (HadGEM2-ES365 and NorESM1-M) under two warming scenarios (RCP4.5 and RCP8.5). The 'status quo' projections of the change from the present period c (2015–2019) to the future period d (2048–2052) are computed as $\left(\exp\{\Delta\widehat{y}_{i(d,c)}\} - 1\right) \times 100\%$, where $\Delta\widehat{y}_{i(d,c)} = \widehat{\boldsymbol{\beta}}_c(s_i)\Delta\overline{\mathbf{z}}_{i(d,c)}$. Regardless of their magnitude or sign, all statistically insignificant projections are shown using the same shade of gray.